NATIONAL BUREAU OF STANDARDS
MICROCOPY RESOLUTION TEST CHART

A Study on the Use of Positron Annihilation
as a Non-Destructive Evaluation Tool for
Micro-Structure Defects in Aluminum, Titanium
and their Alloys and Nickel Base Superalloys

Reported by S.J. Tao
The New England Institute
Ridgefield, Connecticut 06877

ADA046441

AD No.
DDC FILE COPY

DDC
RECEIVED
NOV 7 1977
F

REPORT DOCUMENTATION PAGE	READ INSTRUCTIONS BEFORE COMPLETING FORM

1. REPORT NUMBER	2. GOVT ACCESSION NO.	3. RECIPIENT'S CATALOG NUMBER
FINAL REPORT. Dec 75-Feb 77,		

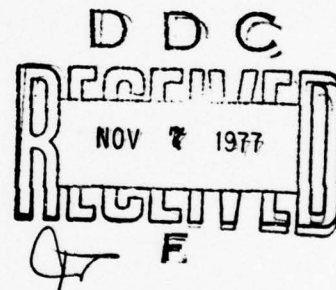| 4. TITLE (and Subtitle)	5. TYPE OF REPORT & PERIOD COVERED
A Study on the Use of Positron Annihilation as a Non-Destructive Evaluation Tool for Micro-Structure Defects in Aluminum, Titanium and Their alloys and Nickel Base Superalloys.	Final Dec.1975-Feb. 1977,
	6. PERFORMING ORG. REPORT NUMBER N.A.

7. AUTHOR(s)	8. CONTRACT OR GRANT NUMBER(s)
Shu-Jen Tao	N00019-76-C-0447

9. PERFORMING ORGANIZATION NAME AND ADDRESS	10. PROGRAM ELEMENT, PROJECT, TASK AREA & WORK UNIT NUMBERS
THE NEW ENGLAND INSTITUTE Ridgefield, Connecticut 06877	320 A-113-4

11. CONTROLLING OFFICE NAME AND ADDRESS	12. REPORT DATE
Office of Naval Research Arlington, Virginia	Mar 1977
	13. NUMBER OF PAGES 107

14. MONITORING AGENCY NAME & ADDRESS(if different from Controlling Office)	15. SECURITY CLASS. (of this report)
	UNCLASSIFIED
	15a. DECLASSIFICATION/DOWNGRADING SCHEDULE

16. DISTRIBUTION STATEMENT (of this Report)

APPROVED FOR PUBLIC RELEASE
DISTRIBUTION UNLIMITED

DDC
RECEIVED
NOV 7 1977
F.

17. DISTRIBUTION STATEMENT (of the abstract entered in Block 20, if different from Report)

19. KEY WORDS (Continue on reverse side if necessary and identify by block number)

Vacancy Concentration, Defects, Aluminum Alloys, Aluminum, Titanium Alloy, Nickel Base Superalloys, Positron Annihilation, Non-Destructive Evaluation.

20. ABSTRACT (Continue on reverse side if necessary and identify by block number)

The work carried out during the three year 1973-1977 period on the evaluation of positron annihilation as a non-destructive evaluation tool for micro-structure defects in some engineering materials, such as aluminum, titanium and their alloys and nickel base superalloys are reported. Positron annihilation has been found to be useful as a non-destructive evaluation tool for microstructure defects in the engineering materials tested. However, the method used, positron lifetime measurement, is well established but relatively

DD FORM 1473 EDITION OF 1 NOV 65 IS OBSOLETE
1 JAN 73
S/N 0102-014-6601 |

time consuming.   Further studies on more engineering materials with various kinds of microstructure defects using a relatively fast method, positron annihilation gamma-ray Doppler Broadening is recommended.

TABLE OF CONTENTS

S U M M A R Y

The work carried out during the three year 1973 - 1977 period on the
evaluation of positron annihilation as a non-destructive evaluation
tool for microstructure defects in some engineering materials, such
as aluminum, titanium and their alloys and nickel base superalloys
are reported. Positron annihilation has been found to be useful as
a non-destructive evaluation tool for microstructure defects in the
engineering materials tested. However, the method used, positron
lifetime measurement is well established but relatively time-con-
suming. Further studies on more engineering materials with various
kinds of microstructure defects using a relatively fast method, posi-
tron annihilation gamma-ray Doppler Broadening is recommended.

I. THE ANNIHILATION PROCESS

The theoretical considerations that determine the probability of the various modes of annihilation of slow positron-electron pairs are discussed in detail in texts on Quantum Electrodynamics and Reviews.[1,2] Here we shall recall some processes and formulas which are used directly for the experimental works.

The annihilation process will release an energy $2M_o c^2$ (M_o - rest mass of electron, c - speed of light in vacuum), the mass energy, plus the energy of the annihilating pair. For slowly moving pairs, conservation of momentum demands that at least two bodies be involved; both before and after the process. The two-photon annihilation process is the most probable one for the annihilation of a "free" positron-electron pair. For three-photon annihilation, the additional particle reduces the annihilation probability by a factor of the order of the fine structure constant, $\alpha = 1/137$. The single-photon annihilation process is less likely because of the need of the presence of a third body. Naturally, annihilation with a higher number of photons is less likely.

At low positron energies, the annihilation probability for two-photon annihilation is

$$\Gamma_2 = \pi \gamma_o^2 c \rho_e$$

where γ_o is the classical radius of electron and ρ_e the density of electrons.

A positron can bind an electron to form a positronium Ps atom. The ground states of the Ps atom are the singlet ^1S state or the para-Ps and the triplet ^3S state, or the ortho-Ps. By the conservation of angular momentum and charge parity that p-Ps decays into an even number, two most probable, of photons and o-Ps into an odd number, three most probable, of photons. The

annihilation lifetime (inverse of annihilation rate) of p-Ps is 123 psec, and
that of o-Ps, 140 nsec. It should be noted that both of these lifetimes,
particularly o-Ps, will be modified in a medium because of other interactions.

The ratio of three-photon to two-photon annihilation for slow posi-
trons in a medium is ~ 1/370. If positronium is formed the fraction of three
photo events will be larger. However, in metallic or ionic substances, the
increase will be very slight since positronium is generally not formed there.
In metallic or ionic crystals most of the positron-electron pairs are annihila-
ting via the two-photon annihilation mode. The relative emission directions and
the energies of the annihilation photons can provide useful information about
the initial state of the electron-positron system.

In the center of mass frame of the annihilating pair, the two photons
are emitted in opposite directions, each with an energy to one half the total
energy of the system, the mass energy less the binding energy of the pair.
In the laboratory frame, because of the motion of the annihilating pair at a
velocity $v \ll c$, the energies and emission directions are changed.

The change of the emission direction $\delta\theta$ is approximately

$$\delta\theta = \frac{P_t}{M_o c} ,$$

where P_t is the momentum of the pair transverse to the emission direction of
the annihilation photons. The magnitude of $\delta\theta$ is found to be in the order of
milliradians.

With a similar analysis we can obtain an expression for the energies
deviations to be

$$\delta E = c P_e /2 ,$$

where p_e is the momentum of the pair along the emission direction. For 10 eV
electrons, assuming positrons are thermalized in the interstitial region, δE is

2

about 1.5 KeV (E = 0.511 MeV).

In order to interpret the experimental results obtained by life-
time, angular correlation or Doppler broadening measurements in a real system,
an expression for the annihilation of positrons in an arbitrary system of
electrons and external fields is required. The theoretical treatments were
given by Chang Lee,[3] Ferrell,[4] Wallace[2] and others. Many experimental works
were made and they are referred to the original papers and review articles.[5]

II. EXPERIMENTAL TECHNIQUES

(1) Lifetime

Positron (annihilation) lifetime measurements usually are made by
taking advantage of a few radioisotopes with a specific decay scheme, for ex-
ample, the commonly used Na22, which emits a gamma-ray within a time of less
than 10 psec in association of the emission of a positron. This gamma-ray pro-
vides a mark for the time of birth of the positron and the annihilation gamma-
rays, the time of death. The gamma-rays are detected by two detectors and the
time intervals between the electrical pulses produced by them are converted
into amplitude of the coincident pulses. They are selected, analyzed and stored
in a multi-channel analyzer or a similar computer system. The different energies
of the two type gamma-rays serve as an identification of these pulses.

There are many ways to construct a positron lifetime measuring system.[6]
However, the essential parts are all similar. For high time resolution, plastic
scintillators of high light output and fast rise time coupled with high gain fast
photo multipliers are used as the detectors. The schematic of a typical one used
by us is shown in Figure 1 as an example.

The system shown in Figure 1 has the following features. The gamma-
ray energy defining side channel discriminators are as fast as the timing circuits.

3

Therefore, the faster time-to-amplitude converter instead of the slower analogue to digital converter in the multi-channel analyzer is gated. Taking advantage of the high gain of XP1020 photo multipliers, no amplifiers are used for timing and energy selection.

The resolution of the system is defined as the full width at half maximum FWHM of the curve measured for two coincident gamma-rays with the same energy settings as used by positron lifetime measurements. Normally Co60 is used for time resolution calibration. The resolution of a practical system varies around 300 psec depending on various conditions.

The positron source is either deposited directly on the surface of the sample or more commonly, on the surface of a thin foil (< 2mg/cm^2), such as gold, mica or polyester. Since positrons are emitted to all directions, they must be stopped by sandwiching the source between two pieces of same samples in close touch. As the positrons emitted are not monoenergetic and are distributed favoring lower energies, most of the positrons will annihilate near the surface with the higher energetic ones penetrating deeper. The maximum penetration power of the positrons emitted by Na22 (E_{max} = 542 KeV) is estimated to be roughly 150 mg/cm^2.

For our purpose, it is found that thin gold foil (0.001 mm thick, ~ 2 mg/cm^2) is a good source support for metal sample. Due to the high atomic number of gold, it is expected that the backscattering effect may enhance the annihilation of positrons in the lighter sample instead of source support, gold.

For single pieces of sample where the method of sandwiching cannot be applied, we have used a piece of annealed gold (> 1 mm thick) as a backing to sandwich the source between the gold and the sample. We have found that this

method is satisfactory for samples of nickel base superalloys, Ti-6Al-4V, aluminum and perhaps others. Although it might be hard to make a direct theoretical interpretation because of the involvement of the gold backing, however, the systematic change of positron lifetime with the change of the metallurgical conditions of the sample can be detected and an indirect theoretical interpretation can still be worked out.

The end product of the positron lifetime measurement is the so-called positron lifetime spectrum. An example of it is shown in Figure 2. The time positive side of the spectrum is considered to be either a single or a multiple exponential decay. For well annealed pure metals it is usually a single exponential decay. For deformed pure metals it contains two exponentials as interpreted by the trap Theory.[7] In metallic samples, in general, either a single or a two-component exponential decay enalysis is used. The spectrum can be analyzed by a simple method of least squares[8] or by a method where the resolution function is accounted for.[9] If a purely theoretical study is not required and only a relative change of positron lifetime is needed the stripping-off of the resolution function is not really necessary. Any change in the original positron lifetime spectrum will give a systematic change in the actual measured positron lifetime spectrum compounded with resolution function.

The source strength used is around 20 µCi. It takes several hours to a day to obtain a spectrum with reasonable statistical significance. There are two ways to increase the counting efficiency; by using a pair of scintillators of larger size and a stronger source. Using scintillators of larger size usually reduces the time resolution of the system which is not very desirable for work on metallic substances. Using a stronger source increases the relative background which is not very desirable, either.

Both of them increase the counting rate of the detectors, consequently increasing the effect of pile-up of pulses. By optimization, it is believed that a system can be assembled to reduce the time required for each measurement down to a few hours. Further improvement would be harder although not impossible. The long time duration for one measurement is the major disadvantage of the method of positron lifetime measurement.

(2) Angular Correlation

A typical experimental set-up is the long slit geometry as shown in Figure 3. Pairs of parallel long slit collimators are used to define the directions of gamma-rays detected by the system. A pair of detectors, usually scintillation counters with scintillators of long dimensions are required; one is placed stationary and another removable. The coincident counting rate from the detectors are measured by an electronic system such as the one shown in Figure 4.[10] A short coincidence time of about 10 nsec is used to reduce the random background.

In order to obtain good angular resolution < 1 mrad, narrow slits and far separation > 5 meters, are required. Consequently, a strong positron source > 10 mCi is usually needed to give sufficient counting rates. It takes several days to obtain a spectrum with reasonable statistical deviation. The positron source, in general, is placed outside the sample. For specific samples inside the source can be used. Ordinary photo multipliers and common relatively slow electronic circuits can be used. Therefore, a simple angular correlation system with moderate resolution (~ 0.5 mrad) can be assembled with a modest budget. However, using the long slit geometry, only one component of the electron momentum, P_z, can be measured.

After the advant of mini-computers, it is possible to construct a multi detector system or a system with a grid of many detectors.[11] This kind of system can measure two components, P_z and P_y, of the electron momentum. Besides that, the time required for one measurement can be somewhat reduced.

6

However, the system becomes fairly complicated. It is also expensive to construct and operate.

If an outside source is used the penetration of the positrons and the attenuation of the 0.51 MeV photons inside the sample will produce an asymmetric resolution curve which may be largely removed by rotating the sample through a small angle.

Precise measurement of the resultant spectrum, angular correlation curve, can be achieved with a resolution as high as 0.1 milliradians. This method is suited for a detailed measurement of the momentum distribution of electrons in the sample, for example the shape of the Fermi surface of metals. At present stage, it is not well suited for applications in applied field.

(3) Doppler Broadening

The measurement of the longitudinal component of the photo pair energy was made possible after the advant of the solid state detectors with high efficiency and fine energy resolution ~ 1.8 KeV for 1.33 MeV Co60 gamma-rays. This roughly gives an energy resolution at 0.51 MeV equivalent to that of a long slit angular correlation apparatus having an angular resolution of ~ 4 milliradians.

Therefore, this method is not suited for works where a high energy resolution is required. Here, angular correlation is preferred. However, for practical purposes where a change of the spectrum can be represented by a certain parameter derived from the curve the present resolution is sufficient to produce reliable and consistant results as shown by many published works.[12]

Only one detector Ge(Li) or hyperpure (intrinsic) Ge detector is required. The preparation of the positron source and sample is similar to that for lifetime measurements.

7

The only difference is any positron source can be used. As shown in Figure 5, the electronics are seemingly simpler than that used in positron lifetime measurement. However, since a much more stable system is required, the resultant system is not much simpler than that used in positron lifetime measurement. A multichannel analyzer or its' equivalent is also required.

The major advantage of this method is the shorter time duration required for one measurement, several hours or less. Certainly, there are disadvantages. One of them is the requirement of a liquid nitrogen cryostate. For Ge(Li) detector, it must be kept under low temperature without interruption even though it is not used. Otherwise it is ruined and must be either repaired or replaced. For hyperpure Ge detector, cryogenic cooling is still required when it is in operation. But, the present state of art of making hyperpure Ge detectors has not reached that of making Ge(Li) detectors. The second disadvantage is the nonuniformity of the parameters used by different workers for the data presentation. However, a recent study by us has shown that some of the parameters used are highly related to the variance of the energy profile of the 0.51 MeV gamma-ray. Therefore, a kind of standardization is possible in the near future.

III. EXPERIMENTAL

For our work conducted during the last three years the method of positron lifetime measurement as described in Section II has been used. The resolution of the apparatus has been very close to 320 psec. In general, one measurement took about one day or one half day. The resultant lifetime spectra were fitted to both a one component exponential decay scheme and a two component exponential decay scheme. If the spectrum was found to be statistically not able to be fitted into a two component exponential decay scheme, the results from the one component decay scheme would be used. The results from the two component exponential decay scheme curve fit give three parameters, τ_1 and τ_2, the meanlife (lifetime) of the two components, and I_2, the intensity of the second (longer) component. From the one component exponential decay scheme curve fit only one parameter τ (or $\bar{\tau}$), meanlife, is obtained.

All of the lifetime measurements, except specifically mentioned were carried out with samples at room temperature $21 \pm 2°C$ and under ambient air. Unless specifically mentioned the surface was cleaned by acetone and wiped by a soft paper tissue.

For the details of the experiments carried out during the first two years, the reader is referred to the two respective final reports.[13,14]

In addition, a brief and thorough review "General Aspects of Positron Annihilation and Its Application to the Study of Defects" is attached to the first report.[13] For many references regarding the study of defects in metals the reader is referred there.[13]

Before the discussion, the experimental work accumulated in the three year study is briefly summarized in Table 1, in an order according to the substructures and materials studied. A major part of section c in Table 1 and some others were carried out in the last year.

Because of the time limitation, the part C3 in Table 1 will be fully reported
at a later date.

TABLE 1 - A SUMMARY OF THE WORK PERFORMED

SUBSTRUCTURES STUDIED	MATERIALS STUDIED	SUMMARY OF RESULTS
A. Dislocation		
1. Creep Induced	Mar-M200* < 100 > oriented	Consistent with the TEM confirmed concept
2. Monotonic uniaxial deformation	99.99% Al	Showing dynamic hardening and recovery characteristics
	Nb*, zone refined monocrystal	Showing dynamic hardening recovery characteristics
	Al-2024-T3	$\bar{\tau}$ vs strain change
	Ti-6Al-4V*	$\bar{\tau}$ vs strain change
3. Commercial Rolling	Al-1100	Showing dynamic hardening and recovery characteristics
4. Cyclic (Fatigue) Strain	Mar-M200* cube-oriented	τ_1, τ_2 increasing with stress
5. Annealed after deformation	99.99%	Recovery and recrystallization observed
	Al-1100-H18	Recovery and recrystallization observed
B. Microstructural Features		
1. Grain Size	Nimonic-115*	$\bar{\tau}$ vs d^{-1}
2. Different Precipitate States	Al-2024-T4	Dispersion of G.P. zones and S^1 precipitation observed

SUBSTRUCTURES STUDIED	MATERIALS STUDIED	SUMMARY OF RESULTS
	Al-7075-T6	Punching out of dislocation loop observed
	Al-7050-T76	Punching out of dislocation loop observed
C. Macroscopic Surface Features		
1. Surface Treatment	Various aluminum alloys	Interesting results, surface defects important
2. Surface Oxides	Fe-Cr-Al and Fe-Cr-Al-Y	Surface defects more important than oxide
	Ti and Ti-6Al-4V	Change of surface oxide noticed
D. Fracture Related Macroscopic Defects		
1. Process Induced Voids	Nickel base* superalloys	Voids 50 µm and up not detected
2. Stress Creep Rupture	Nimonic-115*	Structure level difference detected
	Udimet-700*	Structure level difference detected
3. Surface plastic zone ahead of a fatigue crack	Ti-6Al-4V*	Plastic zone detected

* Source sandwiched with a piece of gold backing

IV. RESULTS AND DISCUSSION

(1) Positrons and Dislocation Substructures

As mentioned, it has been shown that the interaction of positrons with dislocations in metals can lead to long lifetime component, τ_2, in the positron annihilation spectrum.[13-15] The association of such a long lifetime with dislocations prompted us to positron probe the following well-characterized dislocation substructures in alloys generated by various deformation processes and thermal treatments to verify the general applicability of positron annihilation and τ_2 to characterize dislocation-content and through it the plastic states of structural alloys. For completeness we strove to characterize the crept states, monotonically deformed states, rolled states, cyclically deformed states and recovered and recrystallized states.

(1.1) _Creep Induced Dislocation Substructure:_

The system chosen for this purpose was <100> oriented monocrystalline Mar-M-200 (Chemical composition in wt. pct.: 10.2 Cr, 10 Co, 4 W, 0.7 Nb, 2.5 Ti, 11 Al, 0.082 B, 0.74 C, 0.3 Zr, Bal. Ni.), an engineering alloy in which the creep induced dislocation substructure has been extensively studied by transmission electron microscopy.[16-18] The monocrystals were solutionized at 1232°C for 100 hours in an argon atmosphere and aged at 870°C for 32 hours. The resultant microstructure consists of 57 volume percent cuboidal γ' precipitates 0.25 μm on edge, distributed in uniform arrays in the γ nickel solid solution matrix; see Fig. 5. These 1/8 inch gage diameter, $\frac{1}{2}$ inch gage length creep specimens with their stress axes parallel to <100> were crept at 760°C in self-aligning creep machines at a stress of 105 ksi to different strain levels. The resulting creep curve and the strain levels to which the different specimens were crept are shown in Fig. 6a.

13

The two components of the positron lifetime spectrum τ_1 and τ_2, determined from the specimens after creep, are plotted as a function of the total creep strain in Figs. 6b and 6c.[15,19] The value of τ_2 is seen to increase with strain in the primary creep regime and remains reasonably constant in the steady state creep regime. This is very consistent with the TEM confirmed concept[17] that the dislocation substructure density increases during the primary creep state but remains at a steady-state value independent of the total strain in the steady state creep regime. Hence, it appears that τ_2 is a unique signature for dislocations in this particular system. On the other hand, the shorter lifetime component τ_1, which is expected to be a reflection of the vacancy concentration in the alloy, is seen to first increase with strain prior to falling off. This may be indicative of a decrease in nonequilibrium vacancy concentration due to annealing during creep.

(1.2) <u>Monotonic Uniaxial Deformation Induced Dislocation Substructure:</u>

Four different alloy systems were chosen to determine the sensitivity of positrons to dislocations introduced by uniaxial monotonic deformation. The first one was 99.99 pct. pure aluminum tensile strained in the as-rolled condition, the rolled and recovery annealed condition (250°C for one hour), and one standard specimen that was fully recrystallized by annealing at 400°C for one hour.[18,19] The second system chosen was zone refined high purity monocrystalline niobium subjected to different compressive strains.[18,19] The strategy in this phase of study was to use two alloy systems where the dislocation substructures at different extents of deformation are well-characterized through independent means.[20-23] Further, pure aluminum represents a system where substructure can recover dynamically during deformation[20-22] while niobium represents a system where there is no appreciable dynamic recovery of the deformation induced substructure[23] thus representing two extreme types of deformation-recovery behaviors. We also positron probed two more

14

engineering type systems--stress-relief annealed 2024-T3 and Ti-6A1-4V. In these systems only the mean lifetime $\bar{\tau}$ was measured. These latter studies were done to see how much information can be gleaned in deformed systems where τ_1 and τ_2 could not be separated due to resolution problems.

All tension tests were done at a strain rate of $8.3 \times 10^{-4} \text{sec}^{-1}$ at room temperature in an Instron TTC-3 Universal testing machine. The stress-plastic strain curves for the as-rolled as well as recovery annealed aluminum are more or less identical;an example is shown in Fig. 7a. The positron lifetimes in recovery annealed aluminum specimens strained to different levels again consist of two distinct lifetimes as shown in 7b and 7c. The intensity of τ_2 was also determined in this case and is plotted in Fig. 7c. Monotonic increases in the short lifetime, τ_1, and the long lifetime, τ_2, components are observed with increasing plastic strains up to about 3 pct., while at higher strains τ_1 and τ_2 are both observed to decline to lower levels prior to again increasing at strains of 10 pct. and higher. The relative intensity of the long lifetime component, I_2, is observed to vary in a manner opposite to the τ_2 variation with plastic strain, Fig. 7d. In contrast, the positron annihilation in the specimens strained in the as-rolled condition can be characterized by only one resolvable lifetime around 236 picoseconds independent of the plastic strain level imposed on the specimens. The base-line, fully re-crystallized specimen, also exhibits only one positron annihilation lifetime of 155 to 165 picoseconds, which is lower than that constant value exhibited by the cold-rolled aluminum.

We believe that the above set of positron annihilation data strikingly confirms the sensitivity of positron annihilation as an extended defect probe. The single short lifetime component in the recrystallized specimen is in good agreement with the τ_1 value found in well-annealed aluminum.[24] The trends in τ_1 and τ_2 with

plastic strain follow the known room temperature dynamic hardening and recovery characteristics of the pure aluminum used[20-22] and the Rockwell superficial hardness measurements made on the very same strained specimens, see Fig. 8. In fact, the consistency is to the extent that τ_1 and τ_2 drop abruptly at a strain level of around 3-5 pct., which is that strain range defining the onset of dynamic recovery. That τ_2 is dislocation density related is consistent with that it is not observed in the standard fully recrystallized aluminum specimen. Further, the observation that the intensity I_2 increases, when τ_2 itself is decreasing in magnitude, indicates that this long lifetime component is not a result of the positron-vacancy trapping interactions which are characterized by increasing intensity (increased trapping probability) with increasing magnitude of the trapped lifetime (or increased trapping defect density).[25]

Accordingly, it appears that positrons are sensitive to tensile deformation induced dislocation substructures. In the case of aluminum specimens strained in the as-rolled condition, which are expected to be saturated with trapping defects and dislocations, one cannot expect to see the minor changes in the substructure added on by further deformation, and indeed, we did not. However, there is little doubt that even here positrons could distinguish recrystallized versus rolled aluminum.

In the second phase of this part of the study, we used multiple zone refined single crystals of niobium where, as mentioned before, dynamic recovery effects are not expected to occur at room temperature. Single crystal rods used for this purpose had orientations about 5° away from the <111> axis.[15,19] Vacuum fusion analysis of the niobium rods indicated the presence of only 4-7 ppm oxygen, 7-10 ppm nitrogen and about 2ppm hydrogen. Compression specimens of 0.15 in diameter and 0.2 in height were cut from the original rods with a jeweler's saw and then their faces were ground parallel in stages using silicon carbide abrasive paper

16

to a 600 grit finish. The superficial damage of the specimens was rem___ prior
to compression testing by etching. Compression tests were done at a str___ rate of
$1.6 \times 10^{-4} \sec^{-1}$ in the Instron TTC-3 universal testing machine at ambient temperature.

The compressive stress-plastic strain curve and dislocation density
versus strain curve for the niobium single crystals are shown in Figs. 9a and 9b.
Positron lifetime spectra of the strained specimens indicate the presence of both
τ_1 and τ_2 components. τ_1 increased from 145 to 196 picoseconds with increasing
plastic strains up to 7%, Fig 9c. τ_2 was unresolvable in the unstressed specimen
but increased from 458 to 822 picoseconds as the plastic strain was increased,
Fig. 9d. The amplitude I_2 of the long lifetime component initially increased and
reached a maximum at around 1.5% plastic strain, whereafter it monotonically de-
creased with further increase in strain level, Fig. 9e.

Based on the discussion already presented for the crept superalloy
and the tensile tested aluminum, this data on niobium is almost self-explanatory.
It shows conclusively that the existence of τ_2 depends on plastic deformation and
the magnitude of τ_2 on the extent of deformation, or more exactly, the dislocation
substructure density. That τ_1 also increases with deformation is consistent with
increasing density of trapping sites such as deformation induced vacancies or edge
dislocation dipoles that do not anneal out at room temperature in the high melting
niobium. The observed variation of I_2, we believe, is a reflection of the relative
amounts of the trapping defects and dislocations generated at different strain levels.
One could surmise that, with increasing strains up to 1.5% plastic strain, the dis-
location density increases more rapidly than the concentration of deformation-in-
duced vacancies or dipoles, thus increasing the probability of positron annihilation
in the dislocation-positron interaction mode (reflected by the magnitude of I_2).
At higher strains, it is probable that the rate of increase of dislocation density
with plastic strain is overshadowed by the rate of deformation-induced vacancy or
dipole generation, thus leading to a decreasing probability of annihilation by the

τ_2 mode, and hence to a monotonically decreasing I_2.

The stress-plastic strain curve for the stress relieved aluminum 2024-T3 alloy is shown in Fig. 10a. The corresponding positron mean lifetime as a function of plastic strain is shown in Fig. 10b. Again, the trends in the two curves are very similar. It appears that the processes of dynamic hardening and recovery reflected in the pure aluminum data are not evidenced in Fig. 10b, but this is very reasonable since the alloying additions and the resultant precipitation strengthening in 2024-T3 are known to suppress these processes.

The data on the $\alpha-\beta$ titanium alloy Ti-6Al-4V, Figs. 11a and 11b, again indicate consistent trends in stress-plastic strain and average lifetime-plastic strain curves. Accordingly, it appears that the positron annihilation technique either through the long lifetime or average lifetime component can be a sensitive tool to probe for tensile deformation induced dislocation substructures of varying densities, in pure metals as well as engineering systems, provided the initial substructure is not so dense as to be saturated with trapping defects and dislocations.

(1.3) <u>Dislocation Substructure Introduced by a Commercial Rolling Process:</u>

In order to assess whether positrons are sensitive to plastic deformation imposed by more complicated conversion metallurgy processes, we positron probed commercially pure 1100 Aluminum subjected to strain hardening by cold rolling through different thickness reductions. The conditions of the specimens tested correspond to successively increasing levels of strain hardening (or plastic deformation) as described by the H12, H14, H16, H18 and H19 tempers of the Aluminum Association.[26] One standard specimen in the 'O' or the unstrainhardened, well annealed condition was also tested.

The plots of τ_1 and τ_2 as a function of equivalent plastic strain

18

(calculated from thickness reduction ratio during rolling) for the 1100 Aluminum specimens are shown in Figs. 12a and 12b. The trends are very similar to those observed in the case of tensile strained 99.99% pure aluminum, see Fig. 7b and 7c, except that the major recovery features seem to occur at higher plastic strains in the less pure, i.e., impurity strengthened, 1100 Aluminum. Accordingly, it is our opinion that positrons react in the same way to dislocation substructures, regardless of the deformation mode used to induce these dislocations.

(1.4) Cyclic (Fatigue) Strain Induced Dislocation Substructure:

Earlier work on the positron probing of cyclically deformed materials has been confined to pure metals[27] and encouraging results regarding the sensitivity of positron annihilation to the resultant substructural damage has been reported. In the present study, we have attempted to supplement these results by the positron probing of a cyclically deformed alloy of engineering importance. The system chosen was again the coherent precipitation strengthened monocrystalline Mar-M-200 (cube oriented). In addition to being a system of engineering importance, this alloy also happens to be different from the pure metals studied[27,28] in that it exhibits a very pronounced planar slip deformation mode in contrast to the well-defined saturation cell structure formed in the pure metals where ease of cross slip leads to a wavy slip deformation mode.

Cyclic loading of the Mar-M-200 monocrystals was performed in a closed loop hydraulic MTS fatigue testing machine at a frequency of 10 Hz and at three different strain amplitudes under total strain amplitude control.

The plot of number of cycles to failure versus strain amplitude for Mar-M-200 monocrystals is shown in Fig. 13a. It was found, for example (see Fig. 13b), for all the specimens tested that the stress response $\Delta\sigma_f$ for a given total applied strain range dropped with number of cycles and remained more or less constant

19

beginning at about half the total fatigue life. This softening behavior progressing

through the life of the specimen is curious. We have positron probed the specimen

whose stress response behavior is shown in Fig. 13b before its stress response has

dropped to about the plateau value (at about 50 cycles) and at specimen failure. This

basically corresponds to total strain controlled, fatigued specimen state at two $\Delta\sigma_f$

values. We have probed two more specimens at the final but different $\Delta\sigma_f$ values.

Plots of τ_1 and τ_2 as functions of $\Delta\sigma_f$ are shown in Figs. 13c and 13d. As can be

seen both τ_1 and τ_2 increase with $\Delta\sigma_f$. This provides us with the information that as

$\Delta\sigma_f$ increases, both dislocation density and point defect concentration increase.

Conversely, the softening behavior observed is no longer mysterious to us, but appears

to be due to the shakedown of initially tight dislocation substructure as cyclic

deformation proceeds. Similarly, vacancies or edge dislocation dipoles may also be

recovering. This particular work illustrates to our satisfaction that positron

annihilation technique is ready to be used to decipher mechanical behavior phenomena.

(1.5) Dislocation Substructure Densities in Materials Annealed After Deformation

Positron annihilation has been used to probe well annealed pure metals

through the analysis of positron mean lifetimes[29,30] or through the so-called S or H

parameter which reflect the shape of the angular distribution curve (plot of the y-ray

momenta as a function of the angle of their trajectory measured relative to the ini-

tial positron beam direction).[12] However, a systematic study in which materials of

known purity levels are annealed at different temperatures and subsequently positron

probed has not been done to date. The results of such a study should confirm the

applicability of positrons to the determination of recovered or recrystallized states,

as well as the influence, if any, of impurities on the resulting data. We chose

for this phase of the study aluminum of 99.99 pct purity and the 1100 Aluminum, which

is only 99 pct pure.

The 99.99 pct pure aluminum came in the as-rolled condition, it was

then stress-relief annealed at 120°C for one hour and then held at different temperatures up to 400°C for about twenty-four hours at each temperature during positron probing. Positron lifetime measurements were performed at temperatures through a hot-stage designed especially for this study. Lifetime measurements were made both during heating to and cooling from the 400°C ceiling temperature. The latter measurements, of course, reflect positron lifetimes in the metals after a 400°C, twenty-four hour anneal. The 1100 Aluminum came in the heavily strain hardened H18 condition and it was likewise subjected to positron probing during heat up and cool down up to a temperature of 400°C.

The positron lifetime spectra in either material could be best described by the single mean lifetime component, $\bar{\tau}$. The plot of $\bar{\tau}$ as a function of annealing temperature is shown in Figs. 14 and 15. The curve for the pure aluminum starts around 210 picoseconds, a value much higher than the value of about 165 picoseconds characteristic of well-annealed pure aluminum.[29,30] This higher value indicates that there is still a substantial amount of dislocation substructure present in the material after the stress relief annealing at 120°C, which is to be expected. The major change in $\bar{\tau}$ with annealing occurs between 160°C and 280°C where a sharp drop in its value from 210 to 190 picoseconds is observed. This temperature range corresponds well to previously reported recovery and recrystalliza- tion range observed in cold worked aluminum of comparable purity[31] which had been subjected to similar annealing. The subsequent increase in the $\bar{\tau}$ value after 280°C could be due to recrystallization which should create more grain boundary area per unit volume and also due to the trapping contribution of the thermal equilibrium vacancies generated in appreciable numbers at these higher temperatures. The trends in the data are similar to those reported earlier in pure metals.[29,30] The curves of $\bar{\tau}$ as a function of temperature during the cool down and the reheating, see Fig. 14,

21

are direct indications only of grain boundary area per unit volume and the thermal vacancy concentrations at the appropriate temperatures, since the material, by then, is in the fully recrystallized condition and dislocation contents in such material would be low, and hence, not expected to contribute appreciably to positron lifetimes. Again, note that the room temperature lifetimes in these two curves is about 165 picoseconds, in good agreement with earlier data on very well annealed aluminum.[24,29] The dip in the $\bar{\tau}$ temperature plot for the reheated specimen at around 240°C, we believe, is a result of grain growth occurring in the recrystallized material. This would lead to a decreased grain boundary area per unit volume and hence a lowering of $\bar{\tau}$.

The $\bar{\tau}$-temperature curves for the 1100-H18 Aluminum, Fig. 15, differ markedly from those of pure aluminum discussed above. The mean lifetime $\bar{\tau}$ in the initial state is about 240 picoseconds, which is only slightly higher than that for pure aluminum. The difference begins during heat-up in that the decrease in $\bar{\tau}$ does not commence until about 260°C--instead of the lower 160°C for the pure aluminum case. This can be rationalized by noting that impurities in this commercial material are expected to slow down dislocation rearrangement processes involved in the recovery and recrystallization stages, thus necessitating higher annealing temperatures and thermal energy before these processes can commence. As such, it appears that the positron annihilation data now tell us that the recovery processes do not begin until 260°C for the 1100 Aluminum initially in the H18 state. Unfortunately, due to experimental heating difficulties, at-temperature $\bar{\tau}$ measurements could not be made beyond 400°C, and thus we cannot be certain whether or not the upward rising parts of the $\bar{\tau}$-temperature curves (similar to those in Fig. 14) are present for this material. The lifetime values measured on the cool down cycle are indicative of thermal vacancy concentration in the material and this curve is similar in appearance to that for the pure aluminum in this temperature range. The

22

$\bar{\tau}$ value measured at room temperature after the annealing cycle is about 198 picoseconds, higher than the 165 picoseconds value measured for pure aluminum. This could be due to the fact that recovery and recrystallization are not fully completed in the 1100 Aluminum, which is consistent with the higher recrystallization temperature observed. In addition, the presence of a larger quantity of impurities produced defects which cannot be removed by annealing.

(2)   Positrons and Microstructural Features

This set of experiments was designed to determine the sensitivity of positrons to such microstructural features as grain boundaries with and without precipitates on them and second phase precipitates of differing degrees of coherency. Again, since some work has already been done on the positron probing of similar microstructural features in simple systems,[32,33] we have chosen systems of engineering importance so as to complement the already existing information.

(2.1)   Grain Size in a Nickel-Base Superalloy:

A wrought nickel-base superalloy of the Nimonic-115 type (Nominal composition in wt. pct. 0.15C, 15 Cr, 3.5 Mo, 4 Ti, 5 Al, Bal. Ni.), whose microstructure consists of the nickel-rich fcc solid solution γ phase, the ordered γ' precipitate phase (about 30-40 volume pct) and a small volume fraction of alloy carbide phases, was chosen for study to ascertain whether positrons can detect changes in the grain boundary area per unit volume in constitutionally complex engineering alloys. Previously, it has been determined that in simple metals[32,33] τ_1 increases with decreasing grain size or equivalently increasing grain boundary area per unit volume.

The superalloy was initially in the as hot rolled condition and had an average grain size of 20 μm. Larger sizes were obtained by holding the as-rolled specimen at temperatures ranging between 1190°C and 1220°C for two hours. The grain sizes so obtained ranged from 60 μm to 145 μm, most of them tending to be near the

23

upper value. After the grain growth anneals, these specimens were cooled rapidly by a jet of cold air to room temperature in order to suppress carbide precipitation at the grain boundary; see Fig. 16a. One specimen of 60μm grain size, however, was intentionally subjected to 100 hours aging at $982^{\circ}C$ subsequent to the grain growth treatment to cause precipitation of $Cr_{23}C_6$ carbides at the grain boundaries; see Fig. 16b. This specimen was used to elucidate possible effects of the presence of an intergranular carbide "wall" on the sensitivity of positrons to grain boundaries.

The plot of the positron mean lifetime $\bar{\tau}$ as a function of d^{-1} which, but for a proportionality constant, is the same as the grain boundary area per unit volume at a grain size d, is shown in Fig. 17. $\bar{\tau}$ is expected to increase with increasing d^{-1} and this is observed only at fine grain sizes, while at the coarser end of grain sizes (or smaller d^{-1} values), the $\bar{\tau}$ value seems to increase with decreasing d^{-1}. We believe that this trend at small d^{-1} values (coarse grain sizes) is a result of the presence of nonequilibrium vacancies quenched into these coarse grained specimens as a consequence of these particular specimens having been subjected to the higher temperature grain growth heat treatments.

Finally, $\bar{\tau}$ values for the 60 μm grain size material heat treated to precipitate carbides at the grain boundaries was found to be 160 ± 3 picoseconds which is very close to the 168 ± 3 picoseconds observed for the corresponding material without grain boundary carbides. Thus, it appears that the positron annihilation technique can distinguish between different grain sizes at fine grain sizes and this does not seem to be affected by the constitutional complexity of the alloy or by the presence of precipitates at the grain boundaries.

(2.2) Different Precipitate States in Commercial Aluminum Alloys:

In the present study, we chose commercial aluminum alloys heat treated to contain second phase precipitates in different states of precipitation. The alloys chosen include the 2024 aluminum alloy hardened mainly by the Cu rich

24

G.P. zones and precipitates: the 7075 alloy hardened by Zn and Cu rich G. P. zones, and the strong and corrosion resistant 7050 alloy, which is a modified version of the 7075 alloy. The nominal compositions of these alloys and the heat treatments they were subjected to prior to positron probing are given in Tables 2 and 3, respectively. Table 3 also shows the positron mean lifetime $\bar{\tau}$ of the materials after the heat treatments. In addition to these standard "tempers", these alloys were also subjected to at-temperature positron mean life measurements at temperatures up to $400^{\circ}C$ which essentially provided additional isothermal aging at the measurement temperatures. These aging treatments would modify the nature of the precipitate phase (G.P. zones to metastable to stable precipitates), its degree of coherency (coherent to incoherent) and the precipitate particle size, and hence, the effective precipitate-matrix interface area per unit volume. The sensitivity of the positrons to these changes in the precipitate states was thus evaluated through these experiments.

From Table 3, it is clear that the mean lifetime in all the three alloys is lower in the fully annealed 'O' temper as compared to the naturally aged (2024-T4), artificially peak aged (7075-T6) or in the stabilization aged (7050-T76) conditions.

In 2024-T4 and 7075-T6, the major microstructural features are G.P. Zones which represent localized variations in electron density due to their higher solute content, Cu and Mg in 2024-T4 and Cu, Mg and Zn in 7075-T6.[34] These regions should strongly interact with the positrons, probably through the scattering mechanism similar to dislocations. 7050-T76 is aged slightly beyond the peak strength condition, but it still contains G.P. Zones.[35] Hence, the difference in $\bar{\tau}$ values between -T76 and -O tempers of this alloy also seem to result from the same reason as described above. It seems then that positrons are sensitive enough

25

to distinguish between G.P. Zone type regions and coarsened incoherent precipitates.

The at-temperature $\bar{\tau}$ values of 2024-T4, 7075-T6 and 7075-T76 are shown in Figs. 18 through 20 respectively. 2024-T4 starts with a dispersion of G.P. Zones in it. Earlier physical metallurgical studies on aging of 2024-T4 show that below 200°C the G.P. Zones are fairly stable against overaging for 24 hour aging treatments. But beyond this point, G.P. Zones tend to transform to semicoherent S'(Al_2CuMg) phase, incoherent S(Al_2CuMg) phase and coarsened S phase in that order, with increasing aging temperatures. The overaging is very rapid (within a few hours) at temperatures above 250°C.

This behavior is indeed reflected in the $\bar{\tau}$ versus annealing temperature curves we obtain. The $\bar{\tau}$ value varies slowly from 210 to 200 picoseconds in the temperature range up to 200°C, see Fig. 18, and this is probably associated with the coarsening of the G.P. Zones formed during the natural aging process which would reduce the G.P. Zone-solid solution interface area per unit volume and thus lead to a lowering of $\bar{\tau}$. Beyond 200°C, the $\bar{\tau}$ value rapidly increases and reaches a value around 225 picoseconds (a change of 25 picoseconds) where it levels off in the 250°C-350°C range. This increase could be a reflection of the stages of rapid semicoherent S' precipitate formation which then loses coherency during growth by punching out dislocation loops.[36] This would essentially add a number of dislocation loops that can interact with the positron and extend its lifetime. Also, one is tempted to propose that the formation of the incoherent interfaces between the S phase and the solid solution

26

matrix during this stage could add new interphase boundaries that can also interact with positrons and increase their mean lifetime. However, this, we believe is less likely, particularly considering the fact that 2024-O consisting of incoherent precipitates shows a smaller $\bar{\tau}$ value as compared to 2024-T4 with the G.P. Zones, indicating thereby that the incoherent interfaces are less capable of extending positron mean lifetime than the G.P. Zones. The increase of $\bar{\tau}$ beyond 350°C, we believe, reflects the increase in the thermal vacancy concentration in the alloy as no further microstructural changes are expected to occur until the solvus temperature of the alloy (about 480°C) is reached. The cool down part of the annealing curve is essentially a reflection of the decrease in the thermal vacancy concentration in the alloy with decreasing temperature.

To our knowledge, there is no aging data on the 7075-T6 material. However, it is known that the peak aging temperature for this alloy (see the -T6 treatment in Table 3) is lower than that for 2024-T4 and is only about 120°C, with overaging occurring at temperatures only slightly higher than 120°C.[34] This is indeed reflected by the $\bar{\tau}$ versus annealing temperature curve for 7075-T6; see Fig. 17. The $\bar{\tau}$ value changes very slightly up to 150°C (242 ± 3 to 248 ±3) after which it rapidly increases to a value close to 270 picoseconds around 300°C. This again, we believe, is the result of the punching out of dislocation loops during the coherency loss process. These dislocation loops would, of course, anneal out during the subsequent annealing at higher temperatures. In this alloy we do not see the rising branch of the curve indicative of the thermal vacancy concentration in the material; compare Figs. 18 and 19. This is probably due to formation of vacancy-solute complexes which can reduce the number of free vacancies that can trap the positrons. There is some indication that chromium, which is present in this alloy, (and not in 2024) is capable of forming such

27

complexes at least when the solution heated alloy is quenched to room temperature.[34]

The plot of at-temperature $\bar{\tau}$ values for 7050-T76 annealed at different temperatures, shown in Fig. 20, is qualitatively similar to the curve for 7050-T6. The aging kinetics in 7050-T76 have been studied[35] and it appears that this alloy by virtue of its higher copper content is more stable with respect to aging than 7075 and can retain higher strength level even in the -T76 temper which involves aging slightly beyond the peak aging condition. This is again reflected in Fig. 20. The major changes start only beyond $150^{\circ}C$ which is close to the aging temperature for the second step in the -T76 treatment; see Table 3. Again, the change is one of increase in $\bar{\tau}$ values from about 210 picoseconds to 248 picoseconds over the temperature range $150^{\circ}C$ to $300^{\circ}C$, which probably corresponds to the coherency loss process as described earlier. Again, the thermal vacancy branch is not clearly seen in this case. Note also that the annealing out of punched out dislocation loops probably occurs on subsequent annealing during the cool down cycle between $400^{\circ}C$ and $250^{\circ}C$ as indicated by the sharp drop in $\bar{\tau}$ in the lower curve of Fig. 20, after which the lifetime is fairly constant.

In summary, therefore, we can say that positron mean lifetime measurement can be quite sensitive to the differences between the various precipitated states in commercial aluminum alloys where sequential precipitation is observed. Our findings also agree well with the results of other workers such as the specially prepared ternary aluminum alloys,[37] order-disorder changes in β-brass[38] and mantensite-austenite transformations in iron-nickel binary alloys.[39]

28

(3) Positrons and Macroscopic Surface Features

In this category we investigate the ability of positrons
to probe macroscopic surface features, a level of coarseness above that of
microstructural variations discussed in Section IV-2. The systems chosen
include aluminum-base alloys with different degrees of polishing finish and
subjected to different surface cleaning procedures. Also studied were
aluminum alloys in the anodized condition leading to a porous oxide layer on
the surface; two titanium alloys; and experimental iron-chromium-aluminum-
oxidation resistant coating alloys with and without yttrium additions that were
subjected to different oxidation treatments. Again, the aim was to use positrons
to distinguish between the various practical surface features on alloys of en-
gineering importance.

(3.1) Aluminum Alloys with Various Surface Treatments:

Table 4 shows the various aluminum alloys and the surface treatments
they were subjected to and the corresponding values of the positron mean lives.
The mechanical polishing reflects a 600 grit surface finishing, while ultrasonic
cleaning was done by immersing the specimens in acetone and applying ultrasonic
vibrations using a Biosonik III (Bronwill Scientific) at a relative intensity
setting of 30 for about 30 minutes. Chemical brightening was done using a 93.5%
phosphoric-6.5% nitric acid bath between 93° and 104^OC for about 180 to 240 seconds.[40]
Anodizing was done in four stages including electrobrightening in a sodium carbonate-
trisodium phosphate bath, smut removal in dilute sulfuric acid, anodizing in dilute
sulfuric acid and sealing in boiling distilled water.[40] The surfaces of the spe-
cimens after these four stages are bright with a slight grey hue.

The results distinctly show that anodizing, which involves the formation
of a porous and probably non-perfect oxide layer, increases the position mean life-

time over the relatively clean chemically brightened acetone rinsed or ultra-sonically cleaned surface finishes. This is understandable since the defects in an anodized oxide layer, which can include anion or cation vacancies, dis-locations and grain boundaries, can interact with positrons by trapping as well as scattering interactions leading to extended positron lifetimes. Mechanical polishing introduces surface deformation and can be expected to increase near-surface dislocation density. This is again consistent with the higher mean life-time observed in the mechanically polished specimens; see Table 4.

(3.2)   Surface Oxide Scales Formed After Elevated Temperature Oxidation:

In this set of studies, the effect of an oxide scale formed on alloy substrates by elevated temperature oxidation on the positron mean lifetime was investigated. The systems chosen include the single phase commercially pure titanium Ti-35A, the $\alpha-\beta$ alloy Ti-6Al-4V and experimental oxidation resistant iron base alloys (Fe-25 Cr-4Al) with and without 0.2% yttrium addition. The titanium alloys were oxidized at different temperatures from 400°C to 1200°C for 24 hours and quenched in water prior to lifetime measurements. In specimens oxidized at temperatures less than 400°C the lifetime measurements were made at temperature as described in Section IV - 1.5. Fe-Cr-Al and Fe-Cr-Al-Y alloys were oxidized for different lengths of time up to 25 hours at 1200°C and then subse-quently positron probed at room temperature.

The mean lifetimes as a function of oxidation temperature for the two titanium alloys are shown in Figs. 21 and 22. The initial drop in the life-time in the 200°C to 400°C range is probably a result of recovery of the dislocation substructures introduced in the material during the processing history. The interesting change in the lifetime curves occurs at around 800°C where there is a discontinuous decrease in the $\bar{\tau}$ value. This jump is not associated with the $\alpha-\beta$ transition since it is not expected to occur in these alloys till about 900°C.

30

Besides, since one would expect that the α-β transition temperature in the two alloys to be different, the lifetime change if it were related to the α-β transition should have occurred at different temperatures. In fact, the change occurs at about the same temperature in both the alloys. We feel that this jump in $\bar{\tau}$ values is related to changes in the oxide scale on these alloys.

It has been shown that around $800^{\circ}C$ the oxide scale on titanium alloy changes from Ti_2O_3 to a more complex and defected oxide which allows increased oxygen diffusion into the alloy substrate.[41] This added amount of interstitial oxygen can tie up vacancies by forming complexes, thus reducing the number of free vacancies available to trap the positrons. This could lead to the observed jump in $\bar{\tau}$ to lower values.

The positron lifetimes in Fe-Cr-Al and Fe-Cr-Al-Y are shown in Table 5. It is seen that the $\bar{\tau}$ value in Fe-Cr-Al decreases from 202 picoseconds in the unoxidized specimen to 186 picoseconds in the specimen oxidized for two hours and thereafter remains nearly constant. The observed decrease in the $\bar{\tau}$ value, we believe, is an indication of the recovery of the dislocation substructure or annealing out of vacancies in the substrate material at the high temperatures used in the oxidation treatment. The formation of oxide per se does not seem to really change the $\bar{\tau}$ appreciably, particularly since the $\bar{\tau}$ is nearly constant for oxidation times up to 25 hours. In the case of Fe-Cr-Al-Y, the $\bar{\tau}$ values are smaller than the corresponding values in Fe-Cr-Al. This, we believe, is due to the fact that vacancies are likely to be captured by the large sized yttrium atoms, thus reducing the number of trapping sites for positrons. There have been suggestions of other indirect proofs for such yttrium-vacancy interactions in these alloys.[42] There seems to be no appreciable change in the $\bar{\tau}$ itself for this alloy with oxidation time; see Table 5. This again seems to support our suspicion that the $\bar{\tau}$ values in Fe-Cr-Al as well as the Fe-Cr-Al-Y are indications of changes,

if any, in the substrate material due to elevated temperature exposure rather than being related to the oxide scale formed during the exposure.

It appears then that the sensitivity of positrons to high temperature oxide scales can be system dependent and in general the mean lifetimes seem to be more sensitive to changes in the defect density in the substrate occurring during the high temperature oxidation exposure or occurring as a result of the formation of the oxide layer.

(4) Positrons and Fracture-Related Macroscopic Defects in Engineering Alloys

In this section, we describe the results of our evaluation of positron annihilation as a probable tool to probe for macroscopic defects related to fracture processes in engineering alloys. As such, it reports on our results during 1976. This essentially represents the coarsest scale of the materials probed by positrons in the present study. The specimens tested include wrought nickel-base superalloy specimens with intentionally introduced large (up to about 0.2 mm in diameter) grain boundary void type defects, specimens of wrought nickel-base superalloys subjected to elevated temperature stress rupture tests and fracture mechanic specimens of an α-β titanium alloy subjected to fatigue crack propagation tests. Since probing for such large defects is of interest only in engineering structural alloys, the above choice of alloy systems has been made with that interest in mind.

(4.1) Large Processing Induced Voids in a Superalloy:

Specimens of a nickel-base superalloy intentionally chosen so as to have a large density of intergranular voids, see Fig. 23a, were used for this purpose. The specimens selected were those which failed catastrophically on loading at the start of intended creep tests which are expected to run for 100 hours or more in specimens of good microstructural integrity; see Fig. 23b.

32

Due to the admittedly crude specimen selection procedure, the variation in the void contents between different specimens was very small and the corresponding τ_1 and τ_2 values are very close (160 to 163 $\pm$ 1 picoseconds and 254 to 263 $\pm$ 8 picoseconds.) However, the τ_1 and τ_2 values from the specimens free of voids were 167 $\pm$ 1 and 256 $\pm$ 8 picoseconds, respectively, and these do not differ appreciably from those in the specimens with a lot of voids. Thus, it appears that positron probing may not be a sensitive technique for detecting the presence of large voids (50 μm in diameter at least) although it has been found to be sensitive to the very fine "swelling" voids ($\leq 10^{-8}$m) formed by neutron or electron irradiation.[43-48]

(4.2) Nickel-base Superalloys Failed by Stress Rupture:

In Section IV - 1.1, we described the results of positron probing nickel-base superalloy monocrystals subjected to different creep strains. In this section, we present the results of positron probing two polycrystalline wrought nickel-base superalloys fractured under creep loading conditions (stress rupture). The alloys chosen were Nimonic-115 of about 60 μm grain size with and without grain boundary carbides (described in Section IV - 2.1) stress ruptured at 760°C and 569 MN/m^2 and Udimet-700 (Composition in wt. pct. 0.08 C, 15.1 Cr, 17.5 Co, 0.14 Fe, 4.9 Mo, 3.25 Ti, 4.15 Al, 0.029 B, Bal. Ni.) of 250 μm grain size tested at 760°C and 982°C at different stress levels. The test conditions, number of hours to failure and the corresponding τ_1, τ_2 and I_2 values are shown in Tables 6 and 7.

As seen from Table 6, the values of τ_1 and τ_2 for Udimet-700 increase with increasing test stress at both 760°C and 982°C. The reasons for this behavior could be twofold. First, at higher stresses the creep deformation induced damage in the form of vacancies and dislocation substructures would be larger than at lower

33

stresses. Second, during the low stress and long time tests, some of the defects (at least the vacancies) produced by the deformation could anneal out during the stress rupture test itself.

The longer gage length and larger gage diameter Nimonic-115 specimens (31 mm and 6.3 mm as against 12.7 mm and 3.2 mm, respectively, for the Udimet-700 and Mar-M-200 specimens) used allowed the measurement of life-times near the ruptured end of the specimen and in a region still in the gage length but far away from the ruptured end. The results are shown in Table 7. It seems that in the specimens both with and without carbides, the τ_1 and τ_2 values are smaller near the rupture end than in the region away from rupture. A probable rationalization for this could be as follows. In the region near rupture, numerous cracks initiate and grow during the tertiary creep stage, while in the region away from the rupture end the density of cracks is much lower and the material is still undergoing creep deformation. Thus, creep damage in terms of the dislocation substructure and point defect concentration would continue to build up in the region away from rupture while it will be replaced by crack initiation and growth processes near the rupture end. The positrons would then have longer lifetimes in the substructurally more damaged region away from the rupture. The cracks in the near rupture region, being large defects similar to voids described in Section IV - 4.1, are not expected to interact with positrons strongly and hence are not expected to affect their life-times. Table 7 also shows that τ_1 and τ_2 values tend to be lower in the deformed specimens without carbides than those in specimens with carbides. At this time the reasons for this difference are not very clear.

It appears, again, that positrons do not directly sense macroscopic defects such as voids or cracks formed during creep and stress rupture but do

34

sense the presence and degree of substructural level differences in the alloy
that accompanies the formation of such defects.

(4.3) Surface Plastic Zones Ahead of a Fatigue Crack in a Titanium-base Alloy:

The last fracture-related feature studied in this phase of the
work was the plastic zone damage ahead of a fatigue crack in a fracture
mechanically designed and crack propagation tested specimen of the α-β titanium
alloy Ti-6Al-4V. Plastic zone size measurements, along with metallographic
and fractographic characterization, are of importance in the failure analysis
of structural members where one wants to determine the load history the members
were subjected to in service prior to their failure. In addition, the knowledge
of the plastic zone size and a related quantity, crack opening displacement, is
important to the application of the models of ductile fatigue crack growth,[49,50]
or the models of environment affected fatigue crack growth.[51] Accordingly, it
is interesting to see whether positron probing can be used to measure plastic
zone sizes ahead of fatigue cracks in engineering alloys.

The specimen used in the study was machined from the α-β titanium
alloy Ti-6Al-4V hot rolled to a 3/4" thick plate. The specimen geometry and its
orientation with respect to its parent plate are shown in Fig. 24. The specimen
was tested such that the loading direction (indicated by arrows in Fig. 24) was
parallel to the rolling direction with the crack propagating in the long transverse
(parallel to the width of the parent plate) direction. This loading geometry was
used because it closely represents the kind of loading one would expect such alloys
with highly textured microstructures to be subjected to in service (see Figs. 25a
and b for typical textured appearance of the microstructure of the alloy used).

The nominal 0.2% off-set monotonic yield strength of the alloy was 122 ksi in the rolling direction, and about 135 ksi in the transverse direction.

A fatigue crack was initiated at the notch root and was propagated at room temperature by continued fatigue cycling between applied load limits of 168 lbs and 2100 lbs at a frequency of 6 Hz. These loading conditions, when translated to the fracture mechanical parameter stress intensity range, ΔK, for the specimen geometry on hand,[52] correspond to ΔK values of 11.1 ksi$\sqrt{in}$ to 38.8 ksi$\sqrt{in}$ as the crack grew from its initial length of about 1.13 inch (3cms) to a final length of 2.33 inch (5.93 cms). Correspondingly, the maximum stress intensity at the tip of the crack, K_{max}, varied from 12.1 ksi$\sqrt{in}$ to 43.3 ksi$\sqrt{in}$ over the same crack length range.

Positron probing was done using small rectangular sources which were 1 mm x 2 mm in size. Three different ways of placing the positron source relative to the crack have been used in the present study and these are schematically shown in the insets in Figs. 26a through c.

First, the source was placed with its short axis coincident with the crack tip, see inset in Fig. 26a, and then it was moved in 0.5 mm increments along the crack or on the imaginary line that forms the extension of, and runs in front of, the crack. These are marked -x and +x directions, respectively. The measured positron mean lifetime $\bar{\tau}$ as a function of distance x from the crack tip in either direction is plotted in Fig. 26a. Interestingly, the positron annihilation lifetime increases monotonically from about 190 picoseconds at the crack tip to about 245 picoseconds at about 25 mm behind the crack tip. In contrast $\bar{\tau}$ decreases to a minimum value of about 175 picoseconds at about 1 mm ahead of the crack tip whereafter it again increases monotonically to about 182 picoseconds.

36

In the second set of positron probing experiments, the source was placed with its long axis parallel to the crack and the short axis along an imaginary line running perpendicular to the crack direction and at a distance of 1 mm behind the crack tip, i.e., x = -1 mm, see inset in Fig. 26b. The source was then moved along this line at 0.5 mm increments. The resultant $\bar{\tau}$ as a function of the distance along this imaginary line denoted by +y or -y is shown in Fig. 26b. As seen, the $\bar{\tau}$ value is a maximum when the source is in line with the crack and decreases as we move away in either direction.

In the third set of experiments, the orientation of the positron source is the same as that in the second set but the source was placed with its short axis along an imaginary line running perpendicular to the crack direction at a distance of 1 mm ahead of the crack tip, (i.e., at x = +1 mm), see inset in Fig. 26c. The source was then moved along this imaginary line in 0.5 mm steps. The $\bar{\tau}$ values so measured as a function of distance y are shown in Fig. 26c. This spatial variation of $\bar{\tau}$ is again similar to that in Fig. 26b in that $\bar{\tau}$ is a maximum directly in line with the crack and decreases as the source is moved in either direction.

These sets of data, again, confirm to our satisfaction that positrons are extremely sensitive to the plastic deformation in materials, in this particular case in a plastic zone ahead of a fatigue crack tip. The decrease in the $\bar{\tau}$ value in Fig. 26a, when one initially moves away from the crack tip in the +x direction, seems to indicate that the extent of plastic deformation and the attendant dislocation substructure density are decreasing up to a distance of about x = +1.0 mm. This is very reasonable since the crack tip represents the point of high stress concentration and hence a high substructure density both of which would gradually decrease as one moves away from the crack tip into the plastic zone reaching a minimum at the end of the plastic zone. In fact, if one estimates

37

the maximum plastic zone size ahead of the crack studied using the final K_{max} value of 43.3 ksi$\sqrt{in}$ and the yield strength in the x-direction (which is the transverse direction for the parent plate) of 135 ksi, one arrives at a value of 0.05 inch or about 1.30 mm which is in fair agreement with the position of the minimum in the $\bar{\tau}$ - x curve, Fig. 26a. The small increase in $\bar{\tau}$ for x > 1 mm, we believe, is a result of the gradual increase in hardness from the cyclically deformed material in the plastic zone to the residual hardness of the as-machined material far away from the plastic zone. (Microhardness on the as-machined specimen surface was found to be about 340 VHN and on successive chemical removal of metal layers, the microhardness dropped to about 310 VHN and levelled off at this value for distances greater than 150 μm from the machined surface.) This residual hardness will be modified in the plastic zone region due to the shake-down of the dislocation substructure during the cyclic plastic deformation. The increase in the $\bar{\tau}$ value for x < 0, or behind the crack tip is again interesting. This is probably a result of the rubbing together of the crack faces during the cyclic loading due to crack closure considerations[51] and the resultant monotonic hardening and increased substructure density in this region.

The $\bar{\tau}$ versus y curves at x = 1 mm and x = -1 mm, Figs. 26b and c, are similar in appearance and they can be again considered in the light of the extent of the plastic zone, now in the y direction. As before, when we move away from the crack tip in the y direction, the levels of plastic strain the material is subjected to and the resultant substructural density are expected to drop off. This is indeed consistent with the decrease in $\bar{\tau}$ as one goes away from the crack tip. Again, one could estimate the size of the plastic zone in this direction from fracture mechanics, using the final K_{max} value of 43.3 ksi$\sqrt{in}$ and the yield strength of 122 ksi in the y direction (parallel to the rolling direction of the parent plate) and one arrives at

a calculated plastic zone size of 0.063 inch or about 1.6 mms. The total extent of the plastic zone as determined from the width of the $\bar{\tau}$-y peak in Figs. 26b and c is about 6 mm, nearly four times as large as the predicted plastic zone size. This difference is not surprising since the fracture mechanics estimates of plastic zone sizes used in the above comparisons are based on the idealized assumption that the material deforms isotropically leading to a nearly circular shaped plastic zone. On the other hand, more rigorous analyses considering factors such as the state of stress at the crack tip, anisotropy or texture in the material, discrete slip character of the material, etc., lead to more complex shapes for the plastic zone.[53,54] The shape of the plastic zone as indicated by positron probing is such that it is elongated in the softer rolling direction (or loading direction). Such a qualitative shape compares favorably with the shapes of plastic zones calculated for materials such as the alloy presently studied, wherein texture and crystallographic constraints on yielding do lead to more asymmetric plastic zone shapes.[53,54]

A more detailed study using positron sources of 1 mm x 1 mm size is being carried out and will be reported elsewhere.[55]

V. POSITRON ANNIHILATION AND NONDESTRUCTIVE EVALUATION

The sets of data described in the last section form a fairly com-
prehensive experimental data bank on the mechanics of positron interactions in
materials at various scales of the structure and can as such, be of great value
in helping the shaping of the currently available theoretical models of positron
annihilation in metals. A more immediate and perhaps a more rewarding benefit
that one can derive from such an extensive experimental program is the possibility
of being able to indicate whether the new technique studied can be put to practical
use, in this case as a nondestructive evaluation (NDE) tool, and if so, under what
conditions.

For any technique to be viable as a practical NDE tool, it should
meet the following major requirements. First, it should be sensitive to the vari-
ous structural defects or damage states of the materials being examined. Second,
it should be selective in being able to distinctly detect each state or defect of
the material without much of an interference from the other states or defects.
Third, it must be easy to use and does not require specific environment conditions,
such as vacuum. The last, but by no means less important, requirement, is that the
experimental technique involved be reasonably fast and economical for probing the
defects and structural states of interest.

Our experiments indicate that positrons can sensitively detect the
dislocation substructure content of simple as well as microstructurally complex
alloys, in conditions varying from fully annealed to heavily deformed states. In
addition, this sensitivity to dislocation content in deformed materials does not seem
to be affected by the mode of deformation used to introduce the dislocation substruc-
ture, be it high temperature creep, monotonic tension or compression, commercial

40

rolling or cyclic deformation. Thus, we do believe that positron annihilation definitely meets the first two requirements for being a viable NDE tool to probe for dislocation content in certain materials ranging from pure metals, to high strength multiphase engineering alloys. However, one important note of caution must be added to this optimistic conclusion. In all the alloy systems examined, the power of positrons as sensitive probes for dislocations was unveiled conclusively only because fairly detailed knowledge of the physical metallurgical aspects of the nature of the dislocation substructures in these alloy systems and the changes thereof were known. For example, the data on τ_2 being constant irrespective of strain level in Mar-M-200 monocrystals crept in the steady state region would be baffling unless one had the prior knowledge from TEM or other means that the dislocation substructure content in steady state creep regime is indeed expected to be fairly constant. Similarly, the interesting variations in the τ_2 values in recovery annealed pure aluminum strained to different levels would be totally inexplicable unless one knew that dynamic recovery of dislocation substructure content occurs in this system depending on the level of plastic strain. Thus, we have to emphasize the fact that the successful use of positron annihilation to probe for dislocation content in an alloy system rests, in a fair measure, with the availability of a general knowledge of the physical metallurgical aspects of any possible changes in the nature of the dislocation substructure in that system.

We find that positrons, through the mean lifetime $\bar{\tau}$, are reasonably sensitive to the microstructural features in engineering alloys. For example, they are able to detect grain size variations in a multiphase nickel-base superalloy with and without grain boundary carbides, at least in the fine grain size ranges. Here again, the importance of the knowledge of the thermal history the alloy was subjected to and the formation of substructural features that may occur during such

41

a thermal history which can strongly interact with the positrons is clearly seen. The lack of sensitivity of positrons to grain size changes in the larger grain size range due to the presence of an appreciable number of quenched in vacancies which are known to interact strongly with positrons is a very good example of this situation. As far as precipitate states in engineering alloys (G.P. Zones, coherent or incoherent precipitates in aluminum-based alloys) are concerned, again positrons seem to be reasonably sensitive probes. Here again, the importance of the detailed knowledge of the features of the precipitate states and the changes that occur on the various thermal treatments not only in the precipitate state but also in the content of other substructural features, (such as thermal vacancies and punched out dislocation loops in the alloys studied), is clearly borne out.

Positrons seem to be only sensitive to those macroscopic surface features in alloys whose formation in some way affects the content of substructural features such as dislocations or vacancies in the alloy. For example, there is no appreciable difference in $\bar{\tau}$ values of acetone rinsed and ultrasonically acetone cleansed aluminum-based alloys. However, mechanical polished or anodized surface finishes in these alloys yield distinguishably different values of $\bar{\tau}$, only because these latter treatments introduce substructural features such as near surface dislocations or anodized oxide defects which interact markedly with positrons. Similar conclusions also result in the titanium alloy and Fe-Cr-Al and Fe-Cr-Al-Y oxidized at elevated temperatures. In a way, this insensitivity of positrons to many of these macroscopic surface features in alloys is a blessing in disguise, since such features as a surface oxide layer are invariably present in structural alloys used in service at elevated temperatures and it is gratifying that the presence of these features does not measurably alter the positron-material interaction characteristics. This would allow us to use positrons to probe and follow substructural changes in alloys at elevated temperatures, which might change the $\bar{\tau}$ values only by a small

42

amount (see, for example, the annealing and aging data on aluminum and aluminum base alloys) without having to worry about complications due to a surface oxide layer. Then again, the data where the macroscopic surface features do cause measurable changes in the positron annihilation characteristics, as in the mechanical polishing finish, provide useful pointers as to what one should try to preclude when one is interested in probing for the substructural and microstructural features.

The sensitivity of positrons to fracture-related macroscopic defects seems to be again dependent on how the formation of these defects affects, if at all, the substructural defect (dislocations or vacancies) content of the alloy probed. Thus, for example, positrons are not sensitive to large grain boundary voids present in the microstructure of a wrought superalloy, while grain boundary cracks formed in the stress rupture tested superalloys, which would indeed affect the alloy's dislocation content, seem to be picked up by positron annihilation. Again, positrons are sensitive to the macroscopically large plastic zones at the tip of fatigue cracks in a titanium-base alloy only because of the markedly higher dislocation content expected in that region as compared to the undeformed regions. The sensitivity to plastic zones is good to the extent that even indications of the anisotropy in their shape depending on the yield characteristics of the alloy studied are reflected in the positron lifetime data. The plastic zone sizes in the strong titanium alloy studied which is of practical interest were small, since plastic zone size varies inversely as the square of the yield strength of the alloy. Hence, we do feel that a more detailed study in a system with large plastic zone sizes (i.e., in a low strength alloy) would shed more light on this situation.

As a general conclusion, obviously, positron annihilation can be ruled out for the detection of macroscopic defects, such as voids with a dimension of 10^{-4} cm or up. This is evidently due to the fact that the diffusion length of

43

the slow positrons inside the solid phase is roughly of the order of 10^{-6} cm which is much greater than 10^{-4} cm. Positron annihilation is sensitive to microstructure changes and macroscopic changes with which microstructure changes are associated.

Therefore, positron annihilation in general, satisfies the first three requirements to be a viable practical NDE tool. In addition, positron annihilation should be a very valuable tool to assist other tools of physical metallurgy in the study of various kinds of microstructural changes in metals. In meeting the last requirement, the method of positron lifetime measurement is found to be relatively slow, at least several hours for one measurement. This may be satisfactory for research purposes, but could be too slow for other applied purposes, such as quality control.

This time duration can be reduced further, provided faster detectors and electronics are available. However, the development of them requires time and investment. There is an alternative, however, the method of Doppler Broadening. At present, the time required for one measurement by the method of Doppler Broadening is several hours. It is possible to reduce this time to one hour or less.

VI. RECOMMENDATIONS

1. Positron annihilation can be used as a Non-Destructive Evaluation Tool for detecting micro-defects or microstructure changes in certain engineering metallic materials, which cannot be obtained by other NDE methods, such as the ones studied by us. However, because very few engineering materials are pure crystals with very few defects, the high sensitivity of positron annihilation to defects demands that

44

a prioré knowledge of the physical metallurgical aspects of the nature of the
defects or microstructure changes is required for the interpretation of the results.
Consequently, much more work is still needed to enrich our knowledge in this area.

2. The method of positron lifetime measurement is relatively slow, several
hours per measurement or more. Therefore, it is suitable for evaluation of micro
defects or microstructure changes in engineering metallic materials where the time
element is not a serious drawback.

3. For testings where short time duration is required, because of the advant
of the methods of Doppler Broadening, it is recommended to be an alternative
technique. More work along this area is needed.

4. The use of positron annihilation as an NDE tool for detecting micro-defects
or microstructure changes in engineering materials other than metals, such as com-
posites, ceramics, etc. should be explored.

ACKNOWLEDGEMENTS

References

1. A.I. Aklierzer and V.B. Berestetskii, Quantum electrodynamics, Interscience, New York (1965); V.B. Berestetskii, E.M. Lifshitz and L.P. Pitaevskii, Relativistic Quantum Theory, Pergamon, Oxford (1971).

2. P.P. Wallace, Solid St. Phys. 10, 1 (1960); V.I. Goldanskii, Atomic Energy Rev. 6, 3 (1968); R.N. West, Ad. Phys., 22, 3 (1973).

3. C. Lee, Soviet Physics, JETP, 6, 281 (1958).

4. R.A. Ferrell, Rev. Mod. Phys. 28, 308 (1956); Phys. Rev. 108, 167 (1956); Ibid, 110, 1355 (1958).

5. For example: I.Ya. Dekhtyar, Czech. J. Phys. B18, 1509 (1968); S. Berko and F. L. Hereford, Rev. Mod. Phys. 28, 299 (1956); J.A. Merrigan, J.H. Green and S.J. Tao, Physical Methods of Chemistry Vol. 1, Part IIID, ed. A. Weissberger and B.W. Rossiter, John Wiley, Pg. 501 (1972).

6. A. Ogata, S.J. Tao, J. H. Green, Nucl. Instr. Meth. 60, 175 (1968).

7. D.C. Connors, and R.N. West, Phys. Lett. 30A, 24 (1969).

8. S.J. Tao, IEEE, NS-15, 1, 175 (1968).

9. S.J. Tao, unpublished work.

10. J.B. Wang, S.Y. Chuang and S.J. Tao, Nucl. Instr. Meth. 108, 253 (1973).

11. S. Berko, G.M. Beardsley, M. Haghgooie, I. Tal and J. Mader, Fourth International Conf. on Positron Annihilation, Helsingor, Denmark, August, (1976), paper H13:R.J. Douglas, and A.T. Stewart, Ibid, paper H14.

12. For example: I.K. MacKenzie, T.E. Jackman and N. Thrane: Phys. Rev. Lett. 34, 512 (1975); I.K. MacKenzie, T.E. Jackman and P.C. Lichtenberger: App. Phys. 9, 259, (1976); T.E. Jackman, M.S. Thesis, The University of Guelph (1974); P. Hantojarvi, A. Vehanen and V.S. Mikhalankov: Proc. Fourth Intern. Conf. on Positron Annihilation, paper E23, Helsingor, Denmark, 1976; B. Nielsen and K. Petersen: Ibid, paper E24; and many earlier papers.

13. S.J. Tao, "Detection of Vacancy Concentration and Defects in Aluminum, Titanium

and their Alloys and Nickel Base Superalloys by Positron Annihilation".
Final Report, Contract CO0019-74-C-10170 (1975).

14. S.J. Tao, "Positron Annihilation Meanlife and Defects Created by Heat or
Deformation in Aluminum, Titanium and their Alloys and Nickel Base Superalloys".
Final Report, Contract CO0019-75-C-0236 (1976).

15. J.P. Wallace, J.K. Tien, S.J. Tao and S.Y. Chuang, Scripta Met. $\underline{8}$, 1039 (1974).

16. G.R. Leverant and B.H. Kear: Met. Trans. $\underline{1}$, 491 (1970). Also see: B.H. Kear,
G.R. Leverant and J.M. Oblak: Trans. ASM $\underline{62}$, 639 (1969).

17. M.K. Malu: D.Eng. Sc. Thesis, Columbia University, New York, 1975.

18. J.P. Wallace, S. Purushothaman, J.K. Tien, S.J. Tao and S.Y. Chuang:
Proc. Fourth Intern.Conf. on Positron Annihilation, paper E11, Helsingor,
Denmark, 1976.

19. J.P. Wallace, D. Eng. Sc. Thesis, Henry Krumb School of Mines, Columbia
University (1976).

20. E.C.W. Perryman: Acta Met. $\underline{2}$, 26 (1954).

21. T.V. Cherian, P. Pietrokowsky and J.E. Dorn: Trans. TMS-AIME, $\underline{185}$, 948 (1949).

22. G. Taylor and J.W. Christian: Phil. Mag. $\underline{15}$, 873 (1967).

23. G. Taylor and J.W. Christian: Phil. Mag. $\underline{15}$, 893 (1967).

24. R. Cotterill, K. Petersen, G. Trumph and J. Traff: J. Phys. $\underline{F2}$, 459 (1972).

25. A. Seeger: J. Of Phys. $\underline{F3}$, 248 (1973).

26. Aluminum Standards and Data: Published by the Aluminum Association, New York,
1976.

27. J.C. Grosekreutz and W.E. Millet: Phys. Lett. $\underline{28A}$, 621 (1969).

28. H.E. Hjelmroth, J.G. Rasmussen and J. Traff: Proc. Fourth Intern. Conf. on
Positron Annihilation, paper E37, Helsingor, Denmark, 1976.

29. I.K. MacKenzie, T.L. Khoo, A.B. McDonald and B.T.A. McKee: Phys. Rev. Lett. 19, 946 (1967).

30. C.L. Snead, Jr., T.M. Hall and A.N. Goland: Phys. Rev. Lett. 29, 62 (1972).

31. S. Weissman, T. Imura and N. Hosokawa: Chapter in "Recovery and Recrystallization of Metals," L. Himmel (ed.), P. 241, Interscience, New York, 1963.

32. B.T.A. McKee, S. Saimoto, A.T. Stewart and M.J. Stott: Can. J. Phys. 52, 759 (1974).

33. K.G. Lynn, R. Ure and J.C. Byrne: Acta Met. 22, 1075 (1974).

34. H.Y. Hunsicker: Chapter 5 in "Aluminum--Properties, Physical Metallurgy and Phase Diagrams," K.R. Van Horn (ed.), ASM, Cleveland, 1970.

35. J.T. Staley: Met. Trans. 5, 929 (1974).

36. A. Kelly and R.B. Nicholson: Prog. Mat. Sci. 10, 149 (1962).

37. R. Nagai, S. Tanigawa and M. Doyama: Proc. Fourth Intern. Conf. on Positron Annihilation, paper E27, Helsingor, Denmark,1976.

38. P. Schultz, T.E. Jackman, I.K. MacKenzie and J.R. MacDonald: Ibid, paper E6.

39. T.D. Troev, K. Hinode, S. Tanigawa and M. Doyama: Ibid, paper D14.

40. Metals Handbook: Vol. 2. P. 618, ASM, Cleveland, 1972.

41. A.D. McQuillan and M.K. McQuillan: Metallurgy of Rarer Metals, #4: Titanium, Butterworths, London, 1956.

42. J.K. Tien and F.S. Pettit: Met. Trans. 3. 1587 (1972).

43. M. Eldrup, O.E. Mogensen and J.H. Evans: J. Phys. F6, 499 (1976).

44. D. Segers, M. Dorikens, L. Dorikens-Vanpraet and B. Dauwe: Proc. Fourth Intern. Conf. on Positron Annihilation. paper E16, Helsingor, Denmark, 1976.

45. P. Hantojarvi, J. Heinio, M. Manninen and R. Nieminen: Ibid, paper E17.

46. J.H. Evans, O. Mogensen, M. Eldrup and B.N. Singh: Ibid, paper E14.

47. W.B. Gauster: Ibid, paper E10.

48. K. Petersen: Ibid, paper E9.

49. S. Purushothaman and J.K. Tien: Scripta Met. $\underline{9}$, 923 (1975).

50. S. Purushothaman: D.Eng. Sc. Thesis, Columbia University, 1976.

51. R.J. Richards, S. Purushothaman, J.K. Tien, O. Buck and J. Frandsen: Un-published Research, Columbia University, New York, 1976.

52. P.C. Paris and G.C. Sih: ASTM-STP $\underline{381}$, 30 (1966).

53. J.R. Rice: J. Mech. Phys. of Sol. $\underline{22}$, 17 (1974).

54. J.A. Carlson and D.A. Koss: Unpublished Research, Michigan Technological University, Houghton, MI, 1977. Private communication.

55. S.J. Tao, S. Purushothaman and J.K. Tien: "The Use of Positron Annihilation for Mapping Defects in the Surface Plastic Zone Ahead of Fatigue Cracks," To be presented, and published in the proceedings of, Eleventh Symposium on NDE, Southwest Research Institute, San Antonio, TX, June 1977.

LIST OF TABLES

51

TABLE 2. Nominal chemical compositions of the aluminum-based
alloys used in the present study (in wt. pct.).

ALLOY	Al	Cu	Mg	Zn	Cr	Mn	Zr	Si
1100	99 Min.	0.12	———— Not Specified ————					
2024	93.5	4.4	1.5	-	-	0.6	-	-
7075	90.0	1.6	2.5	5.6	0.26	-	-	-
7050	88.4	2.6	2.3	6.5	0.01	0.01	0.10	0.06

TABLE 3. Heat Treatments Used to Achieve Different Precipitate States (Tempers) in the Various Aluminum Alloys Used and the Resulting $\bar{\tau}$ Values.

Alloy and Temper Designation	Heat Treatment Done to Achieve the Temper	Positron Mean Life Time (picosecs)
2024-T4	493°C/1 hr; water quench; Natural Aging at Room Temp.	210 ± 5
2024-0	Annealed 400°C/24 hrs after -T4 treatment	201 ± 5
7075-T6	460°C/1 hr; water quench; Precipitation aged at 121°C/24 hrs.	242 ± 5
7075-0	Annealed 400°C/24 hrs after -T6 treatment	240 ± 5
7050-T76	477°C/20 mins; water quench; 121°C/24 hrs; air cool; 163°C/9 hrs.	225 ± 5
7050-0	Annealed 400°C/24 hrs after -T76 treatment	215 ± 5

53

TABLE 4. Positron Mean Life Times (in picosecs) in Various
Commerical Aluminum Alloys After Different Surface
Treatments.

Alloy	Acetone Rinsing	Mechanical Polishing	Ultrasonic Cleaning in Acetone	Chemical Brightening	Anodizing
1100-H19	-	-	215 ± 1	-	243 ± 2
2024-0	-	-	205 ± 1	-	221 ± 1
7075-0	-	-	214 ± 1	-	230 ± 1
7075-T6	-	-	214 ± 1	-	231 ± 2
7050-0	211 ± 1	228 ± 2	210 ± 1	212 ± 1	218 ± 2
7050-T6	223 ± 1	227 ± 2	216 ± 1	220 ± 1	237 ± 2
7050-T73*	221 ± 1	231 ± 2	219 ± 1	223 ± 1	230 ± 2
7050-T76	227 ± 1	227 ± 2	218 ± 1	223 ± 1	230 ± 2

* -T73: 477°C/20 min; Water Quench; 121°C/24 hrs; Air Cool; 163°C/24 hrs.

TABLE 5.   Positron Mean Life Times Measured at Room
            Temperature in Fe-25Cr-4Al and Fe-25Cr-4Al-0.2Y
            Alloys Subjected to 1200°C Oxidation for
            Different Lengths of Time.

Alloy	Number of Hours at 1200°C	$\bar{\tau}$ (picosecs)
Fe-Cr-Al	0	202 ± 2
	2	186 ± 2
	8	189 ± 2
	16	187 ± 2
	25	190 ± 2
Fe-Cr-Al-Y	0	148 ± 2
	2	150 ± 2
	10	146 ± 2

TABLE 7.   Short and Long Positron Lifetime Components (τ_1 and τ_2)

in Polycrystalline Nickel-Base Superalloy Nimonic-115

Stress Ruptured at 760°C and 82.4 ksi.

Grain Boundary Carbide	Position of Source	τ_1 (picosec)	τ_2 (picosec)	I_2 %
Present	Near Rupture	137 ± 5	284 ± 12	22.2 ± 6.0
Present	Other End	139 ± 4	326 ± 20	12.8 ± 4.2
Absent	Near Rupture	121 ± 5	268 ± 14	21.1 ± 4.6
Absent	Other End	129 ± 5	304 ± 19	15.6 ± 4.5

Figure 1: A Schematic of Positron Lifetime Measurement System.
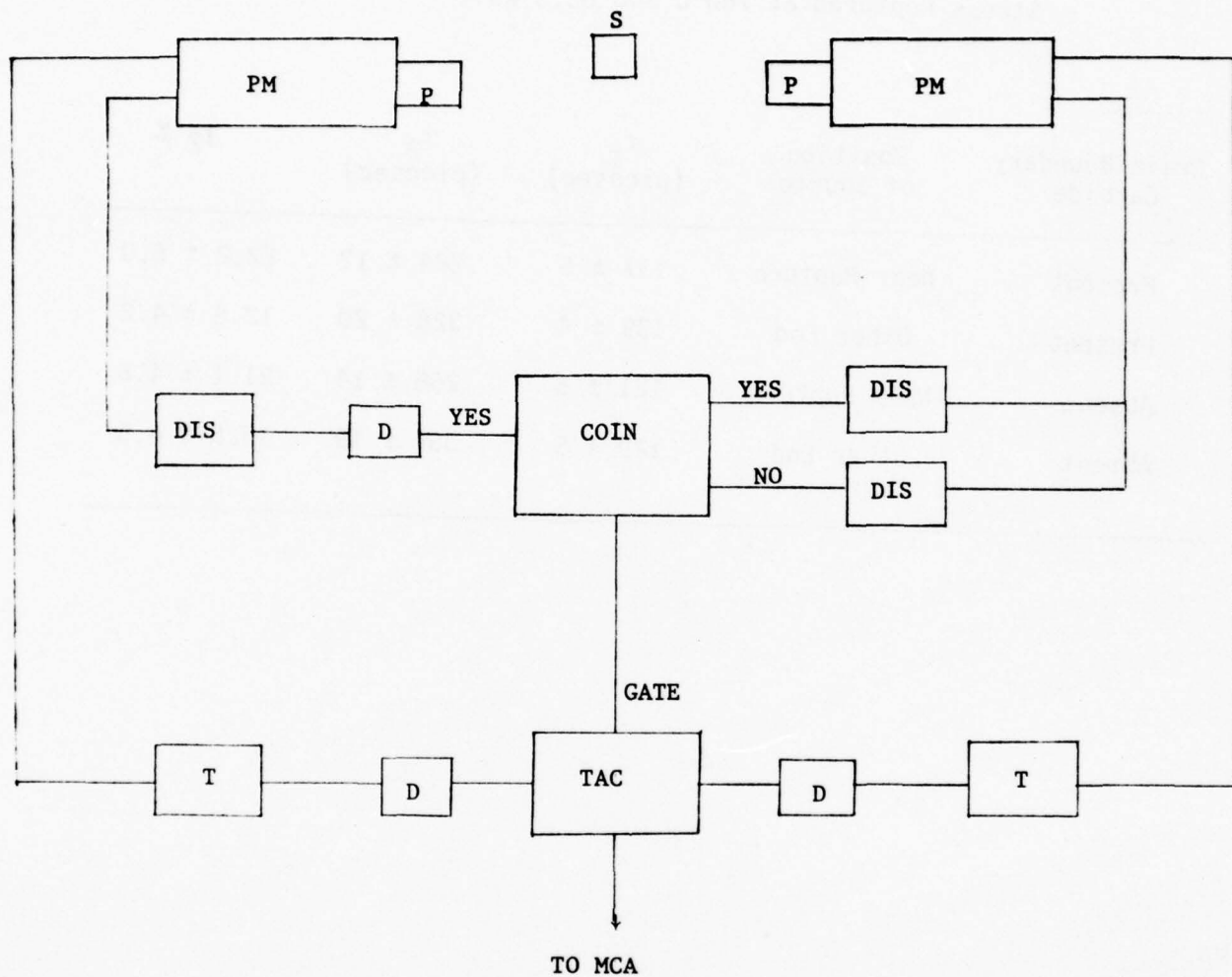
S - Positron source and sample

P - Scintillator NATON 136 1" x 1" Ø

PM - Photomultiplier XP1020

DIS - Discriminator

D - Delay

T - Timing circuit

TAC - Time-to-amplitude converter

MCA - Multichannel analyser

58
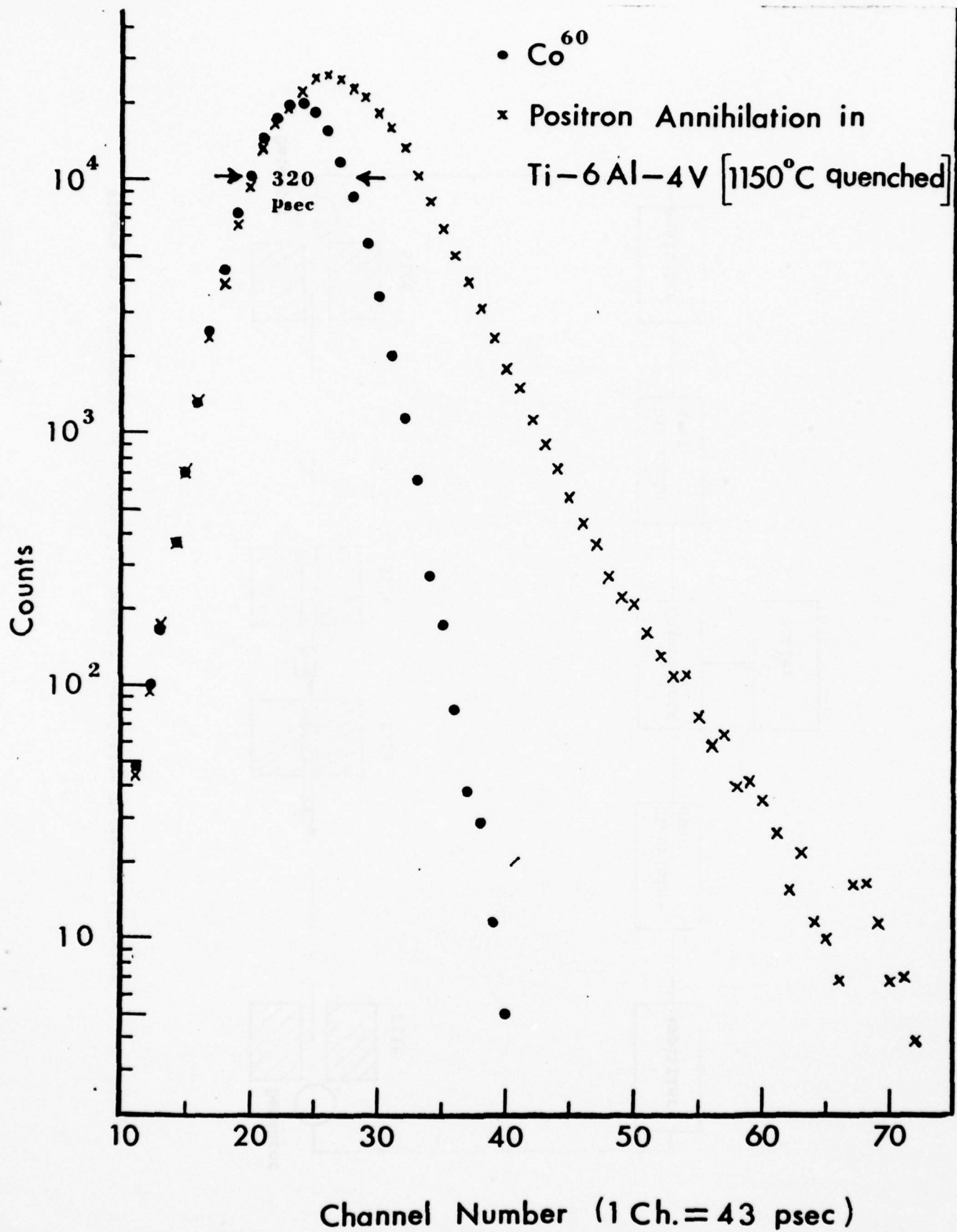
Figure 2: An Example of Positron Lifetime Spectrum

Figure 3: A Schematic of a Long Slit Angular Correlation Measurement System.
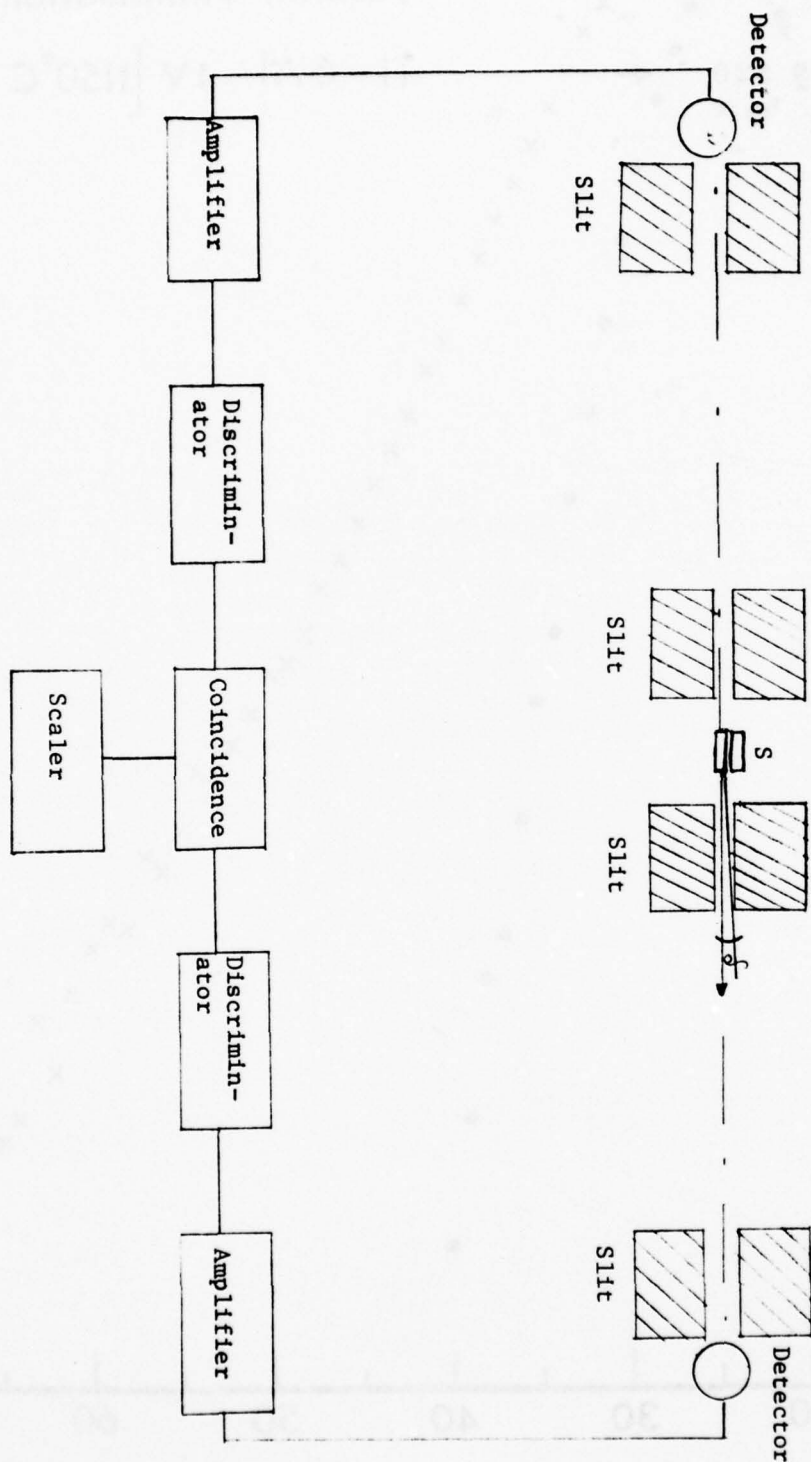
Figure 4: A Schematic of a Doppler Broadening Measurement System
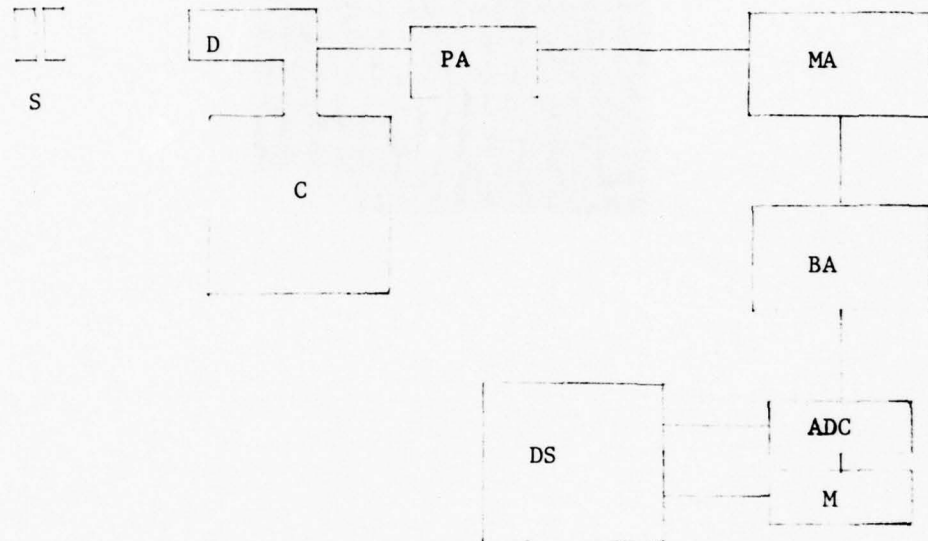
S - Sample

D - Detector

C - Cryostat (liquid nitrogen)

PA - Pre-amplifier

MA - Main amplifier

BA - Biased amplifier

ADC - Analogue-to-digital converter

M - Memory storage

DS - Digital Stabilizer

Highly stabilized power suppliers are required for whole system.

Fig. 5. Replica electron micrograph of the microstructure of Mar-M-200 used in the present study showing the nearly cuboidal array of γ^1 Ni_3 (Al, Ti) precipitates in a nickel rich solid solution matrix.[19]
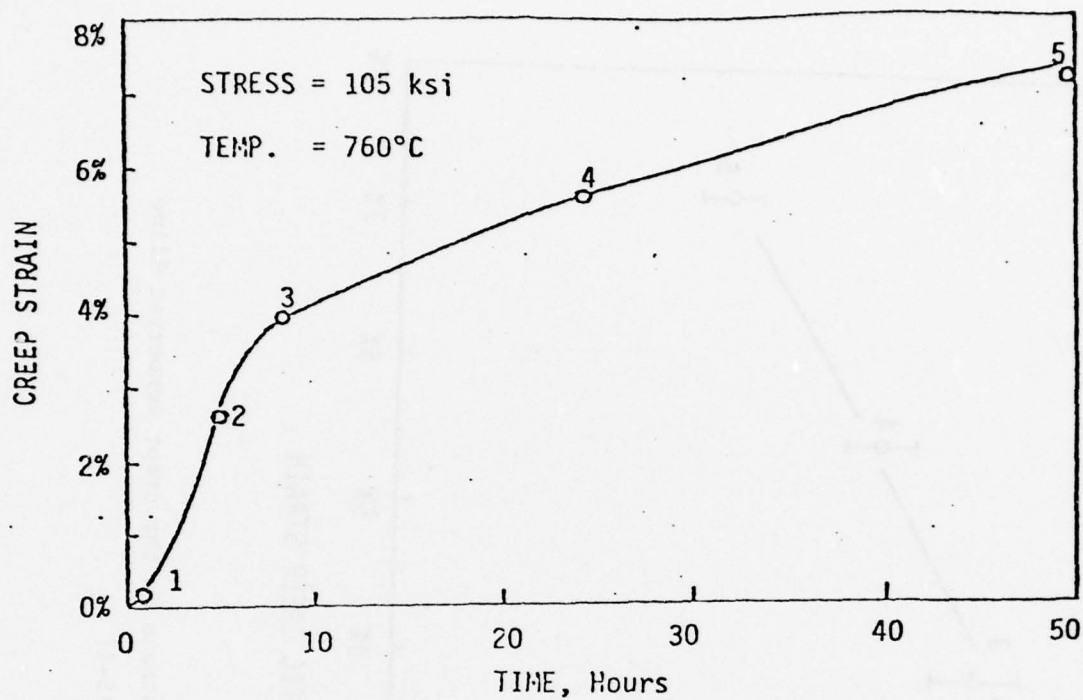
Fig. 6a. Creep curve for monocrystalline superalloy Mar-M-200 tested at 105 ksi and 760°C.[17,19] Note the well defined steady state region. The numerals identify the specimens that were strained to the indicated extents and later positron probed.[15-17]
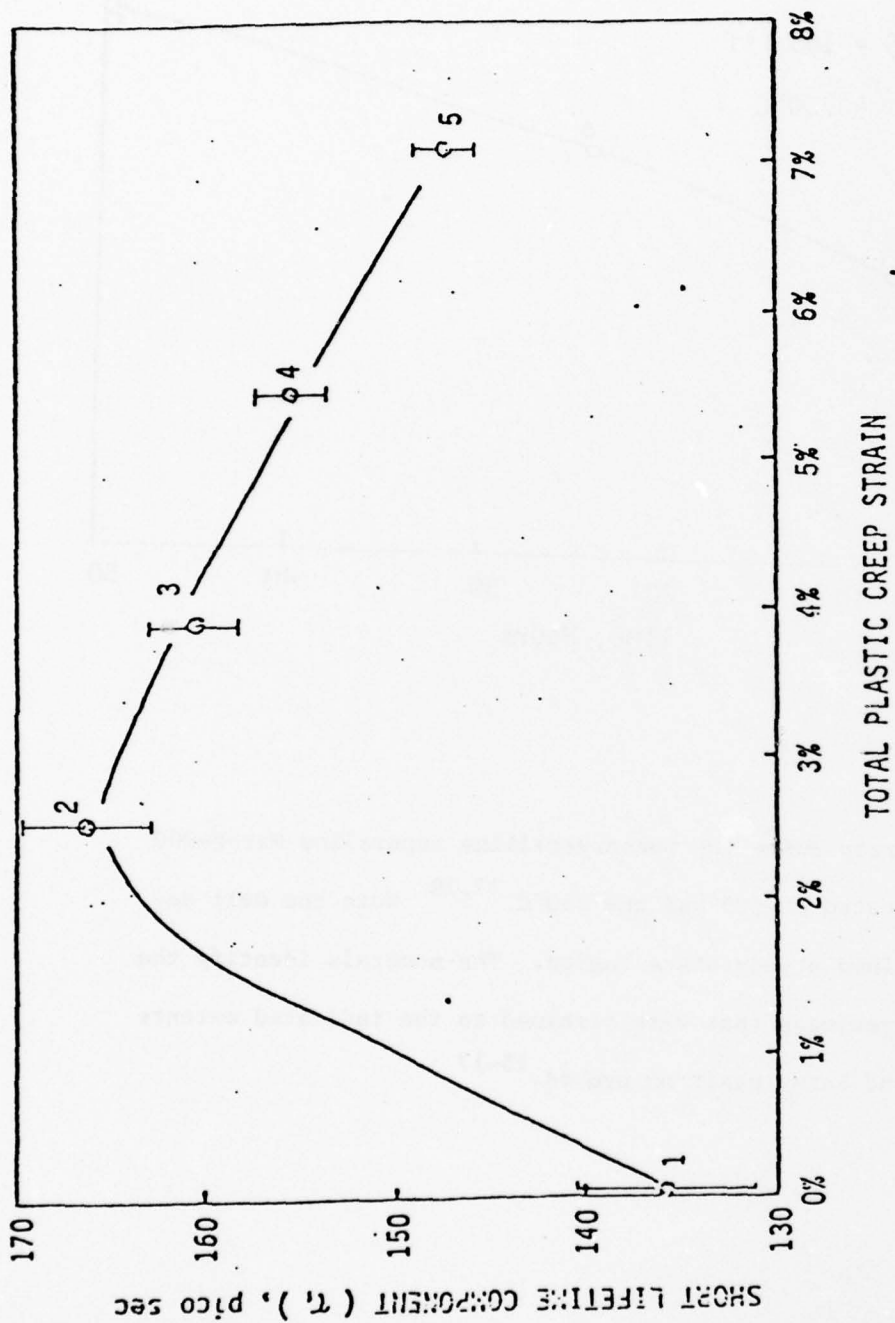
Fig. 6b. Variation of τ_1 with creep strain in the crept monocrystalline Mar-M-200 specimens; after.[15-17]
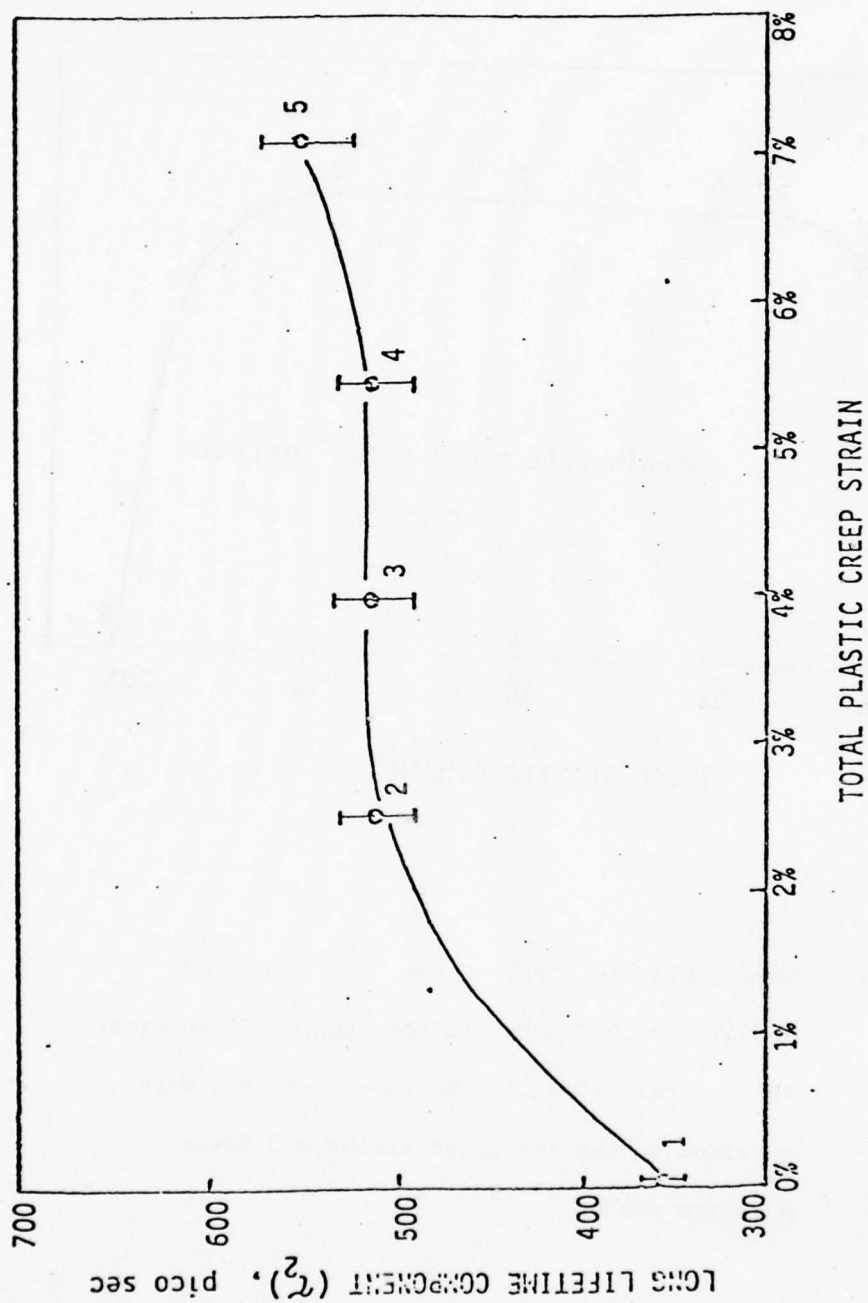
Fig. 6c. Variation of τ_2 with creep strain in the crept monocrystalline Mar-M-200 specimens; after.[15-17]
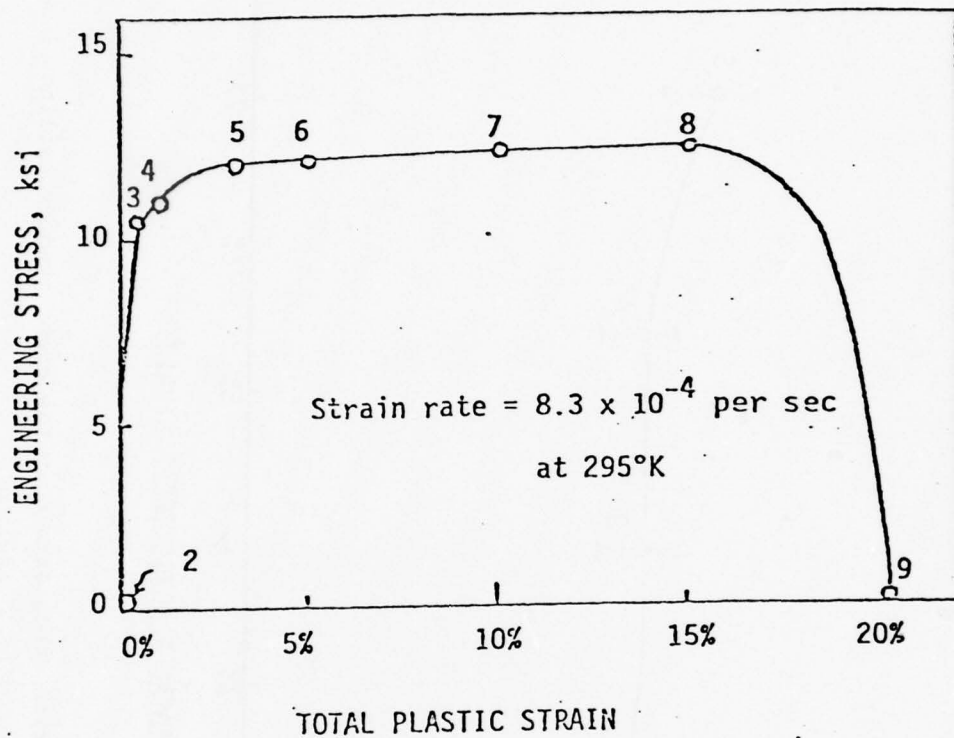
Fig. 7a. Stress-plastic strain curve of the recovery
annealed 99.99% pure aluminum tested in tension.
The numerals identify the specimens that were
strained to the indicated extent and later
positron probed.[15-17]

SHORT LIFETIME COMPONENT (τ_1), picosec.

TOTAL PLASTIC STRAIN

Strain rate = 8.3×10^{-4} per sec.

at 295°K
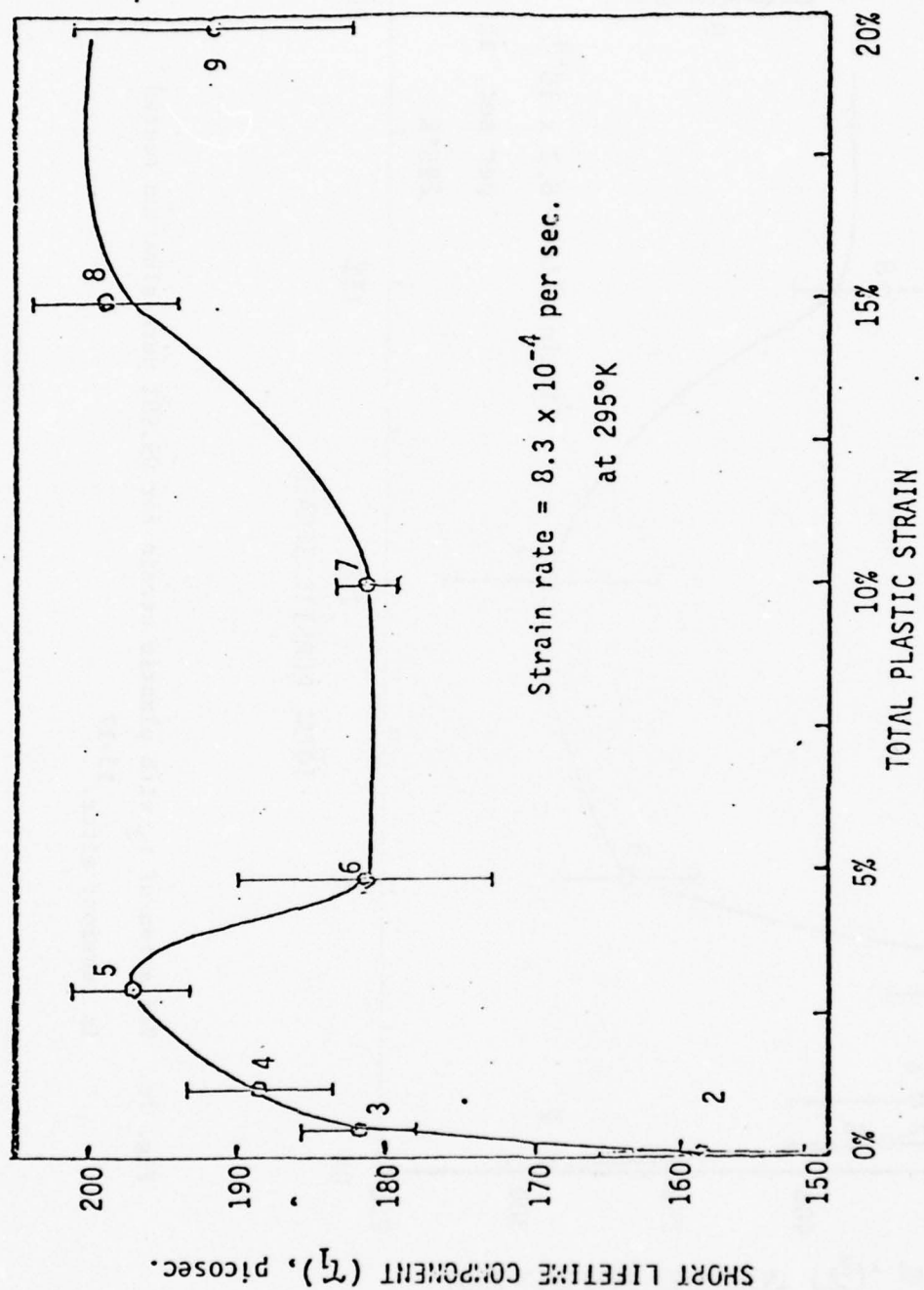
Fig. 7b. Variation of τ_1 with plastic strain for 99.99% pure aluminum tested in tension; after.[15-17]

67
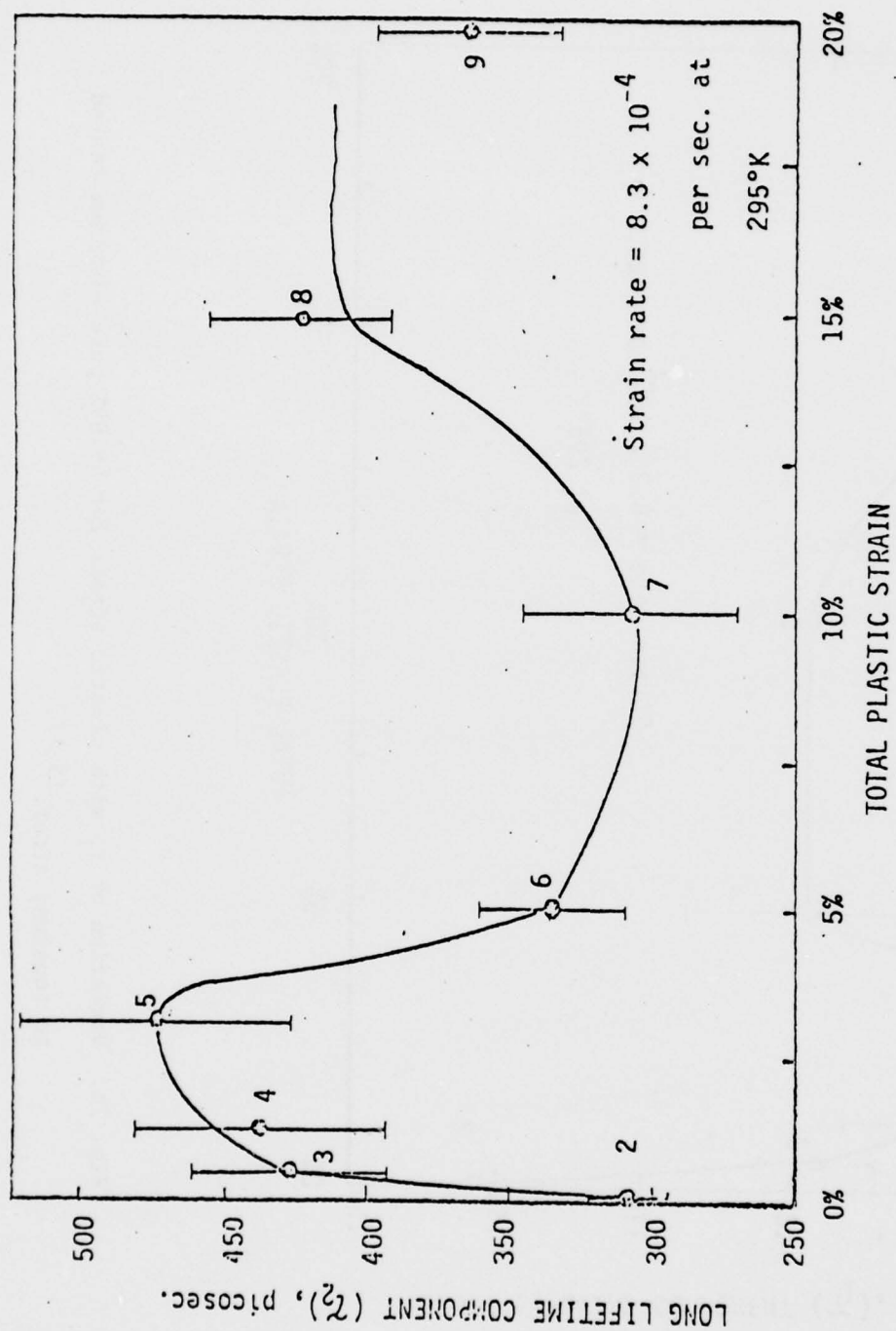
Fig. 7c. Variation of τ_2 with plastic strain for 99.99% pure aluminum tested in tension; after.[15-17]
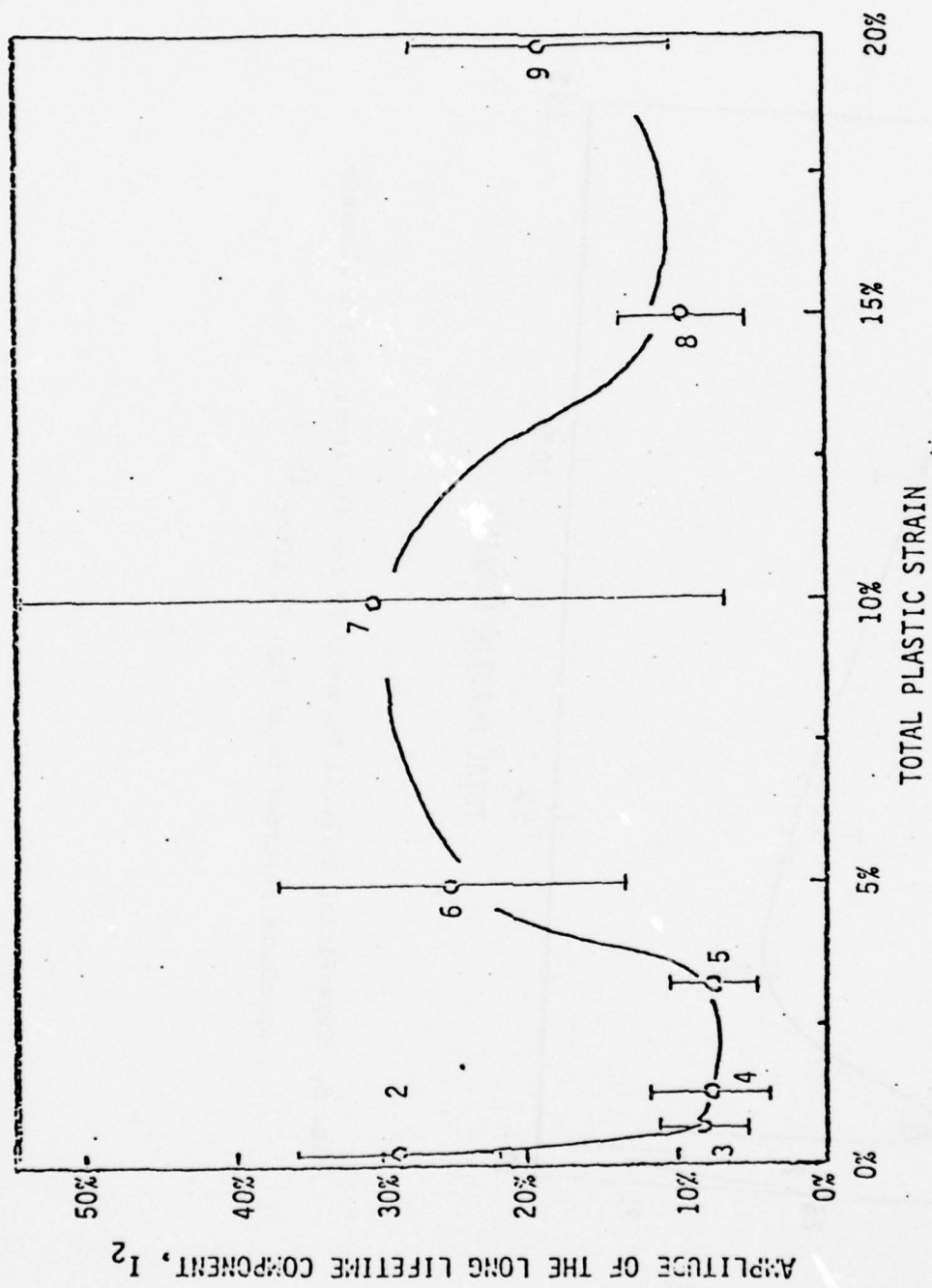
Fig. 7d. Variation of the relative intensity of the long lifetime component τ_2 as a function of plastic strain for 99.99% pure aluminum tested in tension; after.[15-17]

69
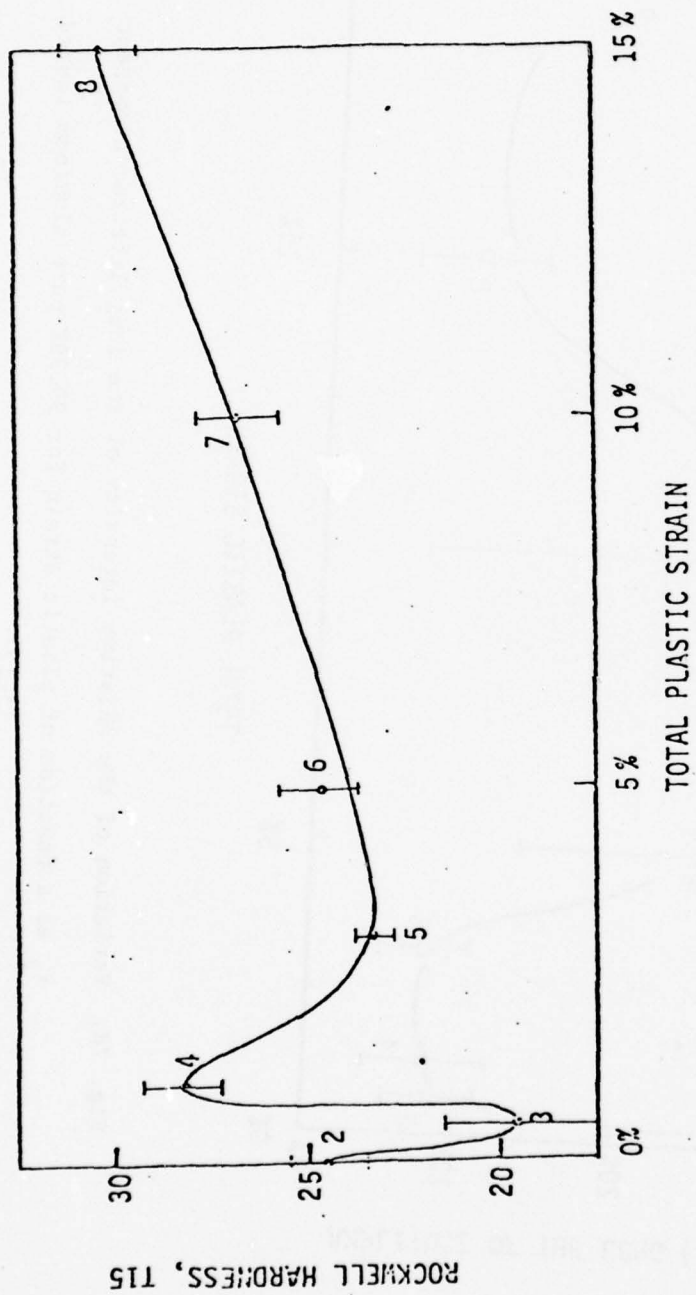
Fig. 8. Superficial Rockwell Hardness of the different 99.99% aluminum specimens referred to in Fig. 7; after.[15-17]

70
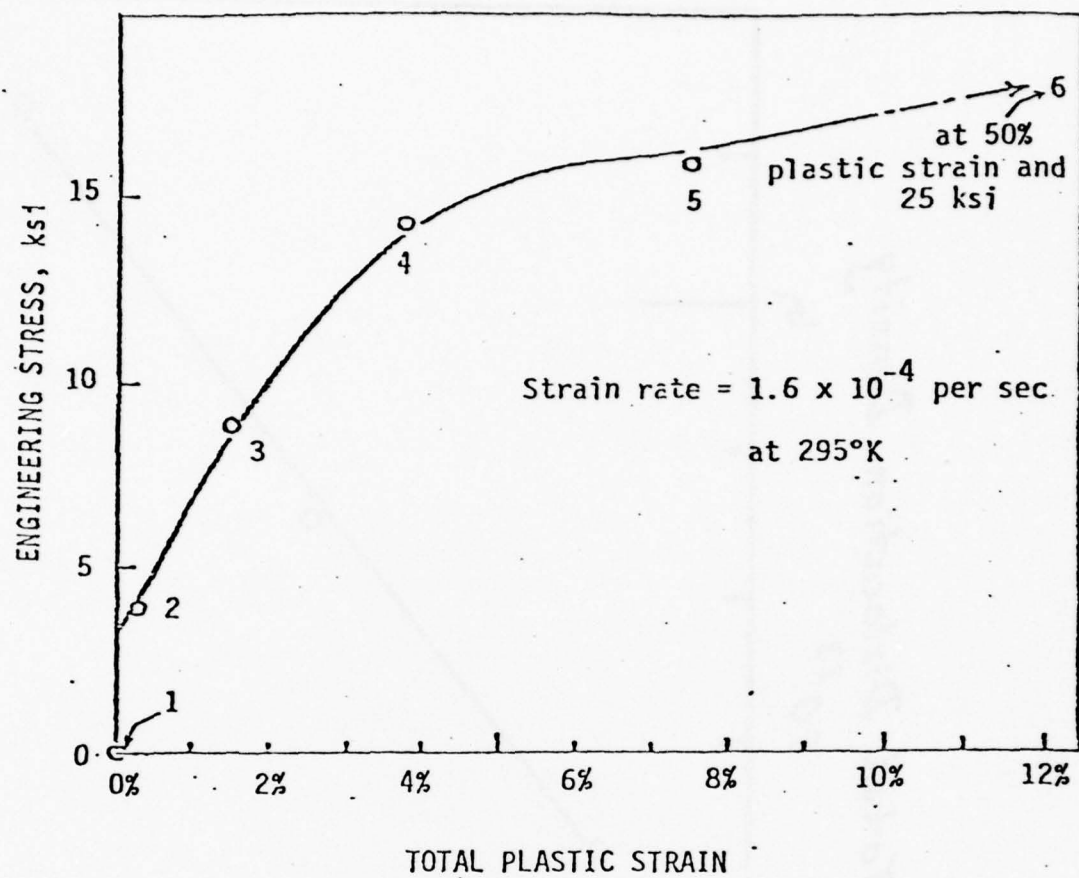
Fig. 9a. Stress-plastic strain curve of the niobium single
crystal tested in compression. The numerals identify
the specimens that were strained to the indicated
extent and later positron probed.[15-17]
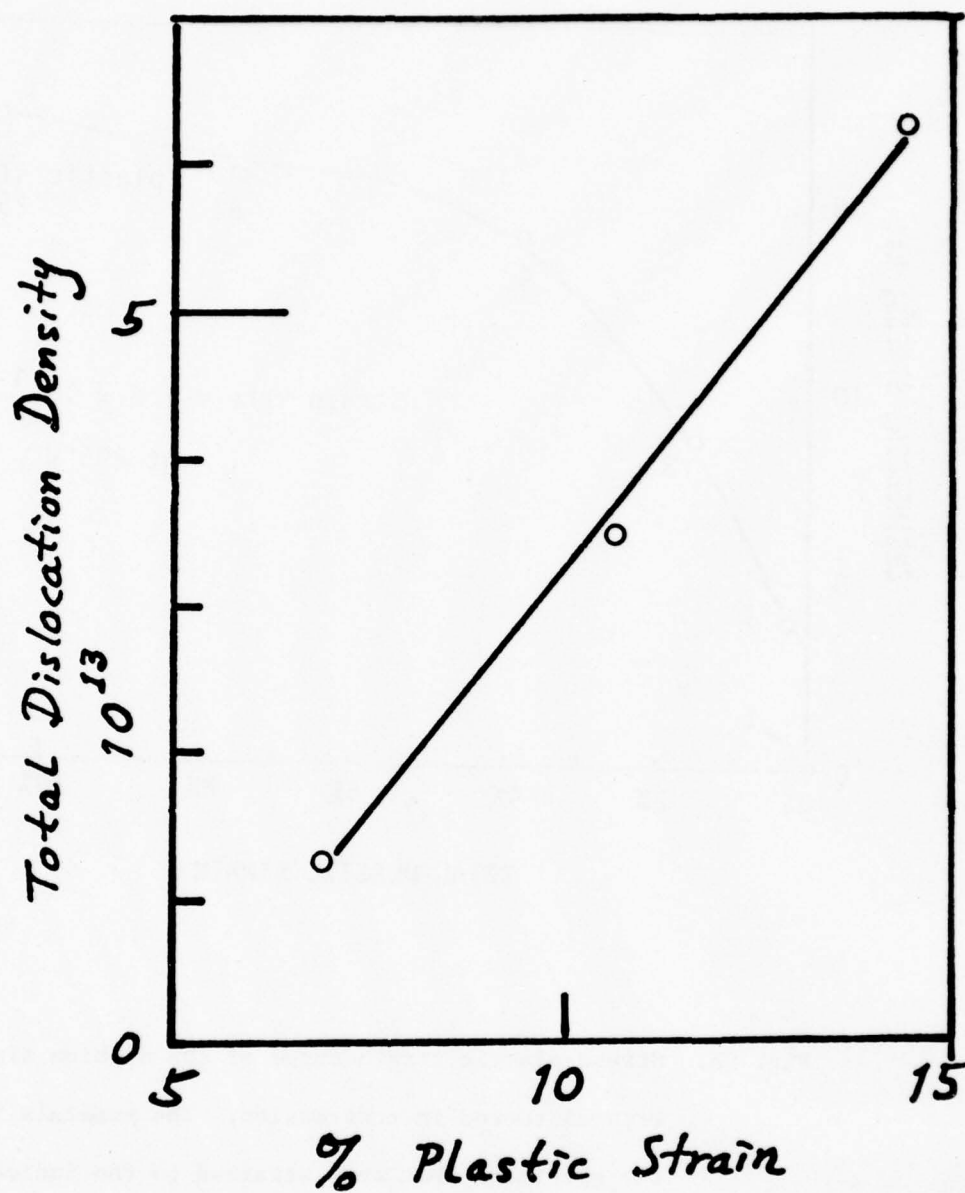
Fig. 9b. Variation of total dislocation density
with plastic strain in niobium strained
in compression; after.[23]

72
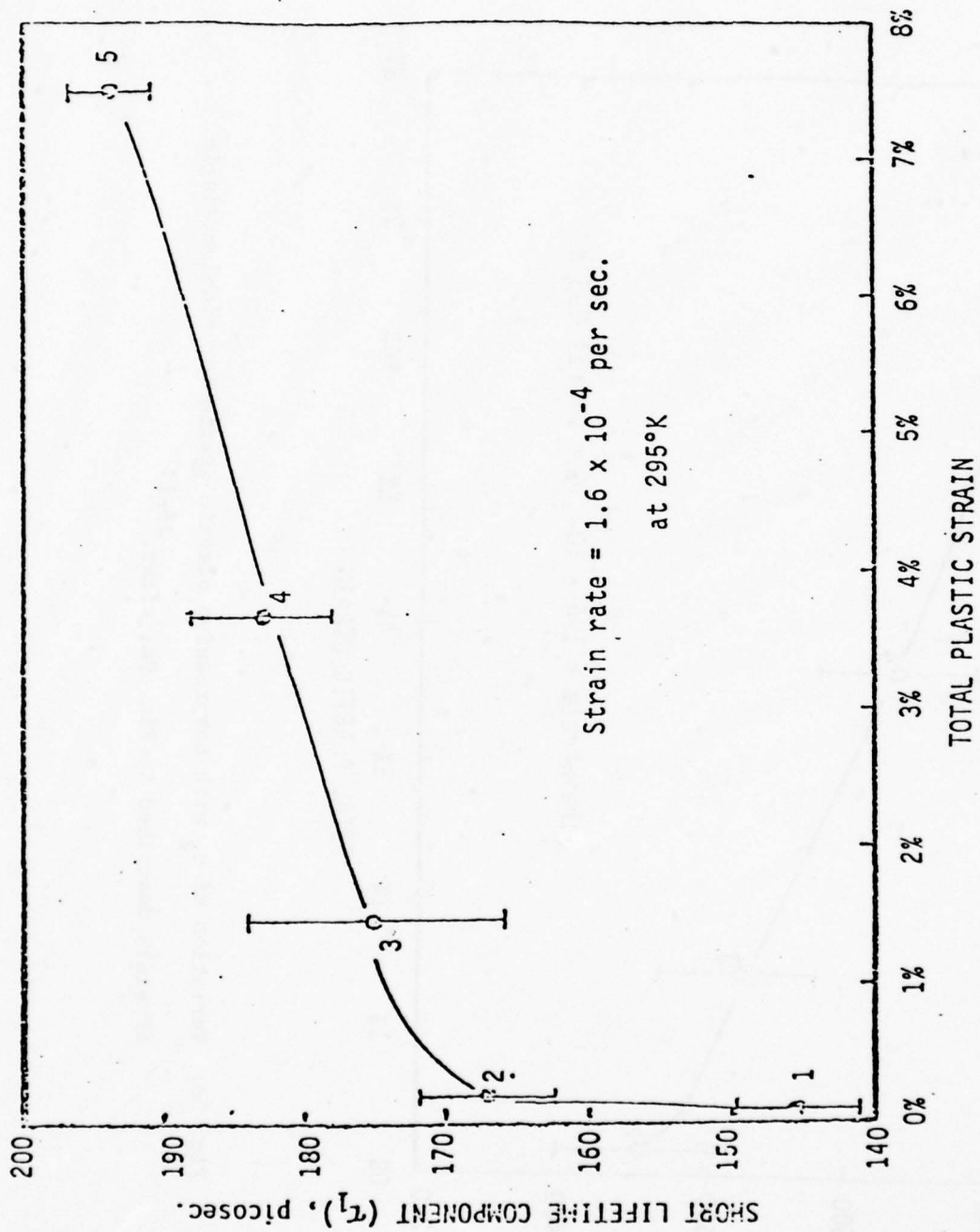
Fig. 9c. Variation of τ_1 with compressive plastic strain for niobium single crystals described in Fig. 9a; after.[15-17]
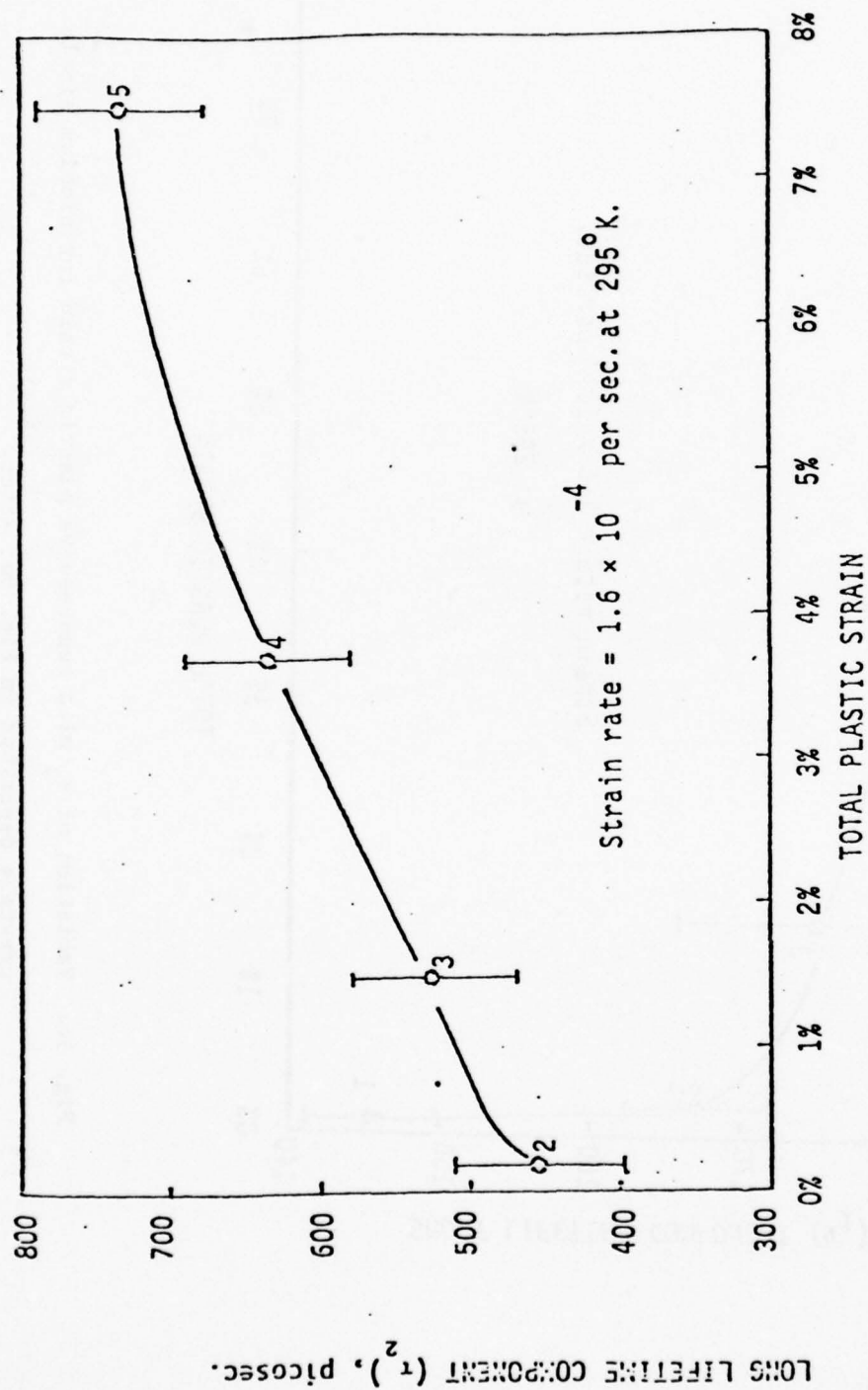
Fig. 9d. Variation of τ_2 with compressive plastic strain for niobium single crystals described in Fig. 9a; after.[15-17]
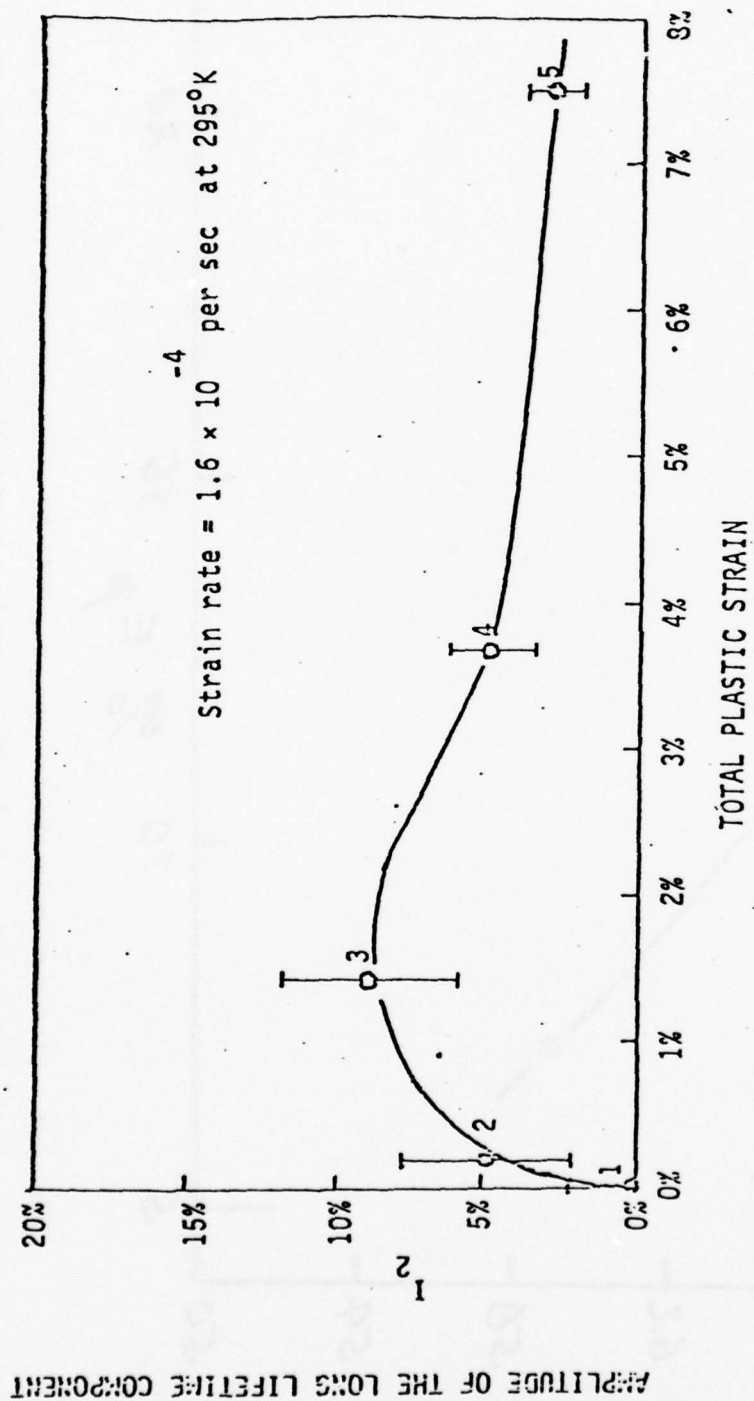
Fig. 9e. Variation of the relative intensity of the τ_2 component with compressive plastic strain for niobium single crystals described in Fig. 9a; after.[15-17]

75
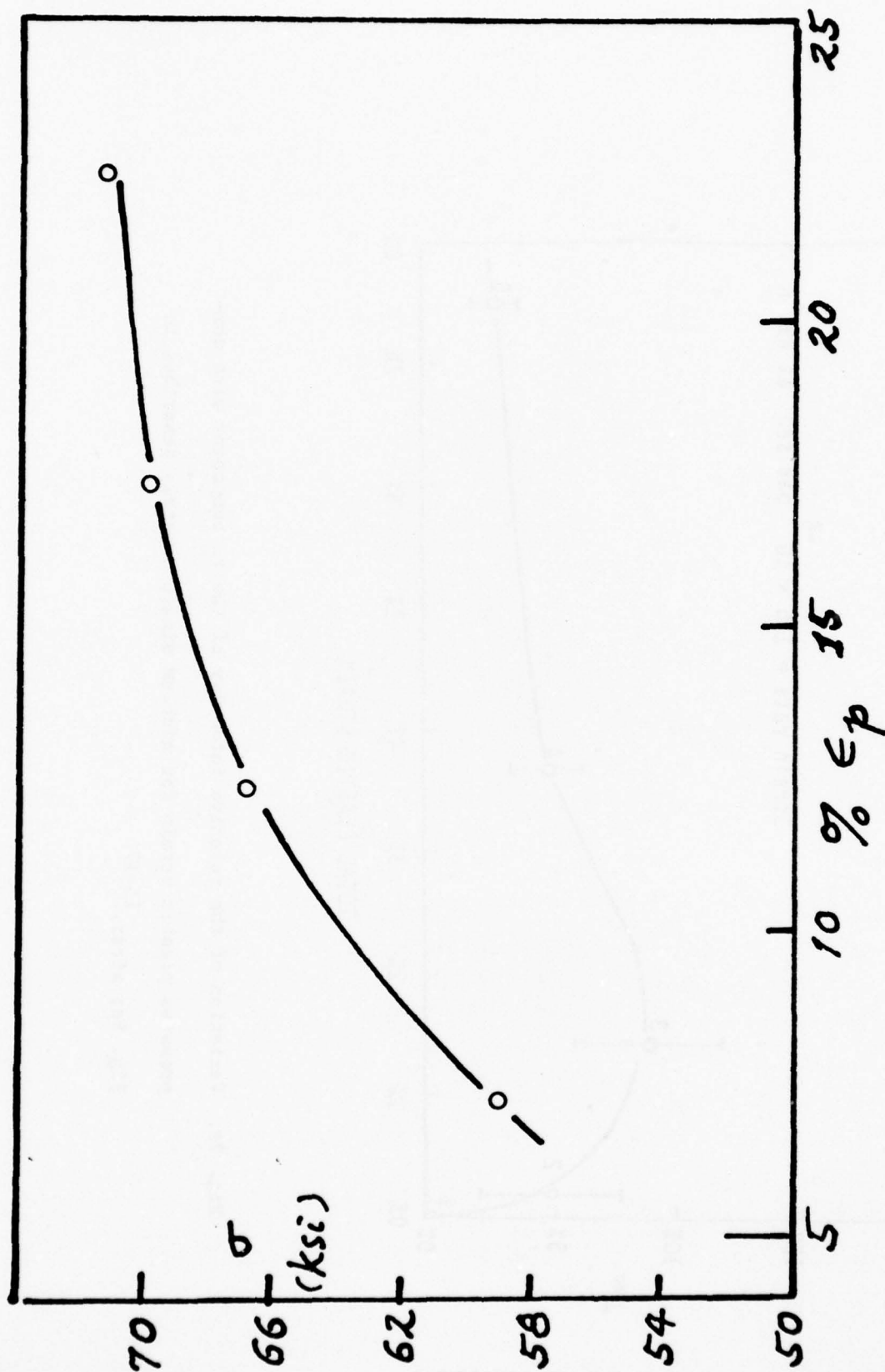
Fig. 10a. Stress-plastic strain curve for 2024-T3 aluminum stress relieved at 100°C for 1 hour and tension tested. The numerals identify the specimens that were strained to the indicated extent and later positron probed.
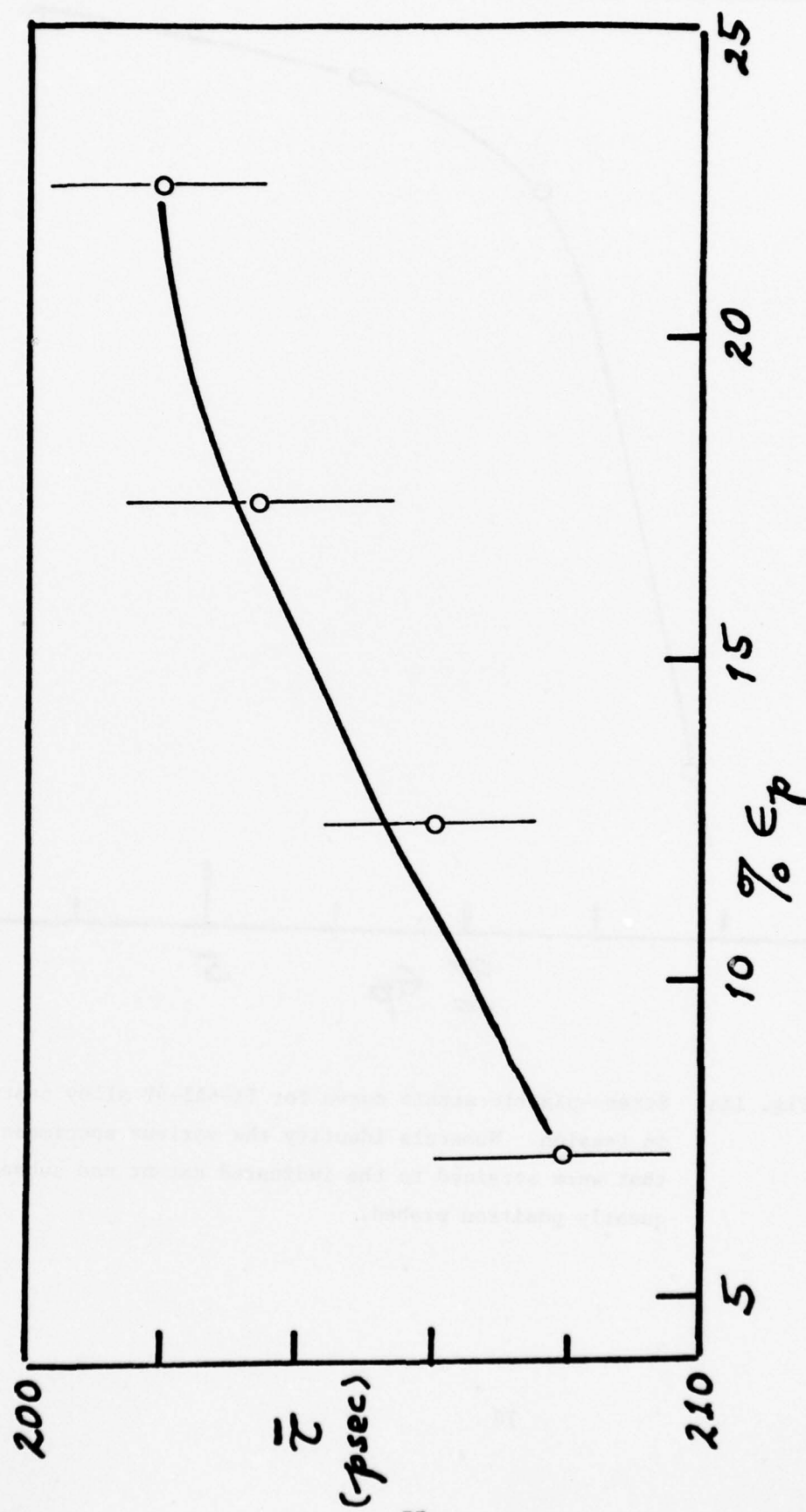
Fig. 10b. Variation of the positron mean lifetime $\bar{\tau}$ as a function of plastic strain in the 2024-T3 specimen described in Fig. 10a.

77
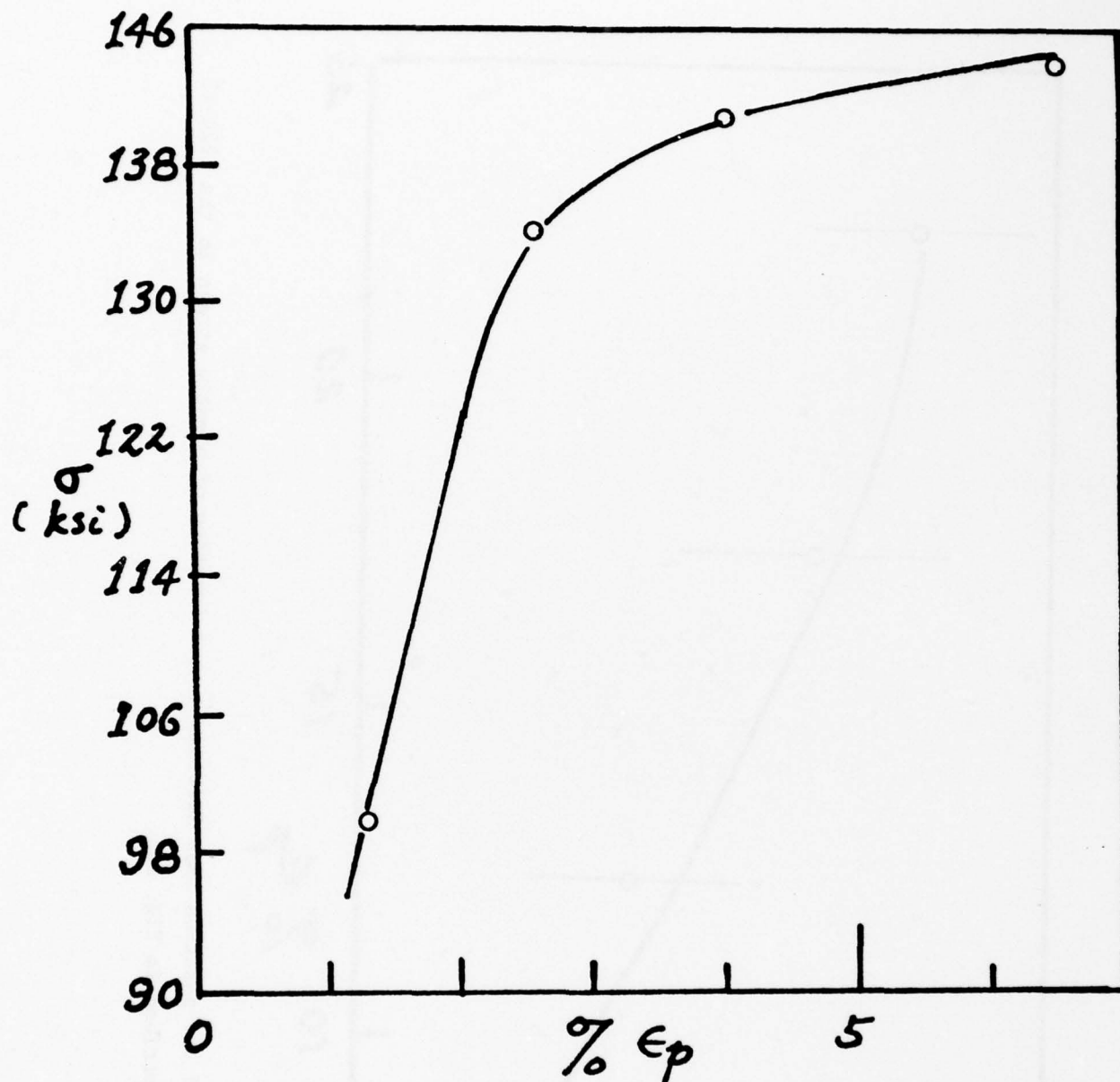
Fig. 11a. Stress-plastic strain curve for Ti-6Al-4V alloy tested in tension. Numerals identify the various specimens that were strained to the indicated extent and subsequently positron probed.

78
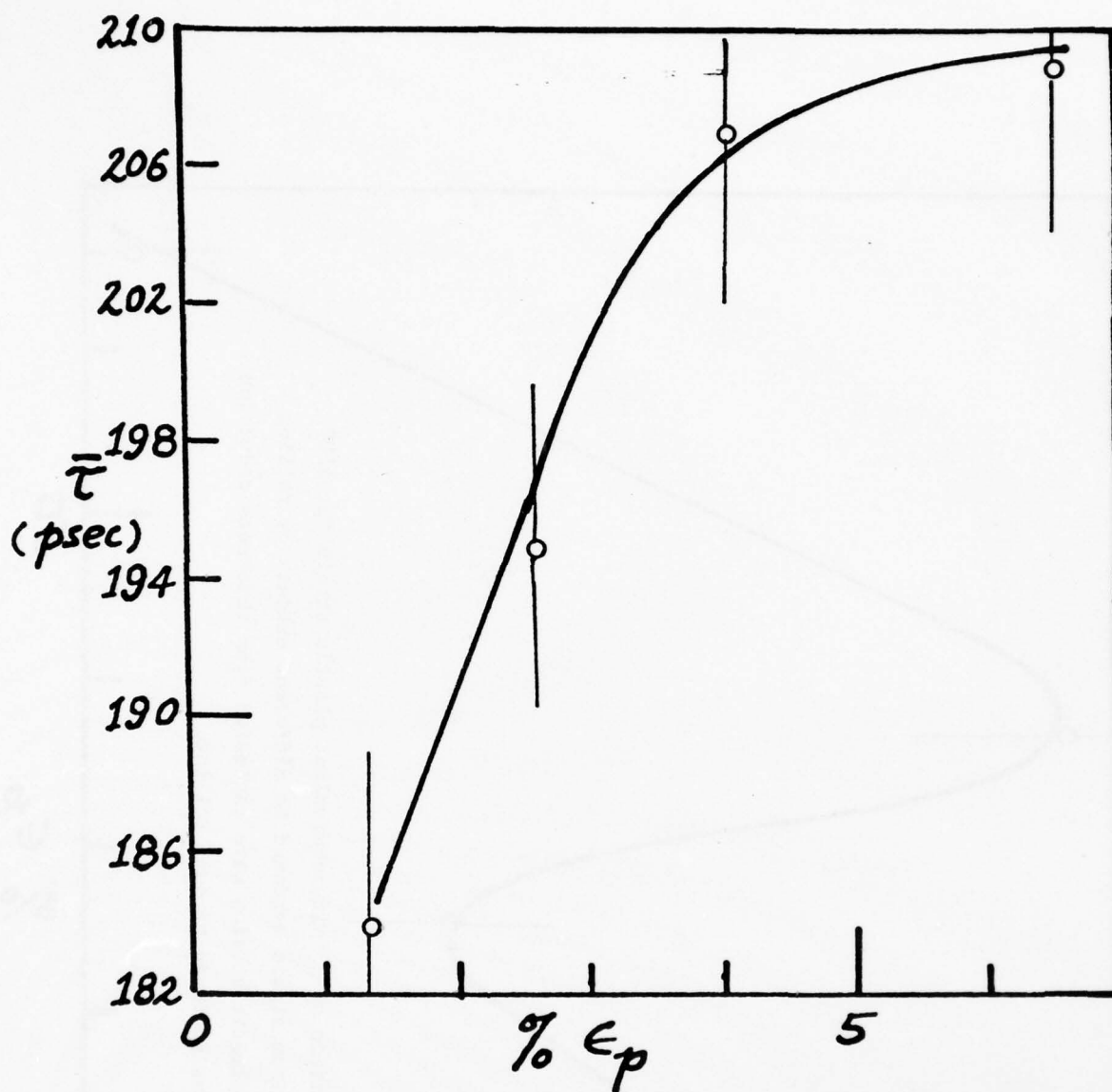
Fig. 11b. Variation of $\bar{\tau}$ with plastic strain for the Ti-6A1-4V specimens described in Fig. 11a.

79
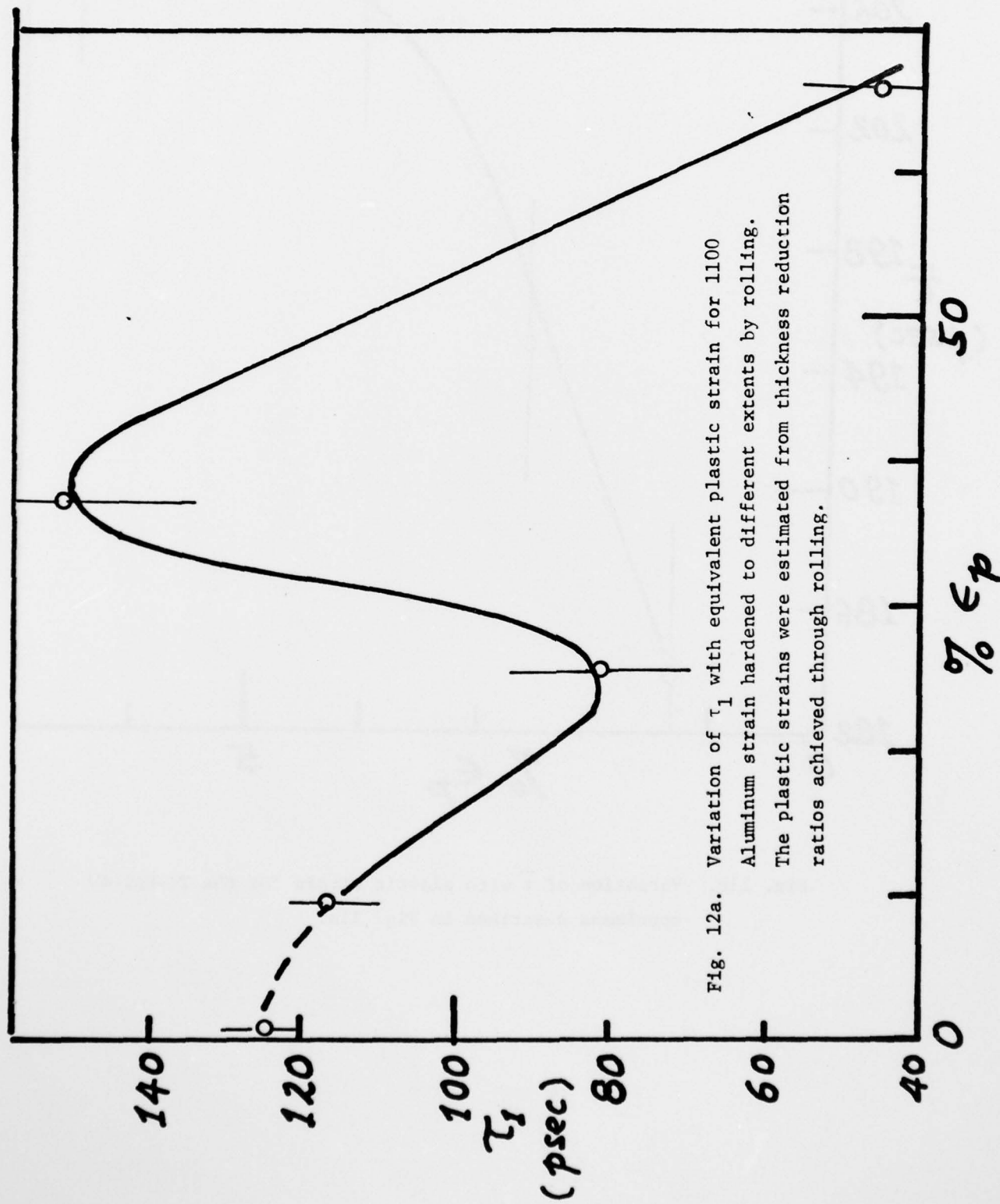
Fig. 12a. Variation of τ_1 with equivalent plastic strain for 1100 Aluminum strain hardened to different extents by rolling. The plastic strains were estimated from thickness reduction ratios achieved through rolling.
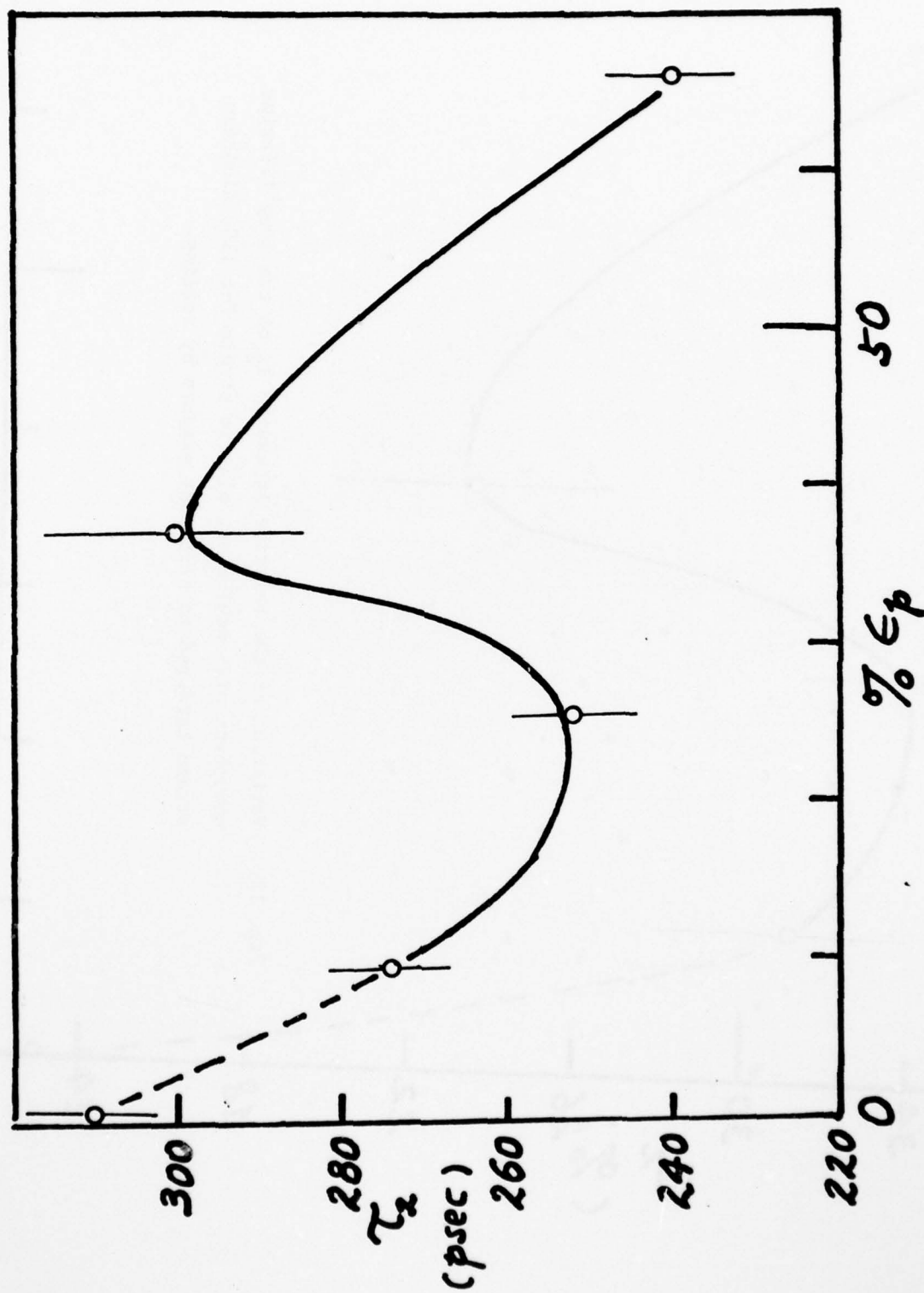
Fig. 12b. Variation of τ_2 with equivalent plastic strain for 1100 Aluminum strain hardened to different extents by rolling.

81
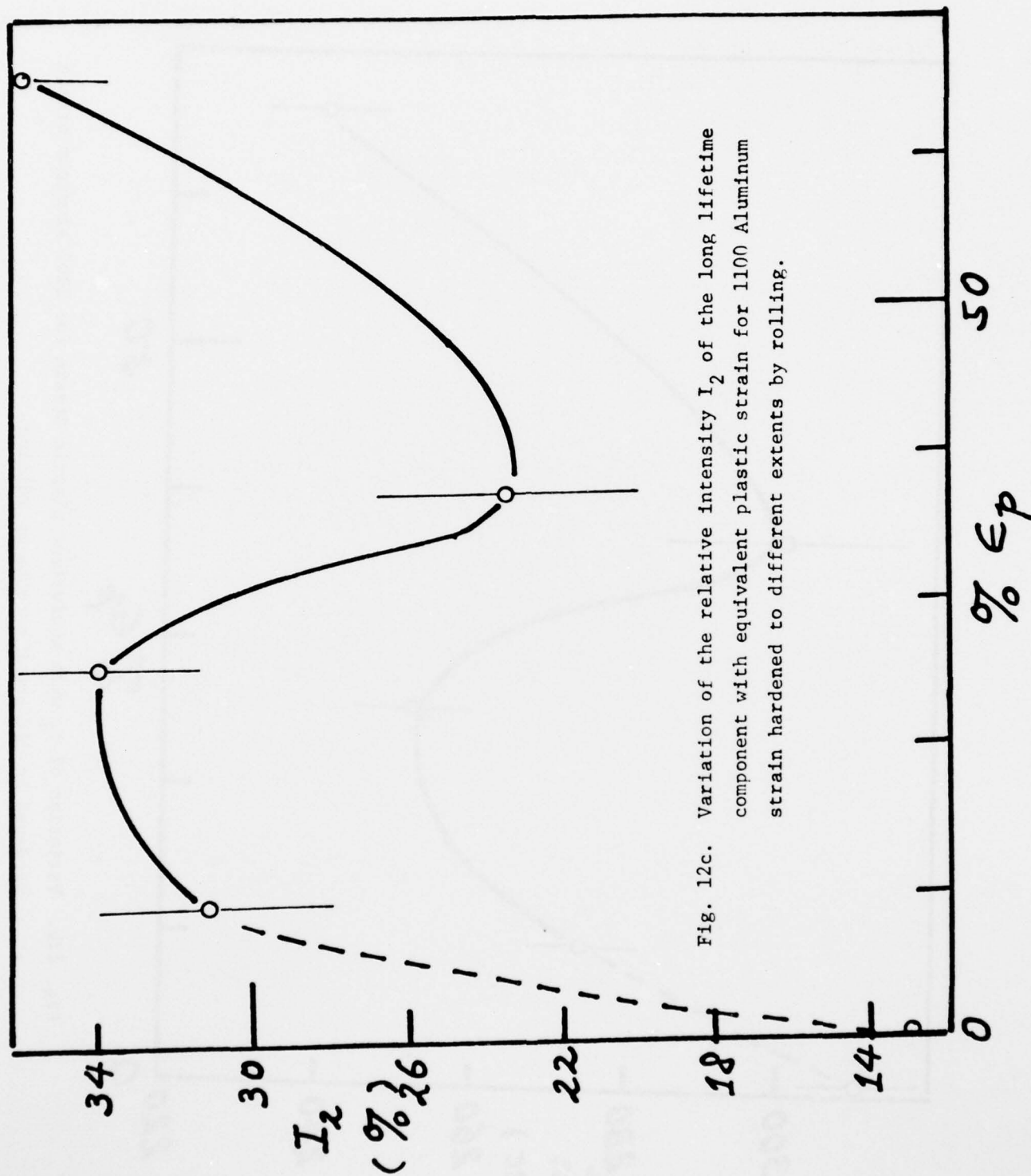
Fig. 12c. Variation of the relative intensity I_2 of the long lifetime component with equivalent plastic strain for 1100 Aluminum strain hardened to different extents by rolling.
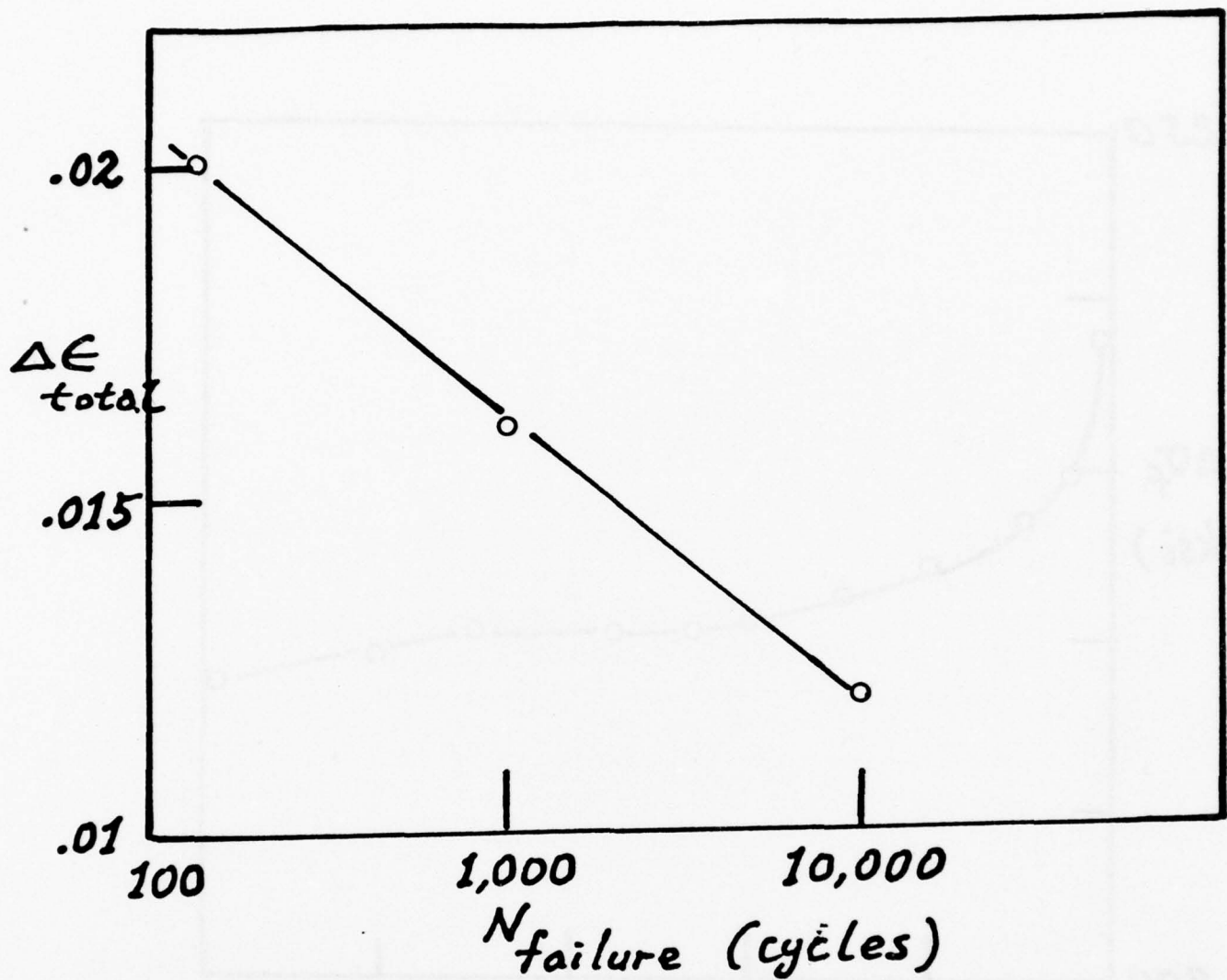
Fig. 13a. Variation of number of cycles to failure with the imposed
total strain range for Mar-M-200 monocrystals fatigue
tested at room temperature; after.
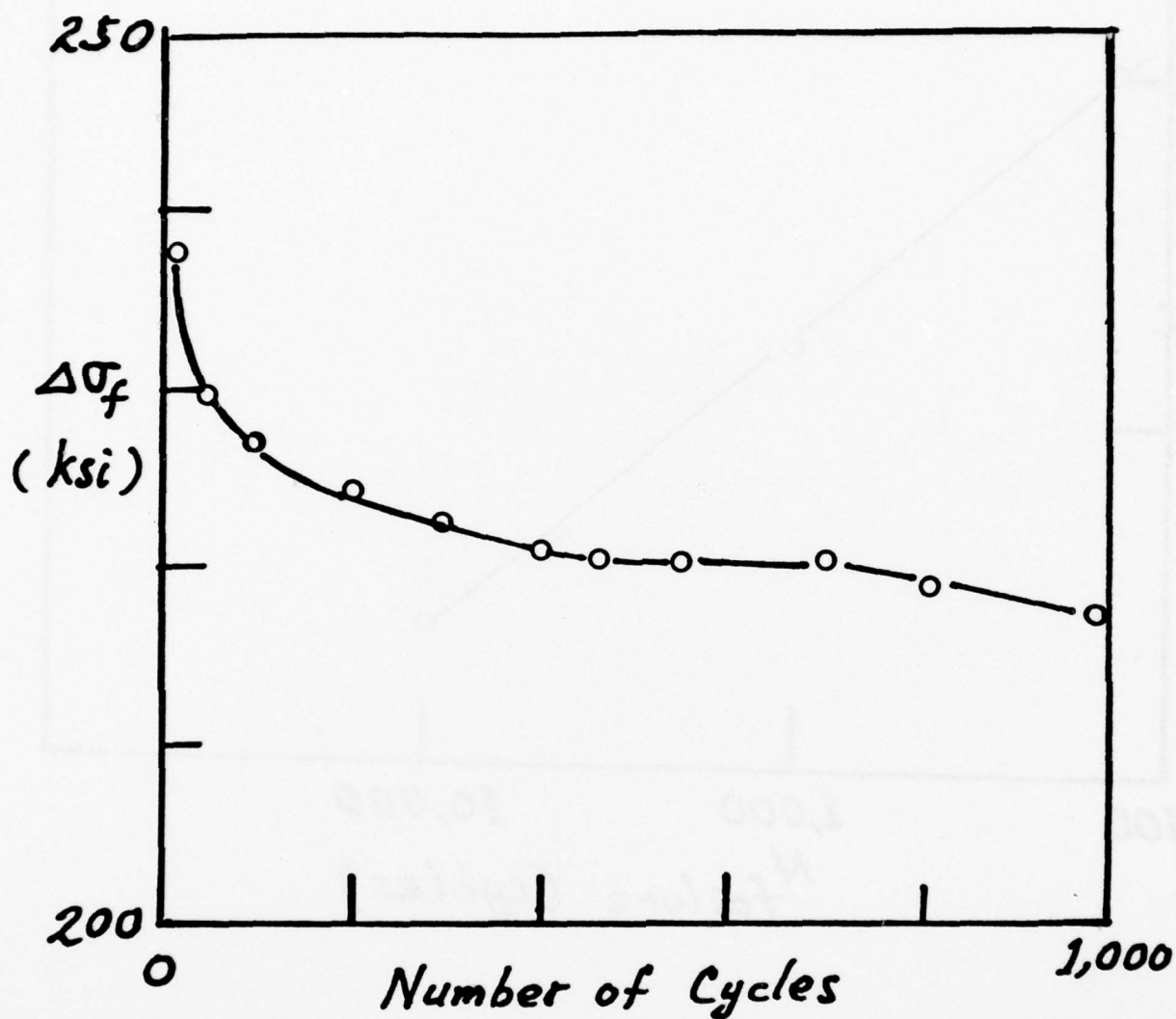
Fig. 13b. Stress response, $\Delta\sigma_f$, of monocrystalline Mar-M-200 as a function of number of cycles at a total strain range of 0.02. Similar behavior was also observed at other strain ranges employed.
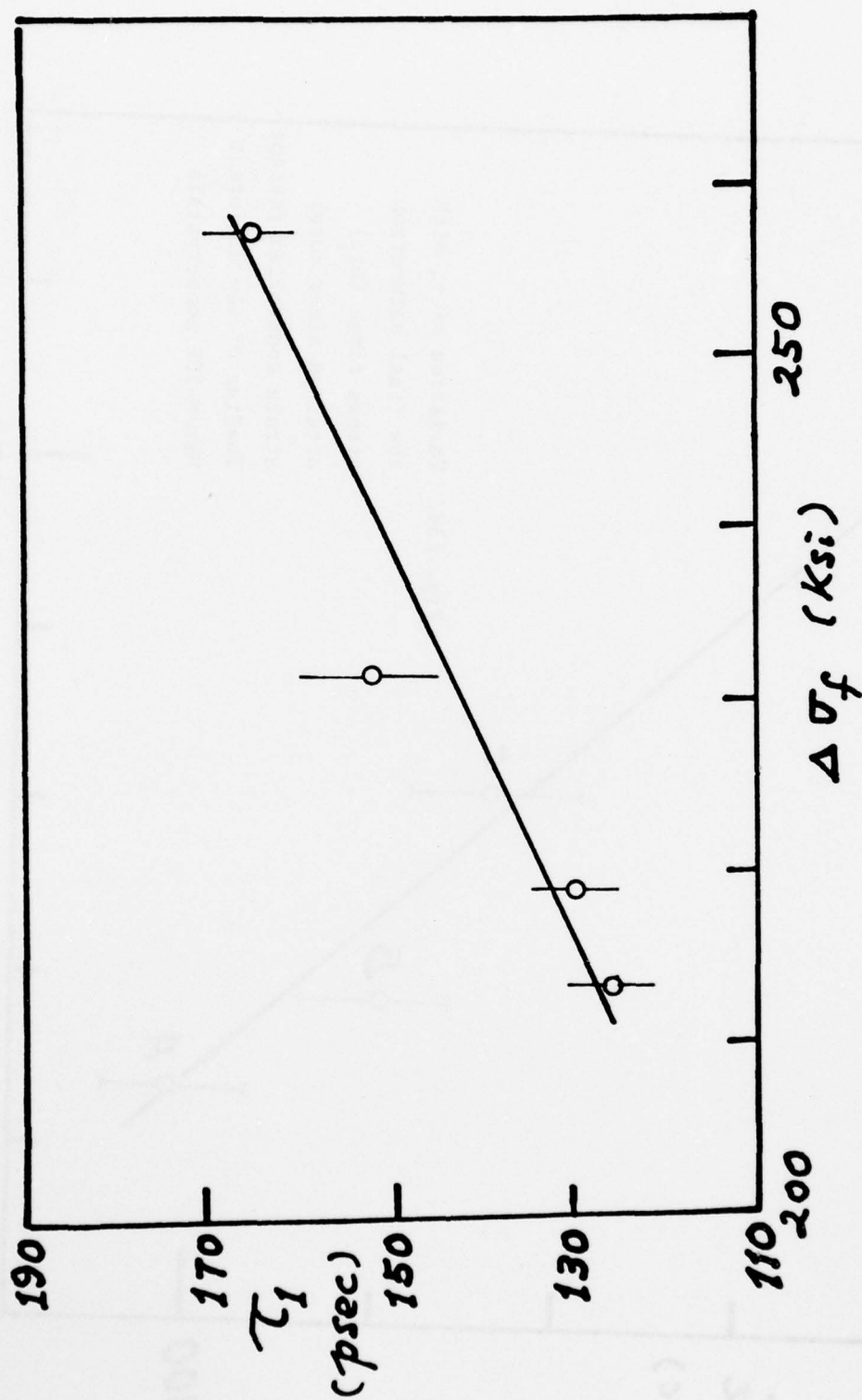
Fig. 13c. Variation of τ_1 with the final saturation stress range ($\Delta\sigma_f$) attained after total strain controlled fatigue loading of the different Mar-M-200 monocrystals.

85
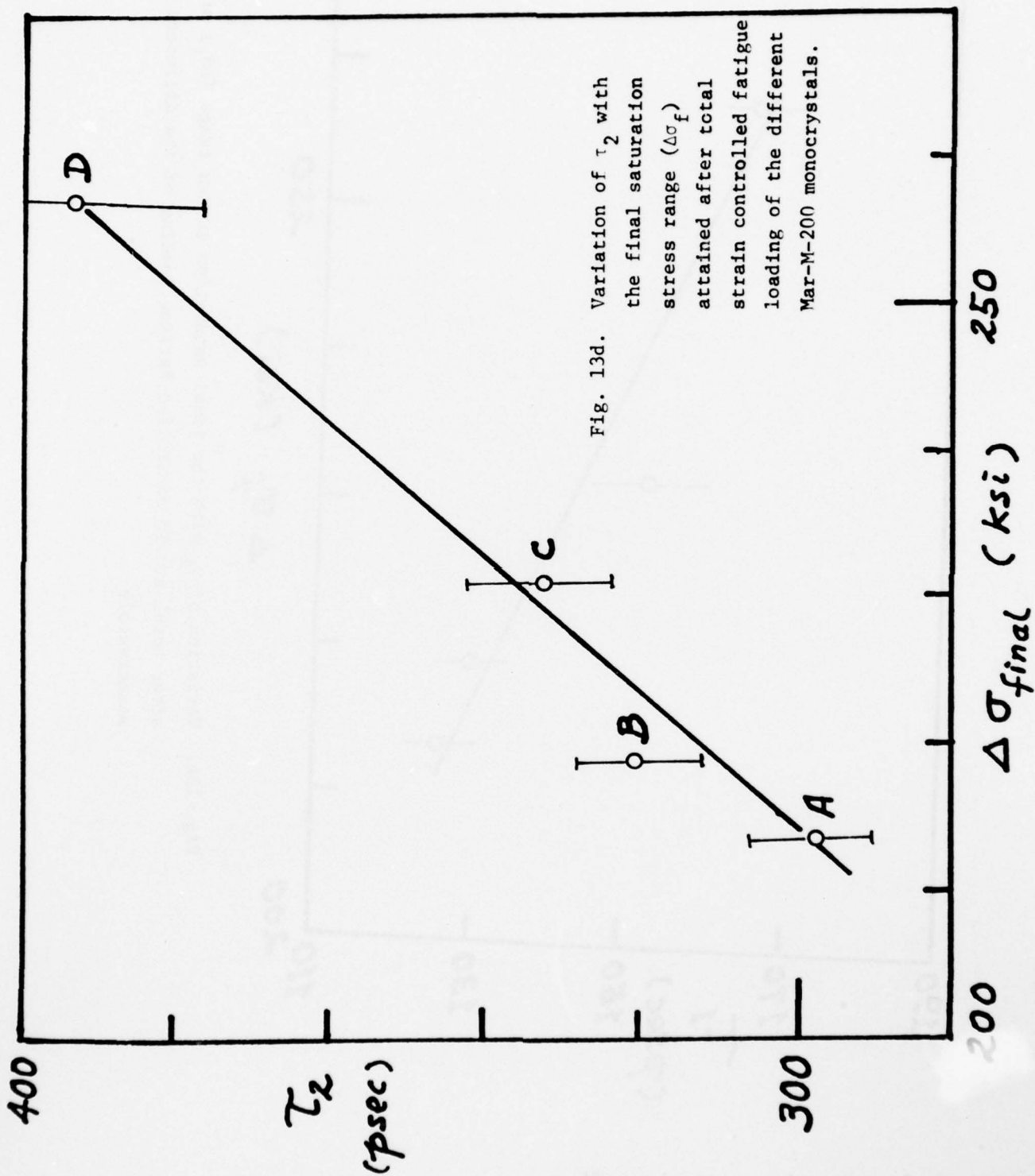
Fig. 13d. Variation of τ_2 with the final saturation stress range ($\Delta\sigma_f$) attained after total strain controlled fatigue loading of the different Mar-M-200 monocrystals.
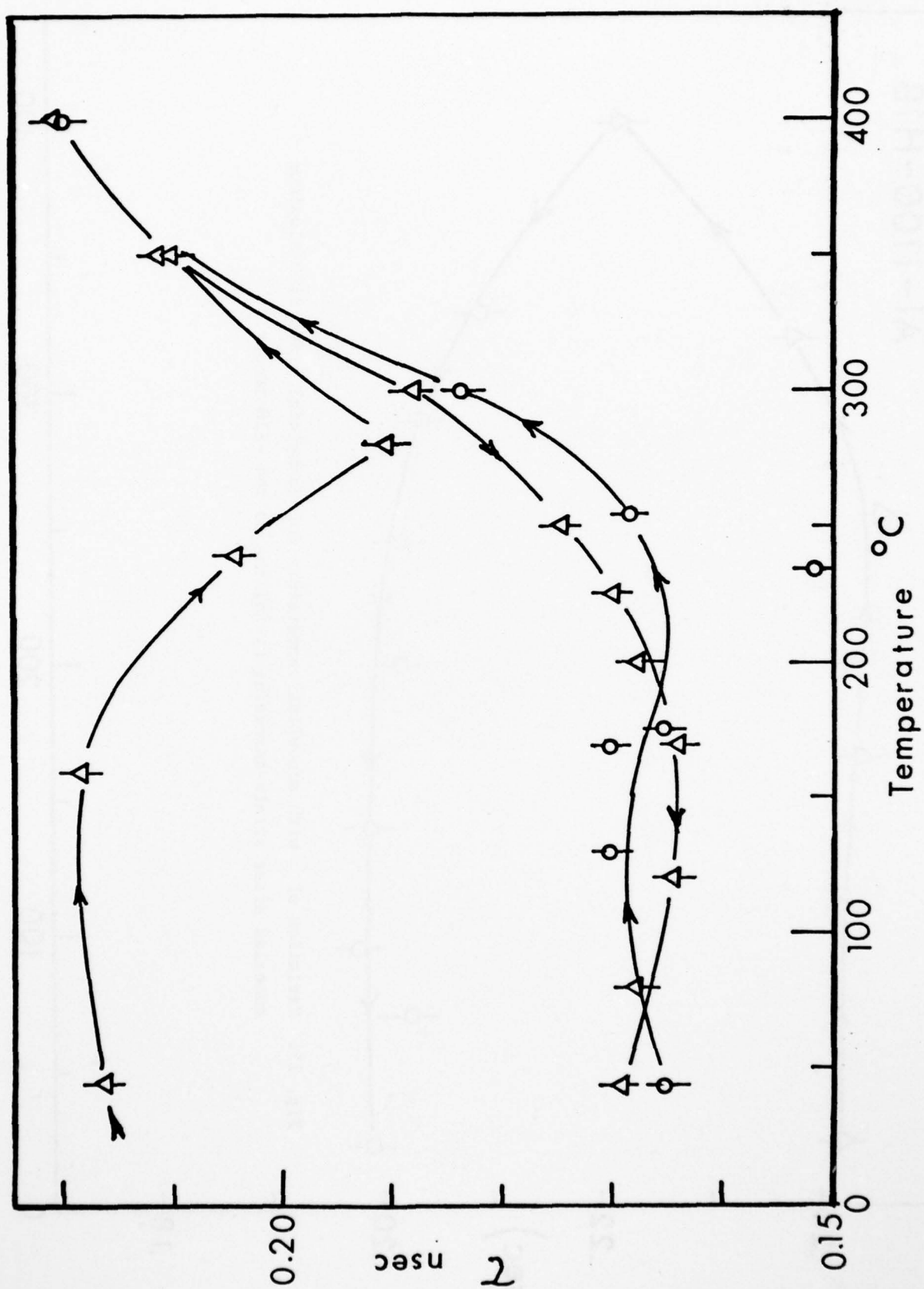
Fig. 14. Variation of the positron mean lifetime τ̄ with annealing temperature for 99.99% pure aluminum annealed after prior cold work.

87

Fig. 15. Variation of $\bar{\tau}$ with annealing temperature for commercial grade 1100 Aluminum annealed after strain hardening by rolling to the -H18 temper.

Al-1100-H18

88
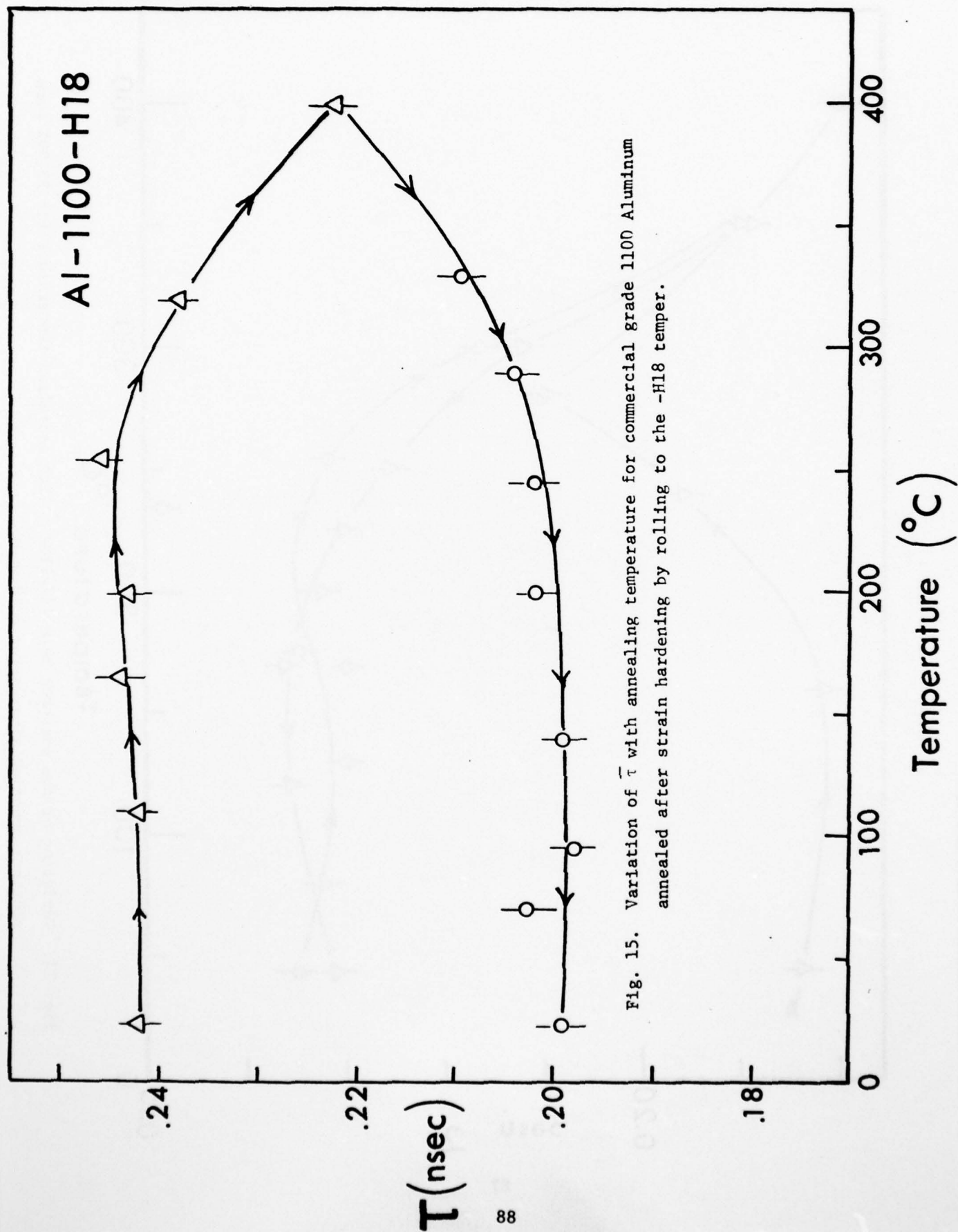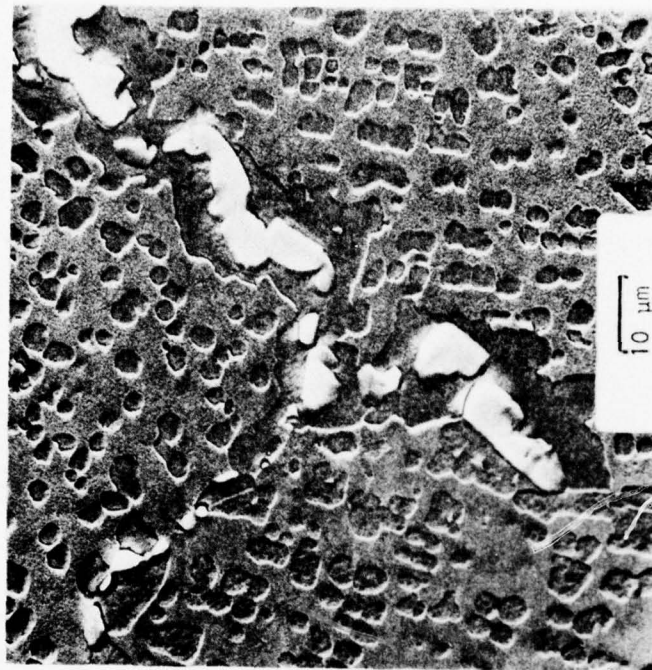
Fig. 16. Microstructure of wrought polycrystalline superalloy Nimonic-115 in the "sliding-heat treated condition" with no grain boundary carbides, (a); and after sliding heat treatment and carbide precipitation treatment, (b). See text for details of the heat treatments. Note the dispersion of γ^1 $Ni_3(AL, Ti)$ precipitates within the grains.

89
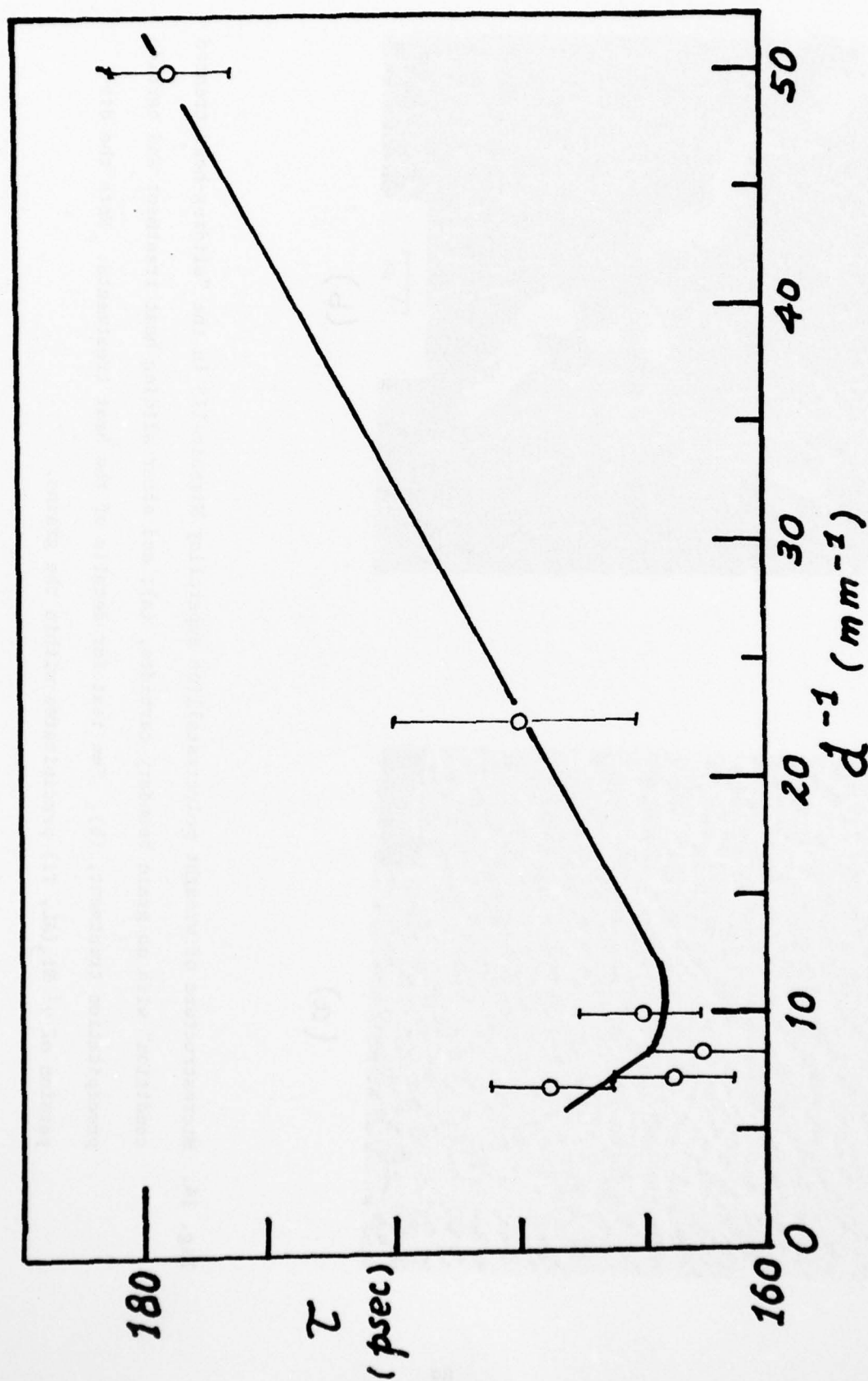
Fig. 17. Variation of $\bar{\tau}$ with inverse grain size for Nimonic-115 with no grain boundary carbides.
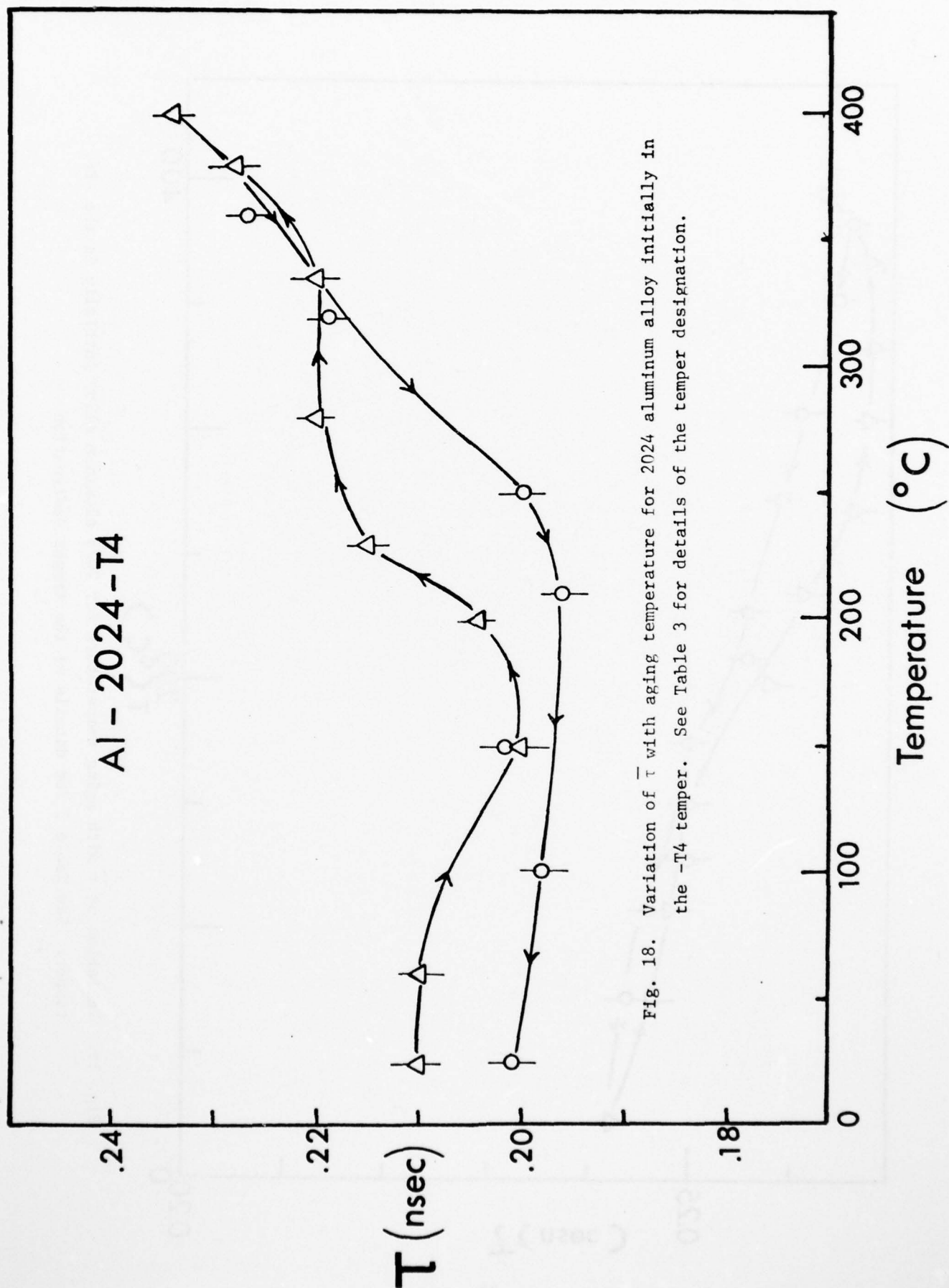
Fig. 18. Variation of $\bar{\tau}$ with aging temperature for 2024 aluminum alloy initially in the –T4 temper. See Table 3 for details of the temper designation.
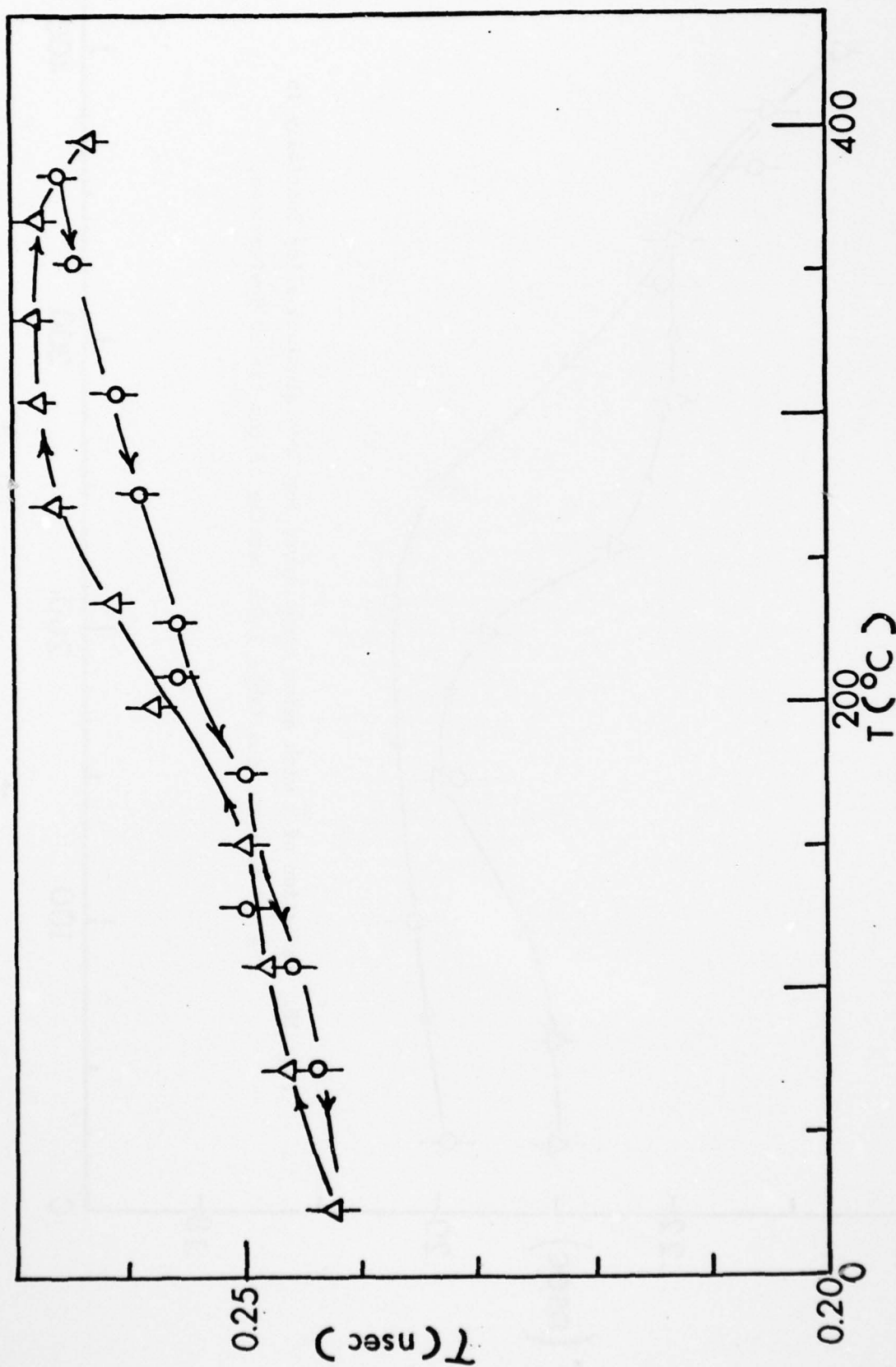
Fig. 19. Variation of $\bar{\tau}$ with aging temperature for 7075 aluminum alloy initially in the -T6 temper. See Table 3 for details of the temper designation.

92

1·0

2·8   2·5

5·0   3·15   2·2

5·6

3·5

6·3

1·1   4·0   2·0

4·5

1·8

1·25   1·4   1·6
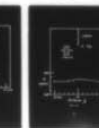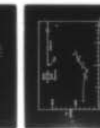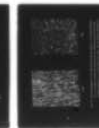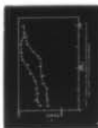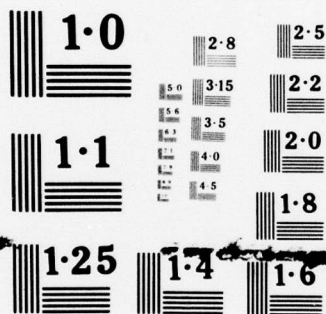
NATIONAL BUREAU OF STANDARDS
MICROCOPY RESOLUTION TEST CHART
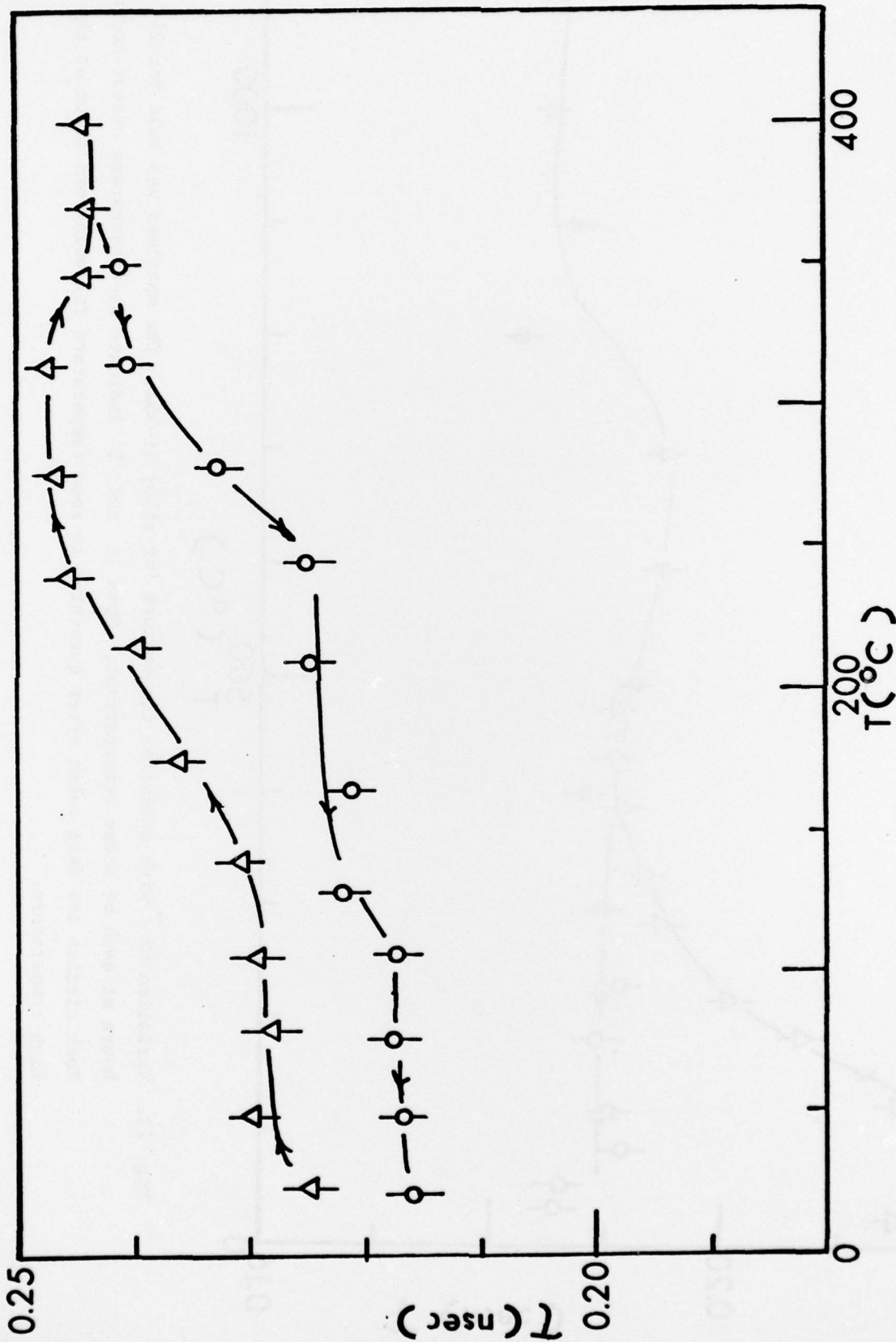
Fig. 20. Variation of $\bar{\tau}$ with aging temperature for 7050 aluminum alloy initially in the -T76 temper. See Table 3 for details of the temper designation.
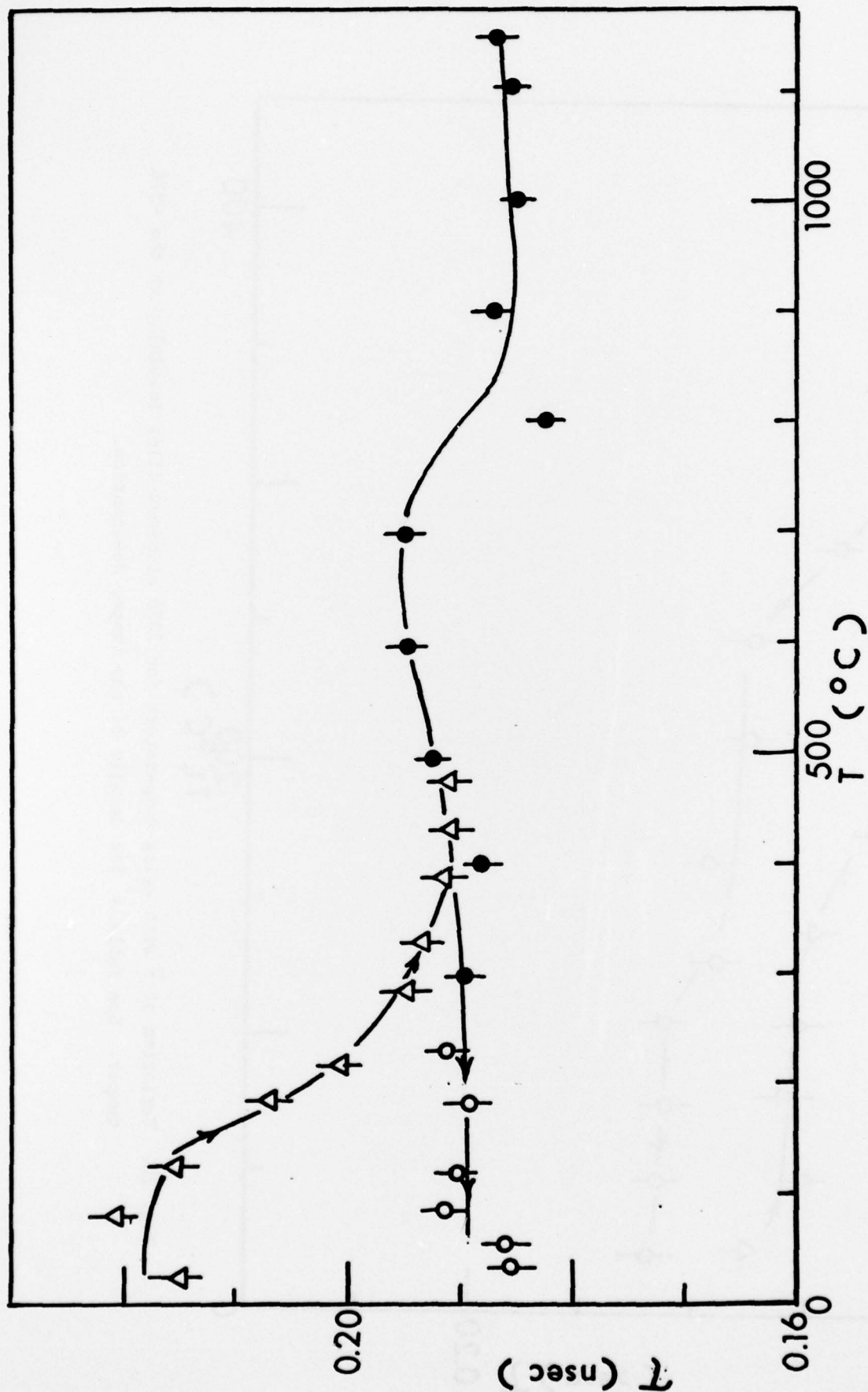
Fig. 21. Variation of $\bar{\tau}$ with oxidation temperature for alloy Ti-35A. The specimen was held for 24 hours at each of these temperatures. Open 'Δ' and 'O' indicate at-temperature measurements. Dark circles are data taken after quenching to room temperature following oxidation at the high temperature.
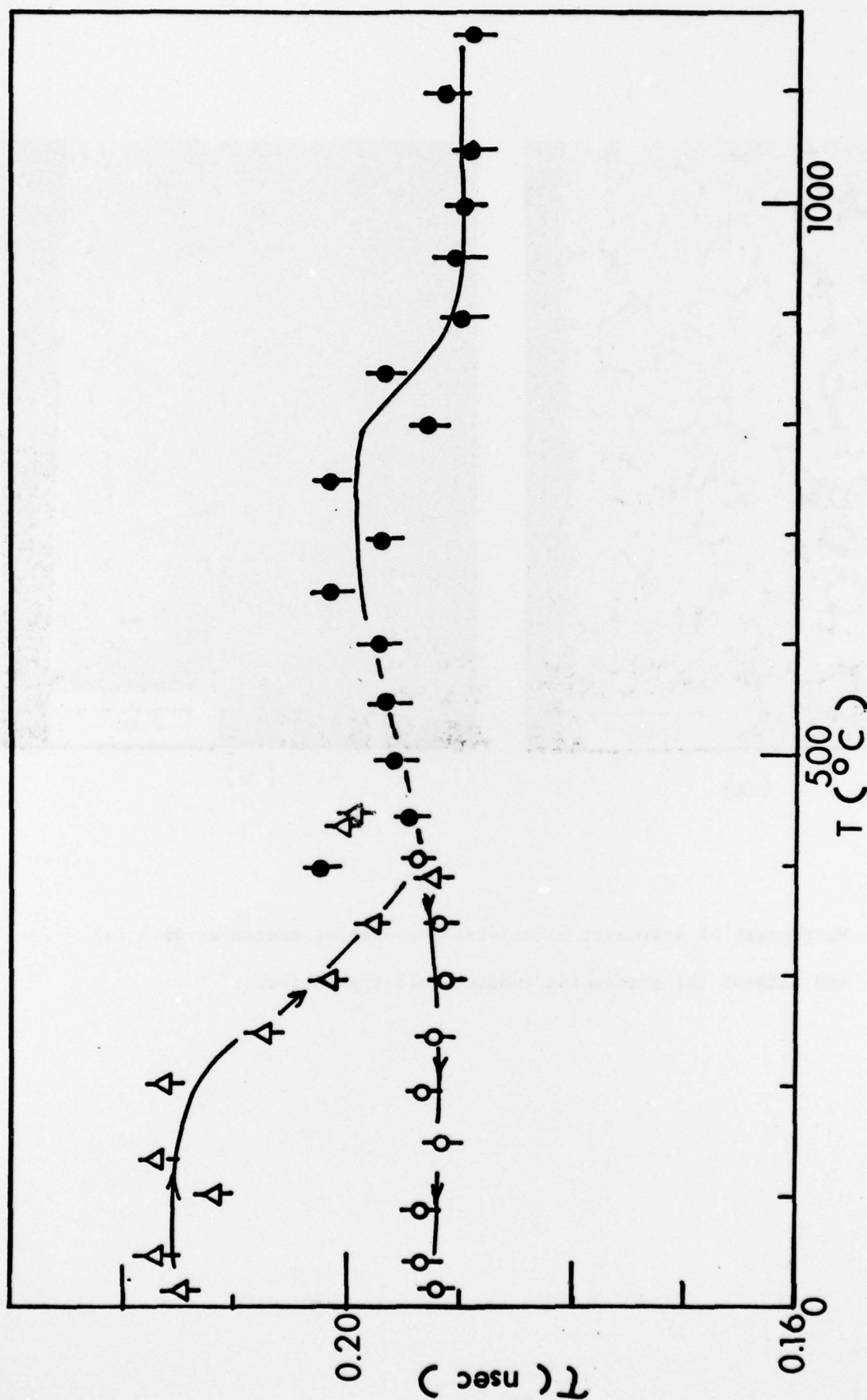
Fig. 22. Variation of $\bar{\tau}$ with oxidation temperature for alloy Ti-6Al-4V. The specimen was held for 24 hours at each of these temperatures. Open 'Δ' and '$\circ$' indicate at-temperature data. Dark circles are data taken after quenching to room temperature following oxidation at the higher temperature.
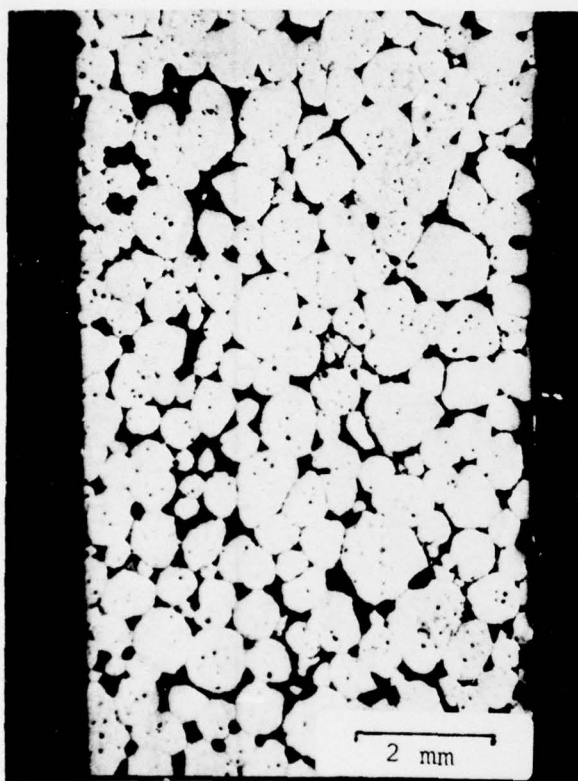
Fig. 23. Macrograph of a wrought nickel-base superalloy specimens with (a) and without (b) processing induced void type defects.
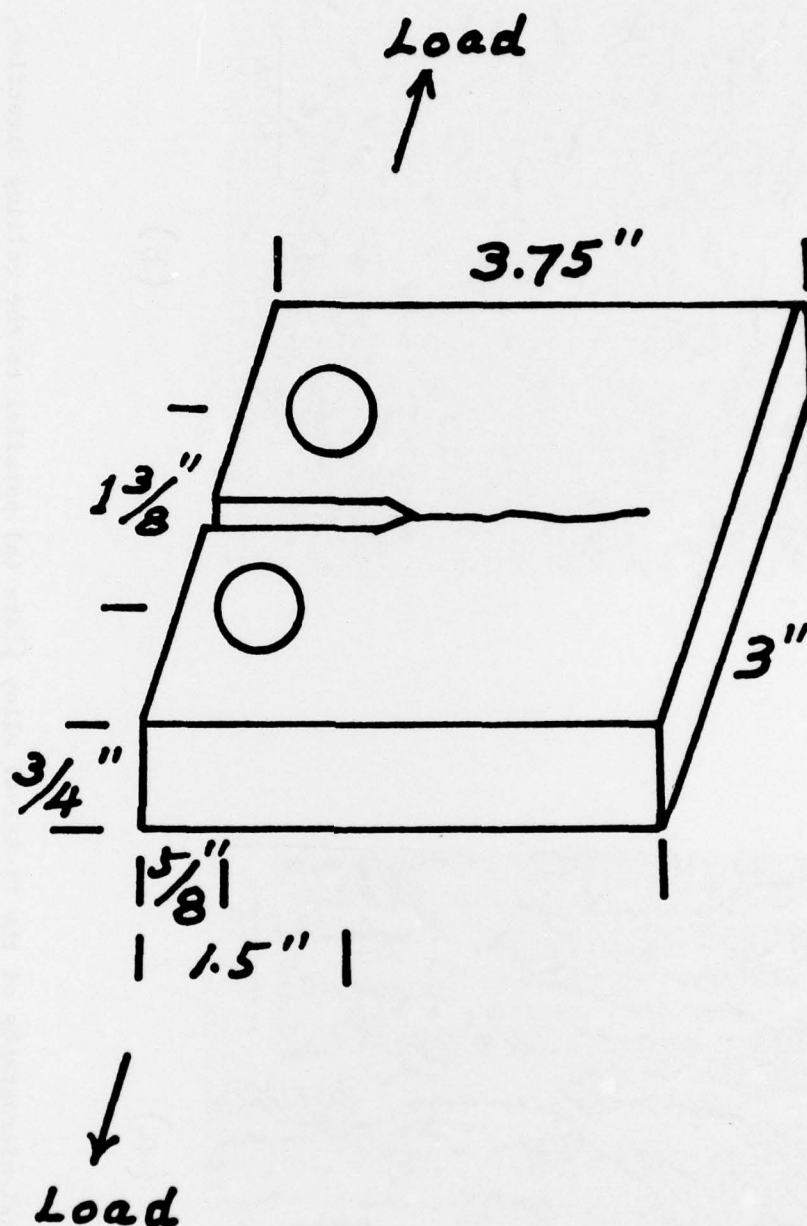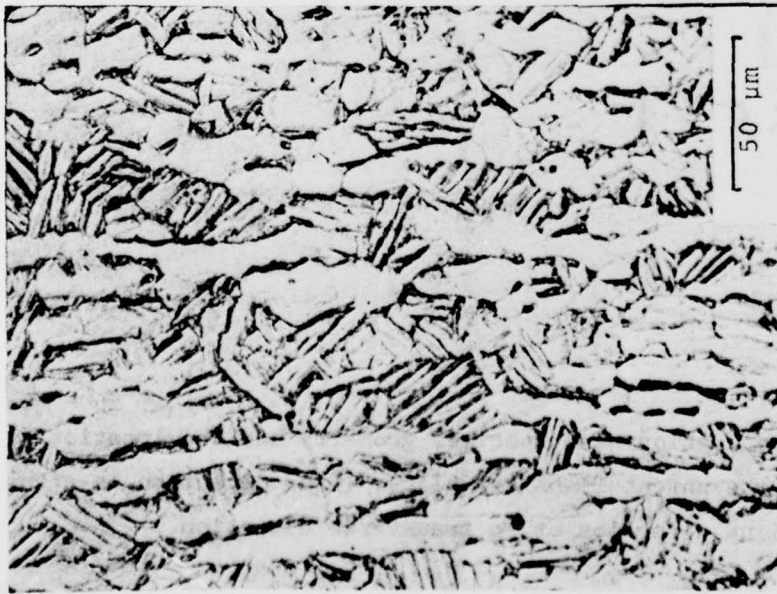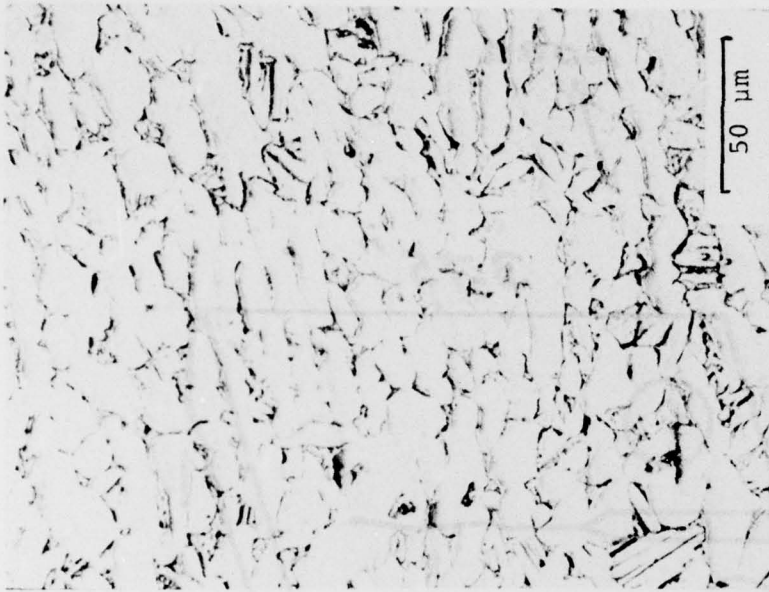
Fig. 24. Fatigue crack propagation test specimen geometry and the location of
the specimen in the parent Ti-6Al-4V plate. (Load direction is either
parallel to rolling direction or to transverse direction.)

Fig. 25. Optical micrographs of the Ti-6Al-4V alloy plate (a) parallel to the rolling direction, i.e., in the plane containing the crack line and the loading direction and (b) in the transverse direction, i.e., in the plane of the crack. Note the distinct difference in the grain shapes in the two directions. Light etching retions are grains of α phase and and the darker etching regions in between are grains of β phase.

98

Figs. 26a through 26c. The three different ways in which the positron source was mounted and traversed relative to the crack in the positron probing experiments on the fracture mechanics speci-mens (see insets) and the corresponding spatial variations in the measured positron mean lifetimes.
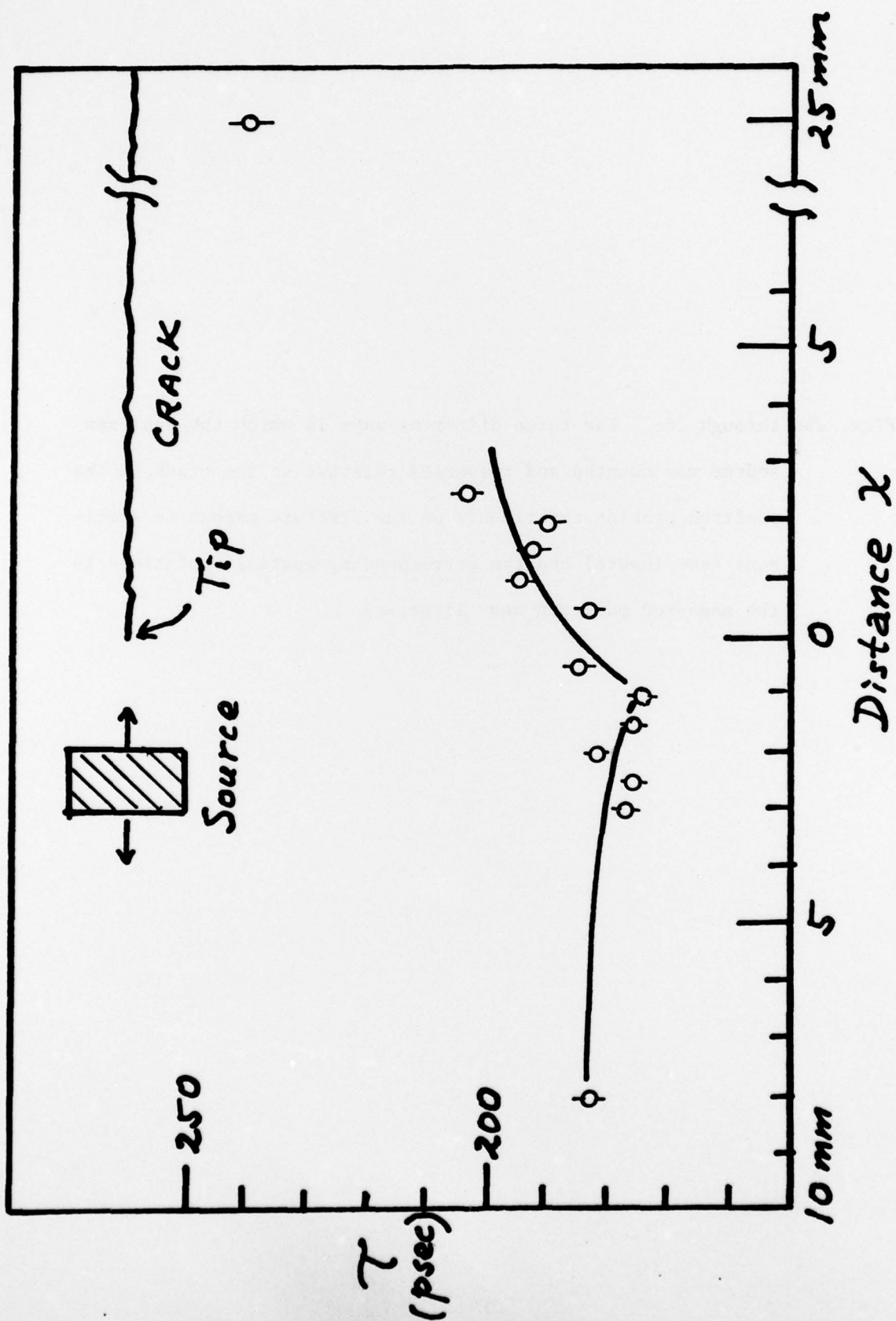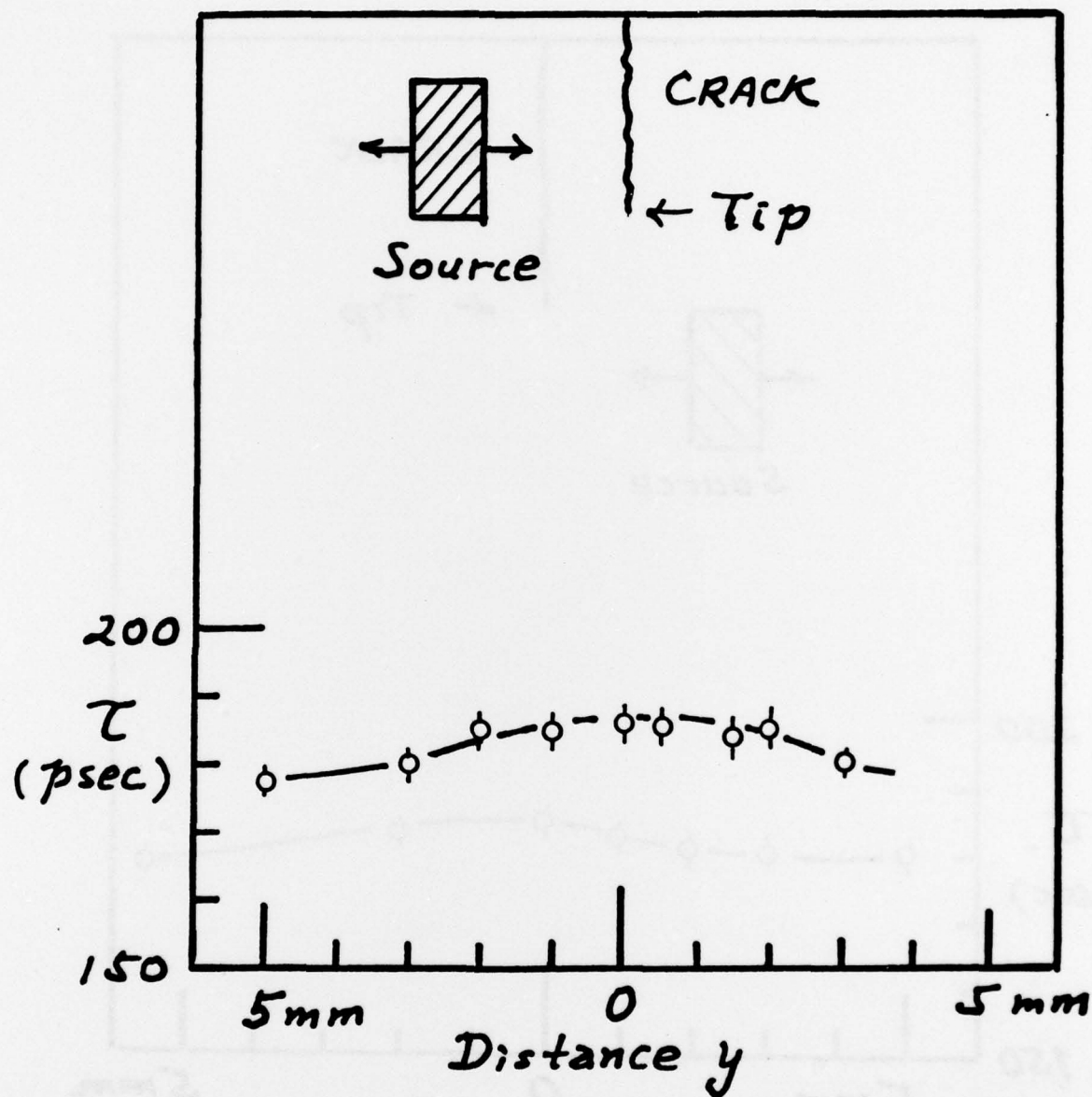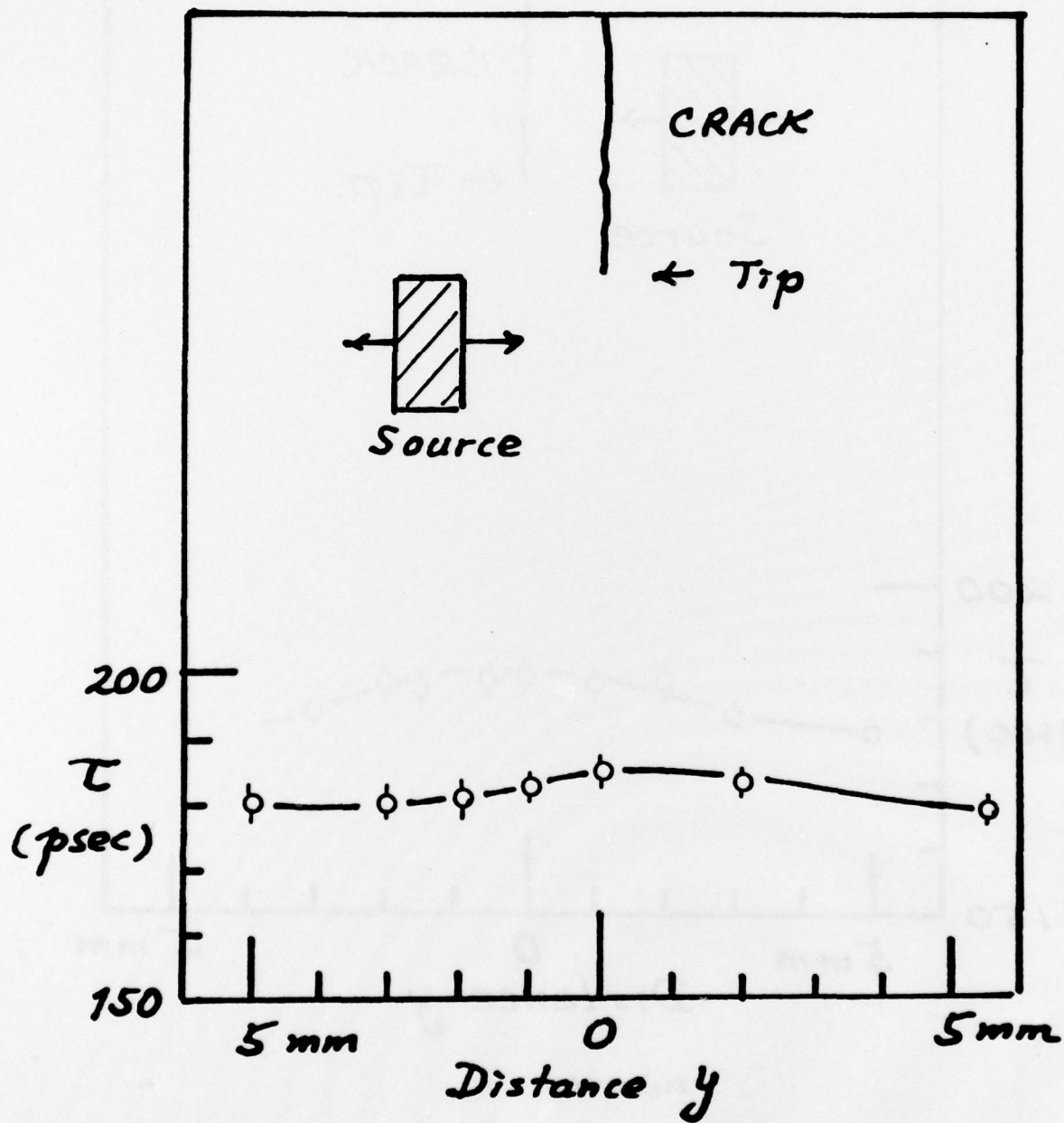
Figure 26a.

Figure 26b

101

Figure 26c